CONTENTS

FIGURES

FIGURES (continued)

FIGURES (continued)

FIGURES (continued)

FIGURES (continued)

TABLES

TABLES (continued)

5. CONTAMINANT FATE AND TRANSPORT

Section 5 presents modeling activities that supported development of this remedial investigation and baseline risk assessment (RI/BRA) for Waste Area Group 7 at the Idaho National Laboratory (INL) Site and addresses the following modeling topics:

- Section 5.1—source-release
- Section 5.2—dissolved-phase transport
- Section 5.3—volatile organic compounds (VOCs)
- Section 5.4—gaseous-phase radionuclides
- Section 5.5—biotic transport.

Modeling in the RI/BRA is largely the same as modeling implemented in the Ancillary Basis for Risk Analysis (ABRA) (Holdren et al. 2002), but with improvements. The differences found when compared to the ABRA models are identified in the following discussions.

The Radioactive Waste Management Complex (RWMC) is a complex site. A single model will not handle source release, fate and transport, and risk calculations with sufficient detail to be acceptable to the Department of Energy, the Idaho Department of Environmental Quality, and the U.S. Environmental Protection Agency; therefore, modeling is divided into modules and separate models or tools that are appropriate for each module are used as follows (see Figure 5-1):

- Waste Inventory and Location Database provides inventory information, in terms of the amount of waste disposed of per year, for each source area
- DUST-MS computes the release of contaminants due to the shallow subsurface
- TETRAD computes contaminant concentration movement in the groundwater and volatile inhalation concentration at the surface
- DOSTOMAN computes biotic uptake concentrations for the other surface pathways, including external exposure, crop ingestion, soil ingestion, and dust inhalation
- Risk calculations convert concentrations from TETRAD or DOSTOMAN into a carcinogenic risk or hazard index.

Numerous model runs were used to define a base-case analysis and to assess the sensitivity of results to select model parameters and assumptions. Contaminants identified for further evaluation in Section 3.4 were simulated. Long-lived progeny were specifically included in the simulations because remedial action may slow transport; this possibility would allow additional ingrowth and influence risk estimates. No additional simulations were performed specifically for ecological analysis. Biotic modeling used to assess human health risk for surface exposure pathways also provided the basis for ecological risk assessment. Contaminants and models used in the RI/BRA are summarized in Table 5-1.

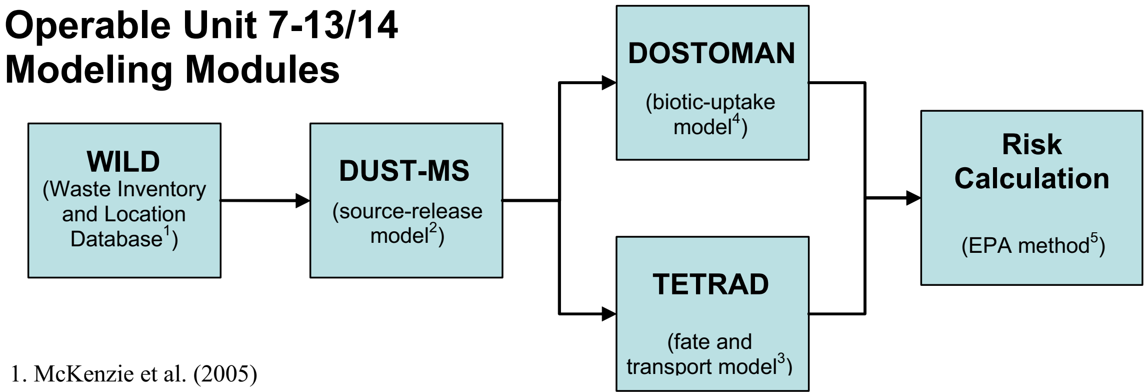

1. McKenzie et al. (2005)
2. Anderson and Becker (2006)
3. Magnuson and Sondrup (2006)
4. See footnote b in Section 3
5. Engineering design file scheduled for development

Figure 5-1. Operable Unit 7-13/14 risk modeling modules.

Table 5-1. Contaminants evaluated in the remedial investigation and baseline risk assessment and the computer models used to assess them.

Contaminant	Screening Results	Primary 1,000-year Exposure Pathway	Computer Models		
			DUST-MS	TETRAD	DOSTOMAN
Ac-227	Contaminant of potential concern	Groundwater ingestion	Yes	Yes	Yes
Am-241	Contaminant of potential concern	Soil ingestion, inhalation, external exposure, and crop ingestion	Yes	Yes	Yes
Am-243	Long-lived parent of Pu-239	External exposure	Yes	Yes	Yes
C-14	Contaminant of potential concern	Groundwater ingestion	Yes	Yes	Yes
Cl-36	Contaminant of potential concern	Groundwater ingestion	Yes	Yes	Yes
Cs-137	Contaminant of potential concern for surface exposure pathways only	External exposure	Yes	No	Yes
I-129	Contaminant of potential concern	Groundwater ingestion	Yes	Yes	Yes
Nb-94	Contaminant of potential concern for surface exposure pathways only	External exposure	Yes	Yes	Yes
Np-237	Contaminant of potential concern	Groundwater ingestion	Yes	Yes	Yes
Pa-231	Contaminant of potential concern	Groundwater ingestion	Yes	Yes	Yes
Pb-210	Contaminant of potential concern	Groundwater ingestion	Yes	Yes	Yes
Pu-238	Contaminant of potential concern and long-lived parent of U-234	Soil and crop ingestion	Yes	Yes	Yes
Pu-239	Contaminant of potential concern	Soil and crop ingestion	Yes	Yes	Yes
Pu-240	Contaminant of potential concern	Soil and crop ingestion	Yes	Yes	Yes
Ra-226	Contaminant of potential concern	External exposure	Yes	Yes	Yes
Ra-228	Contaminant of potential concern	External exposure	Yes	Yes	Yes
Sr-90	Contaminant of potential concern for surface exposure pathways only	Crop ingestion	Yes	No	Yes
Tc-99	Contaminant of potential concern	Groundwater ingestion and crop ingestion	Yes	Yes	Yes
Th-228	Contaminant of potential concern for surface exposure pathways only	External exposure	Yes	No	Yes

Table 5-1. (continued).

Contaminant	Screening Results	Primary 1,000-year Exposure Pathway	Computer Models		
			DUST-MS	TETRAD	DOSTOMAN
Th-229	Long-lived progeny of U-233	Groundwater ingestion	Yes	Yes	Yes
Th-230	Long-lived progeny of U-234	Groundwater ingestion	Yes	Yes	Yes
Th-232	Long-lived progeny of U-236	Crop ingestion	Yes	Yes	Yes
U-232	Parent of contaminant of potential concern (Th-228)	External exposure	Yes	No	Yes
U-233	Contaminant of potential concern	Groundwater ingestion	Yes	Yes	Yes
U-234	Contaminant of potential concern	Groundwater ingestion	Yes	Yes	Yes
U-235	Contaminant of potential concern	Groundwater ingestion	Yes	Yes	Yes
U-236	Contaminant of potential concern	Groundwater ingestion	Yes	Yes	Yes
U-238	Contaminant of potential concern	Groundwater ingestion	Yes	Yes	Yes
Carbon tetrachloride	Contaminant of potential concern	Inhalation and groundwater ingestion	Yes	Yes	No
Chromium	Model performance indicator	NA	Yes	Yes	No
1,4-Dioxane	Contaminant of potential concern	Groundwater ingestion	Yes	Yes	No
Methylene chloride	Contaminant of potential concern	Groundwater ingestion	Yes	Yes	No
Nitrate	Contaminant of potential concern	Groundwater ingestion	Yes	Yes	Yes
Tetrachloroethylene	Contaminant of potential concern	Groundwater ingestion and dermal exposure to contaminated water	Yes	Yes	No
Trichloroethylene	Contaminant of potential concern	Inhalation and groundwater ingestion	Yes	Yes	No

5.1 Source-Release Modeling

The source term for the RI/BRA is defined as waste buried in the Subsurface Disposal Area (SDA). Conceptually, the source-term model is simple. Waste was buried in containers such as drums, boxes, and bags. When containers fail, contaminants can be released over time by one of three release mechanisms: washoff, diffusion, or dissolution. The type of release mechanism and the release rates depend on characteristics of the waste. Mass released from buried waste is available for transport into the subsurface by infiltration or transport to the surface by biotic uptake. If the contaminant is volatile, vapor diffusion into both the vadose zone and the surface is accounted for in the transport model. Source-release modeling for the RI/BRA is summarized in this section. Greater detail on source-release modeling is provided in Anderson and Becker (2006).

Traditionally, the DUST-MS source-release computer code (Sullivan 2006) has been used to estimate the mass available in the SDA for transport. The source-term model simulates release of contaminants into the subsurface from waste buried in the SDA. For the RI/BRA, DUST-MS was again chosen (Anderson and Becker 2006; Appendix D of Holdren and Broomfield 2004) due to its established acceptance, to maintain consistency with previous simulation efforts, and because it was favorably peer-reviewed (Kozak, Yim, and Sullivan 2003). Thirty-one contaminants were modeled for source release, including contaminants of potential concern identified in Section 3.4 and the long-lived daughter products of those contaminants of potential concern. Two of the contaminants (i.e., tritium and chromium) were modeled only as model-performance indicators rather than to assess risk. Table 5-1 lists these contaminants.

Implementation of the source-term model is described in the following sections. Input parameters include source-term inventory, waste types, infiltration rates, release mechanisms, source-area characteristics (i.e., surface area and depth), container types, and container failure rates. Contaminant grouping and assigning SDA contaminants to source areas also are described. DUST-MS is a one-dimensional model; therefore, the SDA is subdivided into 18 separate source areas, which are described in the following subsections, to represent distribution of waste across the SDA. The source-release model provided mass estimates for total yearly releases from all waste-source areas, which were then used as inputs for the subsurface and biotic transport models discussed in the remainder of Section 5.

Radioactive decay was the only mechanism considered to affect source-term inventories. As presented in the Interim Risk Assessment (IRA) (Becker et al. 1998), by decaying isotopes to the present and then initiating fate and transport simulations, results can be biased low for mobile isotopes with short half-lives. Therefore, inventory estimates for most radionuclides were not adjusted directly to account for radioactive decay. Instead, inventories at the time of disposal were input for each year. The DUST-MS code simulated inventory changes over time caused by radioactive decay and ingrowth, thus allowing decay and transport to begin at the actual year of disposal.

Inventories for three parent nuclides (i.e., Pu-242, Cm-244, and Pu-241) were decayed to the daughter and only the daughters were simulated. In the IRA (Becker et al. 1998), risk from Pu-242 was 9E-10; Cm-244 had a risk of 2E-10 and is short-lived; and Pu-241 had a risk of 1E-11 and a short half-life. Therefore, all three parent nuclides were decayed to their daughters to minimize the number of isotopes in the subsurface-transport simulations. This methodology is consistent with that used in the ABRA and is conservative because it has more mass of the daughter available for transport earlier in the simulation.

Inventory for Pu-239 and Pu-240 was divided into a mobile fraction and a nonmobile fraction. Batcheller and Redden (2004) determined that 3.7% of plutonium from Rocky Flats Plant went through high-temperature processes and could be in a colloidal form. This colloidal form would be more mobile and is assumed to be released when the containers fail. Table 5-3 shows how the initial inventory was developed and how mobility was assigned for source-release modeling. While a substantial fraction of Pu-238 came from Rocky Flats Plant, Pu-238 was separated earlier in the process and would not have gone through the high-temperature processes; therefore, Pu-238 is not modeled with a mobile fraction. Colloidal size fraction was not a criterion in eliminating Pu-238 from consideration for colloidal transport. The decision to exclude Pu-238 from having a mobile fraction in the RI/BRA was also based on the small amount of Pu-238 relative to Pu-239/240, as documented in the Second Addendum to the Work Plan (see Section A-3.2.1.1 of Holdren and Broomfield 2004). Any contribution to plutonium concentrations in the environment would be overshadowed by the Pu-239/240 contribution.

5.1.1 Source-Term Inventory

The base case for the remedial investigation represents the current state of RWMC in the absence of any further remedial action, with these three exceptions:

1. Because a non-time-critical removal action is ongoing in the SDA to remove targeted waste from a designated area within Pit 4 (DOE-ID 2004a), an assumption was adopted that the removal action would be completed before the Operable Unit 7-13/14 record of decision was prepared. Therefore, the current inventory was reduced to account for this removal action. The modeling assumption was that 80% of the inventory was removed from waste targeted for retrieval. Waste targeted for retrieval is waste containing the highest concentrations of transuranic isotopes, depleted uranium, or VOCs. The original method of retrieval was based on visual identification of targeted waste streams. For the modeling, the 80% removal was used to estimate the effectiveness of visual identification. To simplify modeling, it was assumed that the Accelerated Retrieval Project remediation would occur at the same time as grouting. Grouting occurred in 2004 and retrieval from the Accelerated Retrieval Project started in 2004; however, retrieval is not complete yet.

2. The active Low-level Waste (LLW) Disposal Facility (referred to as the LLW Pit) will remain open through the year 2009 (Holdren and Broomfield 2004); therefore, inventories projected through the year 2009 are included in the base-case simulations.

3. Organic Contamination in the Vadose Zone Project operations will continue to remove organic vapors from the vadose zone. Current operations are assumed to continue through the year 2009. Details of modeling assumptions for future operations are provided in Section 5.3.1.2.

The non-time-critical removal action to grout beryllium reflector blocks implemented in 2004 (Lopez et al. 2005) also is accounted for. Though grouting did not affect the source-term inventory, it did reduce the modeled contaminant release for the blocks that were grouted. Section 5.1.3 discusses assumptions made to estimate the release from grouted beryllium blocks. Therefore, the base case accounts for grouting that has been completed for beryllium blocks, removal of waste from Pit 4, and projected disposals into the LLW Pit. Annual best-estimate inventories for waste buried in the SDA through 1999 were taken from the Waste Information and Location Database and input into the source-term model. Estimates for projected disposals in the active LLW Pit were provided by Waste Generator Services. Tables 5-2 through 5-5 contain information on the waste streams for each individual contaminant, a brief description of the waste streams, and the release mechanisms and rates identified for modeling the waste streams. (Summaries are provided in Section 4; see Table 4-2 for total disposal inventories for radionuclides and Table 4-3 for nonradionuclides.)

Table 5-2. Radiological waste streams, best-estimate inventories (curies) at time of disposal, and baseline source-release information for Operable Unit 7-13/14.

Contaminant	Waste Stream Code	Percentage in Waste Stream (%)	Inventory (Ci)[a]	Waste Stream Description	Release Mechanism[b]	Release Parameter Value[b]	Release Parameter Units	Parameter Description	Container Type
Ac-227	INTEC-MOD-9H	18.0	7.68E-07	General plant waste (e.g., metal, glass, paper, wood, clothing, plastic, dirt, and shielding material) (1952 through 1983)	Surface wash	2.25E+02	mL/g	Distribution coefficient	No containment
	TRA-670-1N	16.9	7.19E-07	Beryllium waste	Surface wash	2.25E+02	mL/g	Distribution coefficient	No containment
	CFA-690-1	16.4	7.00E-07	Metal—stainless steel	Surface wash	2.25E+02	mL/g	Distribution coefficient	No containment
	INTEC-MOD-5H	10.1	4.32E-07	HEPA filter from Waste Calcining Facility and other filters from miscellaneous facilities	Surface wash	2.25E+02	mL/g	Distribution coefficient	No containment
	INTEC-MOD-6H	6.3	2.68E-07	CPP-603 resins (i.e., basin sludge and miscellaneous storage basin Zeolite filters)	Surface wash	2.25E+02	mL/g	Distribution coefficient	No containment
	INTEC-MOD-7H	6.2	2.63E-07	Contaminated soil from Tank Farm spills	Surface wash	2.25E+02	mL/g	Distribution coefficient	No containment
	TAN-607-3N	5.7	2.45E-07	Activated core, loop components, end boxes, and stainless steel from the Stationary Low-Power Reactor No. 1 reactor	Surface wash	2.25E+02	mL/g	Distribution coefficient	No containment
	TAN-633-5N	5.0	2.14E-07	Material such as core structures, piping, clad assemblies, stainless steel, and combustible waste	Surface wash	2.25E+02	mL/g	Distribution coefficient	No containment
	CFA-RWM-1	4.9	2.07E-07	Central Facilities Area Sewage Treatment Plant unpainted concrete rubble, drying beds soils, clarifier piping, and trickle filter bricks	Surface wash	2.25E+02	mL/g	Distribution coefficient	No containment
	INTEC-MOD-4H	2.4	1.03E-07	One-time-only Navy experiment	Surface wash	2.25E+02	mL/g	Distribution coefficient	No containment
	TAN-607-6RN	1.7	7.09E-08	Metal alloys, end boxes, combustible material, fuel assembly shrouds, concrete, resin, sludge, and equipment from Hot Shop and Hot Cells (1984 through 1993)	Surface wash	2.25E+02	mL/g	Distribution coefficient	3% drums, 97% other
	TAN-633-2N	1.5	6.24E-08	Hot shop waste.	Surface wash	2.25E+02	mL/g	Distribution coefficient	No containment
	D&D-ARA-1	1.2	5.23E-08	Waste stream consists primarily of contaminated metal and debris	Surface wash	2.25E+02	mL/g	Distribution coefficient	No containment
	INTEC-MOD-2H	1.1	4.69E-08	Leached Vycor glass	Surface wash	2.25E+02	mL/g	Distribution coefficient	No containment
	Miscellaneous[c]	2.6	1.06E-07	Various waste types	—	—	—	—	—
Total Ac-227		100	4.26E-06						
Am-241	RFO-DOW-3H	77.8	1.89E+05	Uncemented sludge	Surface wash	2.25E+02	mL/g	Distribution coefficient	99.8% drums, 0.2% wooden boxes
	RFO-DOW-4H	13.4	3.26E+04	Paper, rags, plastic, clothing, wood, and polyethylene bottles	Surface wash	2.25E+02	mL/g	Distribution coefficient	70% drums, 30% wooden boxes
	Pu-241 ingrowth	5.2	1.27E+04	Various Rocky Flats Plant waste streams	Surface wash	2.25E+02	mL/g	Distribution coefficient	Mix of drums and boxes
	RFO-DOW-12H	2.6	6.26E+03	Dirt, concrete, ash, and soot	Surface wash	2.25E+02	mL/g	Distribution coefficient	81% drums, 19% wooden boxes
	RFO-DOW-6H	0.9	2.01E+03	Filters	Surface wash	2.25E+02	mL/g	Distribution coefficient	Wooden or cardboard boxes
	Miscellaneous[c]	0.1	3.02E+02	Various waste types	—	—	—	—	—
Total Am-241		100.0	2.43E+05						

Table 5-2. (continued).

Contaminant	Waste Stream Code	Percentage in Waste Stream (%)	Inventory (Ci)[a]	Waste Stream Description	Release Mechanism[b]	Release Parameter Value[b]	Release Parameter Units	Parameter Description	Container Type
Am-243	TRA-670-1N	60.9	7.03E-02	Beryllium waste	Surface wash	2.25E+02	mL/g	Distribution coefficient	No containment
	INTEC-MOD-9H	19.4	2.24E-02	General plant waste 1952 through 1983. Consists of metal, glass, paper, metal, wood, clothing, plastic, dirt, and shielding material	Surface wash	2.25E+02	mL/g	Distribution coefficient	No containment
	INTEC-MOD-5H	10.9	1.26E-02	HEPA filter from WCF and other filters from miscellaneous facilities	Surface wash	2.25E+02	mL/g	Distribution coefficient	No containment
	Miscellaneous[c]	8.8	1.02E-02	Various waste types	—	—	—	—	—
Total Am-243		100.0	1.16E-01						
C-14	TRA-603-4N	46.0	3.36E+02	Core components	Dissolution	1.19E-05	1/year	Stainless steel fractional corrosion rate	13% drums, 87% other
	TRA-670-1N	12.7	9.31E+01	Beryllium waste	Dissolution	2.65E-03	1/year	Beryllium fractional corrosion rate	No containment
	LLW—metal	9.8	7.17E+01	2000 through 2009 activated metal	Dissolution	1.19E-05	1/year	Stainless steel fractional corrosion rate	No containment
	TRA-632-2N	7.8	5.72E+01	Hot Cell waste	Surface wash	4.00E-01	mL/g	Distribution coefficient	24% drums, 76% other
	NRF-MOD-6H	5.2	3.82E+01	Core structural materials (1953 through 1983)	Dissolution	1.19E-05	1/year	Stainless steel fractional corrosion rate	17% drums, 83% other
	TRA-603-27N	3.8	2.81E+01	Noncompactable waste (e.g., metal, wood, and glass)	Surface wash	4.00E-01	mL/g	Distribution coefficient	No containment
	NRF-MOD-9H	2.3	1.65E+01	Sludge and resins from Expended Core Facility and prototype plant operations (1953 through 1971)	Surface wash	1.90E+01	mL/g	Resins distribution coefficient	18% drums, 82% other
	ANL-MOD-1H	2.2	1.60E+01	Irradiated subassembly hardware (1977 through 1983)	Dissolution	1.19E-05	1/year	Stainless steel fractional corrosion rate	9% drums, 91% other
	ANL-MOD-1R	2.1	1.53E+01	Irradiated subassembly hardware (1984 through 1993)	Dissolution	1.19E-05	1/year	Stainless steel fractional corrosion rate	No containment
	LLW—resins	1.1	7.87E+00	2000 through 2009 resins	Surface wash	1.90E+01	mL/g	Resins distribution coefficient	No containment
	TRA-603-28N	1.0	7.40E+00	Miscellaneous contaminated materials	Surface wash	4.00E-01	mL/g	Distribution coefficient	No containment
	ANL-785-1	1.0	7.11E+00	Subassembly waste from nuclear fuel and materials experiments in the Hot Fuel Examination Facility (1994 through 1999)	Dissolution	1.19E-05	1/year	Stainless steel fractional corrosion rate	No containment
	Miscellaneous[c]	5.0	3.67E+01	Mostly activated metal	—	—	—	—	—
Total C-14		100.0	7.31E+02						
Cl-36	TRA-670-1N	53.3	8.83E-01	Beryllium waste	Dissolution	2.65E-03	1/year	Beryllium fractional corrosion rate	No containment
	LLW—metal	32.5	5.38E-01	2000 through 2009 activated metal	Dissolution	1.19E-05	1/year	Stainless steel fractional corrosion rate	No containment
	NRF-MOD-6H	9.5	1.58E-01	Core structural materials (1953 through 1983)	Dissolution	1.19E-05	1/year	Stainless steel fractional corrosion rate	17% drums, 83% other

Table 5-2. (continued).

Contaminant	Waste Stream Code	Percentage in Waste Stream (%)	Inventory (Ci)[a]	Waste Stream Description	Release Mechanism[b]	Release Parameter Value[b]	Release Parameter Units	Parameter Description	Container Type
	NRF-MOD-6R	2.7	4.49E-02	Core structural materials (1984 through 1997)	Dissolution	1.19E-05	1/year	Stainless steel fractional corrosion rate	No containment
	Miscellaneous[c]	2.0	3.32E-02	Mostly activated metal	—	—	—	—	—
Total Cl-36		100.0	1.66E+00						
Cs-137	INTEC-MOD-2H	27.9	4.69E+04	Leached Vycor glass	Dissolution	1.30E-05	1/year	Vycor glass fractional corrosion rate	No containment
	OFF-ATI-1H	13.3	2.23E+04	Irradiated fuel and chemical byproducts from nuclear research	Surface wash	1.00E+03	mL/g	Distribution coefficient	36% drums, 64% other
	TRA-632-2N	9.8	1.64E+04	Hot Cell waste	Surface wash	1.00E+03	mL/g	Distribution coefficient	24% drums, 76% other
	ANL-MOD-5H	8.3	1.39E+04	General plant waste, mostly from decontamination (1952 through 1983)	Surface wash	1.00E+03	mL/g	Distribution coefficient	6% drums, 94% other
	NRF-MOD-1H	6.3	1.06E+04	Shippingport fuel material, solid (1960 through 1968)	Dissolution	3.47E-02[d]	1/year	Nuclear fuels fractional corrosion rate	No containment
	INTEC-MOD-9H	4.8	8.00E+03	General plant waste (e.g., metal, glass, paper, wood, clothing, plastic, dirt, and shielding material) (1952 through 1983)	Surface wash	1.00E+03	mL/g	Distribution coefficient	2% drums, 98% other
	TRA-603-9N	3.8	6.43E+03	Fuel materials (solids, not dissolved)	Dissolution	3.47E-02[d]	1/year	Nuclear fuels fractional corrosion rate	8% drums, 92% other
	ANL-MOD-2H	2.9	4.82E+03	Irradiated and unirradiated fuel specimens (1971 through 1983)	Surface wash	1.00E+03	mL/g	Distribution coefficient	7% drums, 93% other
	TRA-603-28N	2.7	4.53E+03	Miscellaneous contaminated materials	Surface wash	1.00E+03	mL/g	Distribution coefficient	No containment
	INTEC-MOD-5H	2.7	4.51E+03	HEPA filter from Waste Calcining Facility and other filters from miscellaneous facilities	Surface wash	1.00E+03	mL/g	Distribution coefficient	No containment
	ANL-MOD-3H	2.5	4.26E+03	Irradiated and unirradiated dissolved fuel and fuel-contaminated materials (1952 through 1970)	Surface wash	1.00E+03	mL/g	Distribution coefficient	6% drums, 94% other
	INTEC-MOD-6H	2.5	4.12E+03	CPP-603 resins (i.e., basin sludge and miscellaneous storage basin Zeolite filters)	Surface wash	1.00E+03	mL/g	Distribution coefficient	No containment
	ANL-MOD-2HEXT	2.4	4.00E+03	Irradiated and unirradiated dissolved fuel and fuel-contaminated materials (1984 through 1993)	Surface wash	1.00E+03	mL/g	Distribution coefficient	No containment
	TAN-607-3N	2.3	3.86E+03	Activated core, loop components, end boxes, and stainless steel from Stationary Low-Power Reactor No. 1 reactor	Surface wash	1.00E+03	mL/g	Distribution coefficient	No containment
	INTEC-MOD-7H	1.6	2.77E+03	Contaminated soil from Tank Farm spills	Surface wash	1.00E+03	mL/g	Distribution coefficient	No containment
	Miscellaneous[c]	6.2	1.05E+04	Various waste types	—	—	—	—	—
Total Cs-137		100.0	1.68E+05						
I-129	TRA-603-1N	44.6	8.38E-02	Resins	Surface wash	1.90E+01	mL/g	Resins distribution coefficient	No containment
	LLW—resins	24.8	4.65E-02	2000 through 2009 resins	Surface wash	1.90E+01	mL/g	Resins distribution coefficient	No containment
	INTEC-MOD-2H	9.6	1.80E-02	Leached Vycor glass	Dissolution	1.30E-05	1/year	Vycor glass fractional corrosion rate	No containment

Table 5-2. (continued).

Contaminant	Waste Stream Code	Percentage in Waste Stream (%)	Inventory (Ci)[a]	Waste Stream Description	Release Mechanism[b]	Release Parameter Value[b]	Release Parameter Units	Parameter Description	Container Type
	NRF-MOD-10H	2.5	4.78E-03	Compactable and noncompactable waste from Expended Core Facility and prototype plant operations (1952 through 1983)	Surface wash	0.00E+00	mL/g	Distribution coefficient	7% drums, 93% other
	TRA-632-2N	2.3	4.27E-03	Hot Cell waste	Surface wash	0.00E+00	mL/g	Distribution coefficient	24% drums, 76% other
	NRF-MOD-1H	2.1	3.90E-03	Shippingport fuel material, solid (1960 through 1968)	Dissolution	3.47E-02[d]	1/year	Nuclear fuels fractional corrosion rate	No containment
	ANL-MOD-5H	1.9	3.52E-03	General plant waste, mostly from decontamination (1952 through 1983)	Surface wash	0.00E+00	mL/g	Distribution coefficient	6% drums, 94% other
	LLW—trash	1.4	2.71E-03	2000 through 2009 miscellaneous LLW	Surface wash	0.00E+00	mL/g	Distribution coefficient	No containment
	INTEC-MOD-9H	1.4	2.56E-03	General plant waste (e.g., metal, glass, paper, wood, clothing, plastic, dirt, and shielding material) (1952 through 1983)	Surface wash	0.00E+00	mL/g	Distribution coefficient	2% drums, 98% other
	TRA-603-28N	1.3	2.38E-03	Miscellaneous contaminated materials	Surface wash	0.00E+00	mL/g	Distribution coefficient	No containment
	PBF-620-1	1.0	1.90E-03	Ion exchange resins	Surface wash	1.90E+01	mL/g	Resins distribution coefficient	No containment
	Miscellaneous[c]	7.1	1.34E-02	Mostly fuel-contaminated waste	—	—	—	—	—
Total I-129		100.0	1.88E-01						
Nb-94	TRA-603-4N	45.5	6.63E+01	Core components	Dissolution	1.19E-05	1/year	Stainless steel fractional corrosion rate	13% drums, 87% other
	NRF-MOD-10H	16.5	2.40E+01	Compactable and noncompactable waste from Expended Core Facility and prototype plant operations (1952 through 1983)	Surface wash	5.00E+02	mL/g	Distribution coefficient	7% drums, 93% other
	TRA-632-2N	9.5	1.39E+01	Hot Cell waste	Surface wash	5.00E+02	mL/g	Distribution coefficient	24% drums, 76% other
	LLW—resins	6.2	8.94E+00	2000 through 2009 resins	Surface wash	5.00E+02	mL/g	Distribution coefficient	No containment
	TRA-603-27N	4.7	6.83E+00	Noncompactable waste (e.g., metal, wood, and glass)	Surface wash	5.00E+02	mL/g	Distribution coefficient	No containment
	NRF-MOD-6H	3.5	5.06E+00	Core structural materials (1953 through 1983)	Dissolution	1.19E-05	1/year	Stainless steel fractional corrosion rate	17% drums, 83% other
	LLW—metal	1.9	2.83E+00	2000 through 2009 activated metal	Dissolution	1.19E-05	1/year	Stainless steel fractional corrosion rate	No containment
	TRA-603-1N	1.9	2.82E+00	Resins	Surface wash	5.00E+02	mL/g	Distribution coefficient	No containment
	ANL-MOD-1H	1.9	2.81E+00	Irradiated subassembly hardware (1977 through 1983)	Dissolution	1.19E-05	1/year	Stainless steel fractional corrosion rate	9% drums, 91% other
	ANL-MOD-1R	1.8	2.55E+00	Irradiated subassembly hardware (1984 through 1993)	Dissolution	1.19E-05	1/year	Stainless steel fractional corrosion rate	No containment
	D&D-S1G-1H	1.4	2.00E+00	Decontaminated reactor vessel and processing equipment, components, and piping	Surface wash	5.00E+02	mL/g	Distribution coefficient	No containment
	TRA-603-28N	1.2	1.79E+00	Miscellaneous contaminated materials	Surface wash	5.00E+02	mL/g	Distribution coefficient	No containment
	TRA-603-9N	1.0	1.50E+00	Fuel materials (solids, not dissolved)	Dissolution	3.47E-02[d]	1/year	Nuclear fuels fractional corrosion rate	8% drums, 92% other

Table 5-2. (continued).

Contaminant	Waste Stream Code	Percentage in Waste Stream (%)	Inventory (Ci)[a]	Waste Stream Description	Release Mechanism[b]	Release Parameter Value[b]	Release Parameter Units	Parameter Description	Container Type
	Miscellaneous[c]	3.0	4.26E+00	Various waste types	—	—	—	—	—
Total Nb-94		100.0	1.46E+02						
Np-237	TRA-632-2N	24.9	3.52E-02	Hot Cell waste	Surface wash	2.30E+01	mL/g	Distribution coefficient	24% drums, 76% other
	LLW—trash	16.1	2.28E-02	2000 through 2009 miscellaneous LLW	Surface wash	2.30E+01	mL/g	Distribution coefficient	No containment
	TRA-603-28N	13.9	1.96E-02	Miscellaneous contaminated materials	Surface wash	2.30E+01	mL/g	Distribution coefficient	No containment
	TRA-603-9N	8.9	1.26E-02	Fuel materials (solids, not dissolved)	Surface wash	2.30E+01	mL/g	Distribution coefficient	8% drums, 92% other
	ANL-MOD-5H	7.9	1.12E-02	General plant waste, mostly from decontamination (1952 through 1983)	Surface wash	2.30E+01	mL/g	Distribution coefficient	6% drums, 94% other
	ANL-763-1	5.4	7.55E-03	Soil, rocks, concrete, and sludge solidified with grout from cleanup of Experimental Breeder Reactor II leach pit	Surface wash	2.30E+01	mL/g	Distribution coefficient	No containment
	ANL-MOD-4H	3.1	4.37E-03	Low or unirradiated bulk-actinide waste	Surface wash	2.30E+01	mL/g	Distribution coefficient	25% drums, 75% other
	ANL-MOD-2H	2.7	3.88E-03	Irradiated and unirradiated fuel specimens (1971 through 1983)	Surface wash	2.30E+01	mL/g	Distribution coefficient	7% drums, 93% other
	ANL-MOD-3H	2.4	3.43E-03	Irradiated and unirradiated dissolved fuel and fuel-contaminated materials (1952 through 1970)	Surface wash	2.30E+01	mL/g	Distribution coefficient	6% drums, 94% other
	ANL-MOD-2HEXT	2.3	3.23E-03	Irradiated and unirradiated fuel and fuel-contaminated materials (1984 through 1993)	Surface wash	2.30E+01	mL/g	Distribution coefficient	No containment
	INTEC-MOD-9H	1.9	2.72E-03	General plant waste (e.g., metal, glass, paper, wood, clothing, plastic, dirt, and shielding material) (1952 through 1983)	Surface wash	2.30E+01	mL/g	Distribution coefficient	2% drums, 98% other
	NRF-MOD-1H	1.9	2.66E-03	Shippingport fuel material, solid (1960 through 1968)	Surface wash	2.30E+01	mL/g	Distribution coefficient	No containment
	INTEC-MOD-5H	1.1	1.53E-03	HEPA filter from Waste Calcining Facility and other filters from miscellaneous facilities	Surface wash	2.30E+01	mL/g	Distribution coefficient	No containment
	Miscellaneous[c]	7.5	1.05E-02	Various waste types	—	—	—	—	—
Total Np-237		100.0	1.41E-01						
Pa-231	D&D-ARA-1	97.2	8.56E-04	Waste stream consists primarily of contaminated metal and debris	Surface wash	8.00E+00	mL/g	Distribution coefficient	No containment
	Miscellaneous[c]	2.8	2.46E-05	Various waste types	—	—	—	—	—
Total Pa-231			8.81E-04						
Pb-210	ALE-ALE-1H	94.2	9.10E-06	Building rubble, electric wires, piping, machinery, radioactive tracers and sources, glass, gloves, paper, filters, and vermiculite	Surface wash	2.70E+02	mL/g	Distribution coefficient	No containment
	Miscellaneous[c]	5.8	5.59E-07	Various waste types	—	—	—	—	—
Total Pb-210		100.0	5.62E-07						
Pu-238	Rocky Flats	88.7	1.85E+03	See Rocky Flats Plant plutonium, Table 5-3	Surface wash	2.50E+03	mL/g	Distribution coefficient	Mix of drums and boxes
	TRA-632-2N	3.2	6.68E+01	Hot Cell waste	Surface wash	2.50E+03	mL/g	Distribution coefficient	24% drums, 76% other
	TRA-603-28N	1.8	3.72E+01	Miscellaneous contaminated materials	Surface wash	2.50E+03	mL/g	Distribution coefficient	No containment

Table 5-2. (continued).

Contaminant	Waste Stream Code	Percentage in Waste Stream (%)	Inventory (Ci)[a]	Waste Stream Description	Release Mechanism[b]	Release Parameter Value[b]	Release Parameter Units	Parameter Description	Container Type
	INTEC-MOD-9H	1.6	3.36E+01	General plant waste (e.g., metal, glass, paper, wood, clothing, plastic, dirt, and shielding material) (1952 through 1983)	Surface wash	2.50E+03	mL/g	Distribution coefficient	2% drums, 98% other
	TRA-603-9N	1.2	2.39E+01	Fuel materials (solids, not dissolved)	Surface wash	2.50E+03	mL/g	Distribution coefficient	8% drums, 92% other
	Miscellaneous[c]	3.5	7.30E+01	Mostly debris, some fuel-contaminated waste	—	—	—	—	—
Total Pu-238		100.0	2.08E+03						
Pu-239	Rocky Flats	94.7	6.07E+04	See Rocky Flats Plant plutonium, Table 5-3	Surface wash	2.50E+03	mL/g	Distribution coefficient	Mixed drums and other containers
	Rocky Flats	3.6	2.33E+03	See Rocky Flats Plant plutonium, Table 5-3	Surface wash	0.00E+00	mL/g	Distribution coefficient	Mixed drums and other containers
	Miscellaneous[c]	1.7	1.08E+03	Mostly fuel-contaminated waste	—	—	—	—	—
Total Pu-239		100.0	6.41E+04						
Pu-240	Rocky Flats	93.0	1.35E+04	See Rocky Flats Plant plutonium, Table 5-3	Surface wash	2.50E+03	mL/g	Distribution coefficient	Mixed drums and other containers
	Rocky Flats	3.6	5.20E+02	See Rocky Flats Plant plutonium, Table 5-3	Surface wash	0.00E+00	mL/g	Distribution coefficient	Mixed drums and other containers
	OFF-LRL-2H	3.1	4.49E+02	Concrete, bricks, and asphalt	Surface wash	2.50E+03	mL/g	Distribution coefficient	Drums
	Miscellaneous[c]	0.3	5.39E+01	Various waste types	—	—	—	—	—
Total Pu-240		100.0	1.46E+04						
Ra-226	OFF-USN-1H	66.4	4.33E+01	Animal carcasses, waste paper towels, glassware, tools, and similar laboratory items	Surface wash	5.75E+02	mL/g	Distribution coefficient	12% drums, 88% other
	OFF-ISC-1H	15.3	1.00E+01	Magnesium-thorium scrap, laboratory equipment, and sources	Surface wash	5.76E+02	mL/g	Distribution coefficient	75% drums, 25% other
	OFF-AEF-1H	10.2	6.67E+00	Scrap metal, combustibles, glass, and concrete	Surface wash	5.75E+02	mL/g	Distribution coefficient	91% drums, 9% other
	OFF-DPG-1H	5.1	3.33E+00	Animal and laboratory waste	Surface wash	5.75E+02	mL/g	Distribution coefficient	92% drums, 8% other
	OFF-HEW-1H	1.5	1.00E+00	Radium-contaminated laboratory waste	Surface wash	5.75E+02	mL/g	Distribution coefficient	Drums
	Miscellaneous[c]	1.5	9.50E-01	Various waste types	—	—	—	—	—
Total Ra-226		100.0	6.53E+01						
Ra-228	Projected	70.3	2.57E-05	Projected waste	Surface wash	5.75E+02	mL/g	Distribution coefficient	No containment
	WER-CMP-1	29.3	1.07E-05	Compacted waste a combination of glass, plastic, absorbents, cloth, paper, and wood	Surface wash	5.75E+02	mL/g	Distribution coefficient	No containment
	Miscellaneous[c]	0.4	1.55E-07	Various waste types	—	—	—	—	—
Total Ra-228		100.0	3.66E-05						
Sr-90	INTEC-MOD-2H	31.3	4.26E+04	Leached Vycor glass	Dissolution	1.30E-05	1/year	Vycor glass fractional corrosion rate	No containment
	TRA-632-2N	12.7	1.73E+04	Hot Cell waste	Surface wash	6.00E+01	mL/g	Distribution coefficient	24% drums, 76% other

Table 5-2. (continued).

Contaminant	Waste Stream Code	Percentage in Waste Stream (%)	Inventory (Ci)[a]	Waste Stream Description	Release Mechanism[b]	Release Parameter Value[b]	Release Parameter Units	Parameter Description	Container Type
	ANL-MOD-5H	7.4	1.01E+04	General plant waste, mostly from decontamination (1952 through 1983)	Surface wash	6.00E+01	mL/g	Distribution coefficient	6% drums, 94% other
	TRA-603-28N	7.1	9.62E+03	Miscellaneous contaminated materials	Surface wash	6.00E+01	mL/g	Distribution coefficient	No containment
	INTEC-MOD-9H	5.9	8.00E+03	General plant waste (e.g., metal, glass, paper, wood, clothing, plastic, dirt, and shielding material) (1952 through 1983)	Surface wash	6.00E+01	mL/g	Distribution coefficient	2% drums, 98% other
	NRF-MOD-1H	4.6	6.24E+03	Shippingport fuel material, solid (1960 through 1968)	Dissolution	3.47E-02[d]	1/year	Nuclear fuels fractional corrosion rate	No containment
	TRA-603-9N	4.5	6.18E+03	Fuel materials (solid, not dissolved)	Dissolution	3.47E-02[d]	1/year	Nuclear fuels fractional corrosion rate	8% drums, 92% other
	INTEC-MOD-5H	3.3	4.51E+03	HEPA filter from Waste Calcining Facility and other filters from miscellaneous facilities	Surface wash	6.00E+01	mL/g	Distribution coefficient	No containment
	INTEC-MOD-6H	3.1	4.24E+03	CPP-603 resins (i.e., basin sludge and miscellaneous storage basin Zeolite filters)	Surface wash	6.00E+01	mL/g	Distribution coefficient	No containment
	ANL-MOD-2H	2.6	3.48E+03	Irradiated and unirradiated fuel specimens (1971 through 1983)	Dissolution	3.47E-02[d]	1/year	Nuclear fuels fractional corrosion rate	7% drums, 93% other
	ANL-MOD-3H	2.3	3.08E+03	Irradiated and unirradiated dissolved fuel and fuel-contaminated materials (1952 through 1970)	Surface wash	6.00E+01	mL/g	Distribution coefficient	6% drums, 94% other
	ANL-MOD-2HEXT	2.1	2.90E+03	Irradiated and unirradiated dissolved fuel and fuel-contaminated materials (1984 through 1993)	Surface wash	6.00E+01	mL/g	Distribution coefficient	No containment
	INTEC-MOD-7H	2.0	2.78E+03	Contaminated soil from Tank Farm spills	Surface wash	6.00E+01	mL/g	Distribution coefficient	No containment
	ARA-616-1H	1.6	2.16E+03	Scrap metal, resin, burnable materials, sludge, and some boric acid crystals from Mobile Low-Power Reactor No. 1 and Gas-Cooled Reactor Experiment	Surface wash	6.00E+01	mL/g	Distribution coefficient	1% drums, 99% other
	TAN-607-6RN	1.2	1.65E+03	Metal alloys, end boxes, combustible material, fuel assembly shrouds, concrete, resin, sludge, and equipment from Hot Shop and Hot Cells (1984 through 1993)	Surface wash	6.00E+01	mL/g	Distribution coefficient	3% drums, 97% other
	ARA-602-3H	1.2	1.60E+03	Hot Cell waste consisting of some fuel residue	Surface wash	6.00E+01	mL/g	Distribution coefficient	1% drums, 99% other
	ARA-602-1H	1.0	1.38E+03	Miscellaneous debris from Stationary Low-Power Reactor No. 1 cleanup (e.g., 1,000-gal tank, demineralizer with resin, building materials, pipes, soil, wire, concrete, and insulation)	Surface wash	6.00E+01	mL/g	Distribution coefficient	No containment
	Miscellaneous[c]	6.1	8.55E+03	Mostly debris waste	—	—	—	—	—
Total Sr-90		100.0	1.36E+05						
Tc-99	ANL-MOD-1H	16.3	6.88E+00	Irradiated subassembly hardware (1977 through 1983)	Dissolution	1.19E-05	1/year	Stainless steel fractional corrosion rate	9% drums, 91% other
	INTEC-MOD-2H	15.8	6.67E+00	Leached Vycor glass	Dissolution	1.30E-05	1/year	Vycor glass fractional corrosion rate	No containment
	ANL-MOD-1R	14.8	6.24E+00	Irradiated subassembly hardware (1984 through 1993)	Dissolution	1.19E-05	1/year	Stainless steel fractional corrosion rate	No containment
	TRA-603-1N	8.0	3.37E+00	Resins	Surface wash	1.90E+01	mL/g	Resins distribution coefficient	No containment

Table 5-2. (continued).

Contaminant	Waste Stream Code	Percentage in Waste Stream (%)	Inventory (Ci)[a]	Waste Stream Description	Release Mechanism[b]	Release Parameter Value[b]	Release Parameter Units	Parameter Description	Container Type
	TRA-632-2N	6.2	2.60E+00	Hot Cell waste	Surface wash	0.00E+00	mL/g	Distribution coefficient	24% drums, 76% other
	LLW—resins	4.8	2.05E+00	2000 through 2009 resins	Surface wash	1.90E+01	mL/g	Resins distribution coefficient	No containment
	ANL-MOD-5H	4.0	1.70E+00	General plant waste, mostly from decontamination (1952 through 1983)	Surface wash	0.00E+00	mL/g	Distribution coefficient	6% drums, 94% other
	INTEC-MOD-9H	3.8	1.60E+00	General plant waste (e.g., metal, glass, paper, wood, clothing, plastic, dirt, and shielding material) (1952 through 1983)	Surface wash	0.00E+00	mL/g	Distribution coefficient	2% drums, 98% other
	NRF-MOD-1H	3.5	1.49E+00	Shippingport fuel material, solid (1960 through 1968)	Dissolution	3.47E-02[d]	1/year	Nuclear fuels fractional corrosion rate	No containment
	TRA-603-28N	3.4	1.45E+00	Miscellaneous contaminated materials	Surface wash	0.00E+00	mL/g	Distribution coefficient	No containment
	NRF-MOD-10H	2.8	1.19E+00	Compactable and noncompactable waste from Expended Core Facility and prototype plant operations (1952 through 1983)	Surface wash	0.00E+00	mL/g	Distribution coefficient	7% drums, 93% other
	TRA-603-9N	2.2	9.30E-01	Fuel materials (solids, not dissolved)	Dissolution	3.47E-02[d]	1/year	Nuclear fuels fractional corrosion rate	8% drums, 92% other
	INTEC-MOD-5H	2.1	8.84E-01	HEPA filter from Waste Calcining Facility and other filters from miscellaneous facilities	Surface wash	0.00E+00	mL/g	Distribution coefficient	No containment
	INTEC-MOD-6H	1.9	8.20E-01	CPP-603 resins (i.e., basin sludge and miscellaneous storage basin Zeolite filters)	Surface wash	1.90E+01	mL/g	Resins distribution coefficient	No containment
	D&D-ARA-1	1.5	6.42E-01	Contaminated metal and debris from decontamination and demolition of Auxiliary Reactor Area facilities	Surface wash	0.00E+00	mL/g	Distribution coefficient	No containment
	ANL-MOD-2H	1.4	5.89E-01	Irradiated and unirradiated fuel specimens (1971 through 1983)	Dissolution	3.47E-02[d]	1/year	Nuclear fuels fractional corrosion rate	7% drums, 93% other
	INTEC-MOD-7H	1.3	5.51E-01	Contaminated soil from Tank Farm spills	Surface wash	0.00E+00	mL/g	Distribution coefficient	No containment
	ANL-MOD-3H	1.2	5.20E-01	Irradiated and unirradiated dissolved fuel and fuel-contaminated materials (1952 through 1970)	Surface wash	0.00E+00	mL/g	Distribution coefficient	6% drums, 94% other
	ANL-MOD-2HEXT	1.2	4.90E-01	Irradiated and unirradiated dissolved fuel and fuel-contaminated materials (1984 through 1993)	Surface wash	0.00E+00	mL/g	Distribution coefficient	No containment
	Miscellaneous[c]	3.8	1.59E+00	Various waste types	—	—	—	—	—
Total Tc-99		100.0	4.23E+01						
Th-228	ALE-317-2R	78.3	8.20E+00	Cloth, paper, wood, plastic, cut-up scrap, cut-up glove boxes, and other general plant waste	Surface wash	—	mL/g	Distribution coefficient	No containment
	CEG-CEG-1R	19.1	2.00E+00	Powder solidified in Aquaset	Surface wash	—	mL/g	Distribution coefficient	No containment
	INTEC-MOD-9H	1.3	1.30E-01	General plant waste (e.g., metal, glass, paper, wood, clothing, plastic, dirt, and shielding material) (1952 through 1983)	Surface wash	—	mL/g	Distribution coefficient	2% drums, 98% other
	Miscellaneous[c]	1.3	1.30E-01	Various waste types	Surface wash	—	mL/g	Distribution coefficient	—
Total Th-228		100.0	1.05E+01						

Table 5-2. (continued).

Contaminant	Waste Stream Code	Percentage in Waste Stream (%)	Inventory (Ci)[a]	Waste Stream Description	Release Mechanism[b]	Release Parameter Value[b]	Release Parameter Units	Parameter Description	Container Type
U-232	TRA-603-9N	79.0	8.36E+00	Fuel materials	Surface wash	—	mL/g	Distribution coefficient	8% drums, 92% other
	ALE-317-2R	20.9	2.21E+00	Cloth, paper, wood, plastic, cut-up scrap, cut-up glove boxes, and other general plant waste	Surface wash	—	mL/g	Distribution coefficient	No containment
	Miscellaneous[c]	0.1	1.73E-02	Various waste types	Surface wash	—	mL/g	Distribution coefficient	—
Total U-232		100.0	1.06E+01						
U-233	TRA-603-9N	28.4	6.01E-01	Fuel materials	Surface wash	1.54E+01	mL/g	Distribution coefficient	8% drums, 92% other
	ARA-626-1H	28.4	6.00E-01	Some fuel scraps and waste from disassembly of facilities and Hot Cell waste	Surface wash	1.54E+01	mL/g	Distribution coefficient	2% drums, 98% other
	RFO-DOW-19H	25.5	5.40E-01	U-233	Surface wash	1.54E+01	mL/g	Distribution coefficient	Drums
	SMC-628-2	14.2	3.01E-01	Unsolidified slag	Surface wash	1.54E+01	mL/g	Distribution coefficient	11% drums, 89% other
	SMC-990-1	1.3	2.74E-02	Metals, glass, and gravel contaminated with depleted uranium	Surface wash	1.54E+01	mL/g	Distribution coefficient	66% drums, 34% other
	SMC-628-1	1.1	2.21E-02	Nonacidic evaporator sludge	Surface wash	1.54E+01	mL/g	Distribution coefficient	46% drums, 54% other
	Miscellaneous[c]	1.1	2.43E-02	Various waste types	—	—	—	—	—
Total U-233		100.0	2.12E+00						
U-234	RFO-DOW-18H	33.7	2.15E+01	Enriched uranium	Surface wash	1.54E+01	mL/g	Distribution coefficient	Drums and boxes
	RFO-DOW-16H	22.7	1.45E+01	Depleted uranium	Surface wash	1.54E+01	mL/g	Distribution coefficient	Drums
	PDA-RFO-1A	7.3	4.64E+00	Evaporator salt (nitrate) and roaster oxides (depleted uranium)	Surface wash	1.54E+01	mL/g	Distribution coefficient	Drums
	OFF-ATI-1H	5.7	3.64E+00	Irradiated fuel and chemical byproducts from nuclear research	Surface wash	1.54E+01	mL/g	Distribution coefficient	36% drums, 64% other
	OFF-GEC-1H	4.6	2.95E+00	Core, reactor vessel, and loop components	Surface wash	1.54E+01	mL/g	Distribution coefficient	No containment
	TAN-607-3N	3.6	2.33E+00	Activated core, loop components, end boxes, and stainless steel from SL-1 reactor	Surface wash	1.54E+01	mL/g	Distribution coefficient	No containment
	TAN-607-2	2.9	1.83E+00	Test Area North Hot Shop noncompactable waste	Surface wash	1.54E+01	mL/g	Distribution coefficient	No containment
	INTEC-MOD-6H	2.4	1.56E+00	CPP-603 resins (i.e., basin sludge and miscellaneous storage basin Zeolite filters)	Surface wash	1.54E+01	mL/g	Distribution coefficient	No containment
	OFF-CSM-1H	2.0	1.30E+00	Magnesium fluoride slag with 1% natural uranium, steel metallic salt and silicate, and miscellaneous laboratory waste	Surface wash	1.54E+01	mL/g	Distribution coefficient	Drums
	ANL-MOD-2R	1.5	9.47E-01	Bulk actinide waste from the Zero Power Plutonium Reactor and other facilities	Surface wash	1.54E+01	mL/g	Distribution coefficient	No containment
	ANL-MOD-5H	1.3	8.41E-01	General plant waste, mostly from decontamination (1952 through 1983)	Surface wash	1.54E+01	mL/g	Distribution coefficient	6% drums, 94% other
	ANL-MOD-4H	1.2	7.48E-01	Low or unirradiated bulk-actinide waste	Surface wash	1.54E+01	mL/g	Distribution coefficient	25% drums, 75% other

Table 5-2. (continued).

Contaminant	Waste Stream Code	Percentage in Waste Stream (%)	Inventory (Ci)[a]	Waste Stream Description	Release Mechanism[b]	Release Parameter Value[b]	Release Parameter Units	Parameter Description	Container Type
	ALE-317-2R	1.1	7.10E-01	Cloth, paper, wood, plastic, cut-up scrap, cut-up glove boxes, and other general plant waste	Surface wash	1.54E+01	mL/g	Distribution coefficient	No containment
	ARA-627-1H	1.0	6.38E-01	Plastic bags, brick, HEPA filters, scrap, glove boxes, and fuel	Surface wash	1.54E+01	mL/g	Distribution coefficient	No containment
	Miscellaneous[c]	9.0	5.73E+00	Mostly scrap metal	—	—	—	—	—
Total U-234		100.0	6.39E+01						
U-235	RFO-DOW-16H	22.0	1.08E+00	Depleted uranium	Surface wash	1.54E+01	mL/g	Distribution coefficient	Drums
	INTEC-MOD-3H	19.3	9.47E-01	Unirradiated and irradiated fuel specimens from natural and depleted fuel mockups	Surface wash	1.54E+01	mL/g	Distribution coefficient	2% drums, 98% other
	RFO-DOW-18H	15.1	7.44E-01	Enriched uranium	Surface wash	1.54E+01	mL/g	Distribution coefficient	Drums and boxes
	TRA-603-9N	9.9	4.86E-01	Fuel materials (solids, not dissolved)	Surface wash	1.54E+01	mL/g	Distribution coefficient	8% drums, 92% other
	PDA-RFO-1A	6.6	3.25E-01	Evaporator salt (nitrate) and roaster oxides (depleted uranium)	Surface wash	1.54E+01	mL/g	Distribution coefficient	Drums
	WAG-WG7-02	3.7	1.80E-01	Acid Pit in situ stabilization treatability study	Surface wash	1.54E+01	mL/g	Distribution coefficient	No containment
	OFF-GEC-1H	3.2	1.57E-01	Core, reactor vessel, and loop components	Surface wash	1.54E+01	mL/g	Distribution coefficient	No containment
	OFF-ATI-1H	2.3	1.14E-01	Irradiated fuel and chemical byproducts from nuclear research	Surface wash	1.54E+01	mL/g	Distribution coefficient	36% drums, 64% other
	TAN-607-3N	1.6	8.00E-02	Activated core, loop components, end boxes, and stainless steel from SL-1 reactor.	Surface wash	1.54E+01	mL/g	Distribution coefficient	No containment
	OFF-CSM-1H	1.6	8.00E-02	Magnesium fluoride slag with 1% natural uranium, steel metallic salt and silicate, and miscellaneous laboratory waste	Surface wash	1.54E+01	mL/g	Distribution coefficient	Drums
	OFF-GDA-1H	1.4	7.00E-02	Fuel fabrication items, laboratory equipment, activated metal, and irradiated fuel	Surface wash	1.54E+01	mL/g	Distribution coefficient	48% drums, 52% other
	INTEC-MOD-6H	1.1	5.38E-02	CPP-603 resins (i.e., basin sludge and miscellaneous storage basin Zeolite filters)	Surface wash	1.54E+01	mL/g	Distribution coefficient	No containment
	Miscellaneous[c]	12.2	5.98E-01	Mostly fuel-contaminated waste	—	—	—	—	—
Total U-235		100.0	4.92E+00						
U-236	RFO-DOW-16H	62.4	9.03E-01	Depleted uranium	Surface wash	1.54E+01	mL/g	Distribution coefficient	Drums
	TRA-632-2N	6.3	9.07E-02	Hot Cell waste	Surface wash	1.54E+01	mL/g	Distribution coefficient	24% drums, 76% other
	RFO-DOW-18H	5.6	8.04E-02	Enriched uranium	Surface wash	1.54E+01	mL/g	Distribution coefficient	Drums and boxes
	INTEC-MOD-3H	4.1	6.00E-02	Unirradiated and irradiated fuel specimens from natural and depleted fuel mockups	Surface wash	1.54E+01	mL/g	Distribution coefficient	2% drums, 98% other
	ANL-MOD-5H	3.7	5.42E-02	General plant waste, mostly from decontamination (1952 through 1983)	Surface wash	1.54E+01	mL/g	Distribution coefficient	6% drums, 94% other
	TRA-603-28N	3.5	5.05E-02	Miscellaneous contaminated materials	Surface wash	1.54E+01	mL/g	Distribution coefficient	No containment
	SMC-628-2	3.0	4.37E-02	Unsolidified slag	Surface wash	1.54E+01	mL/g	Distribution coefficient	11% drums, 89% other
	TRA-603-9N	2.3	3.28E-02	Fuel materials (solids, not dissolved)	Surface wash	1.54E+01	mL/g	Distribution coefficient	8% drums, 92% other

Table 5-2. (continued).

Contaminant	Waste Stream Code	Percentage in Waste Stream (%)	Inventory (Ci)[a]	Waste Stream Description	Release Mechanism[b]	Release Parameter Value[b]	Release Parameter Units	Parameter Description	Container Type
	ANL-MOD-2H	1.3	1.87E-02	Irradiated and unirradiated fuel specimens (1971 through 1983)	Surface wash	1.54E+01	mL/g	Distribution coefficient	7% drums, 93% other
	LLW—trash	1.2	1.75E-02	2000 through 2009 miscellaneous LLW	Surface wash	1.54E+01	mL/g	Distribution coefficient	No containment
	ANL-MOD-3H	1.1	1.66E-02	Irradiated and unirradiated dissolved fuel and fuel-contaminated materials (1952 through 1970)	Surface wash	1.54E+01	mL/g	Distribution coefficient	6% drums, 94% other
	ANL-MOD-2HEXT	1.1	1.56E-02	Irradiated and unirradiated dissolved fuel and fuel-contaminated materials (1984 through 1993)	Surface wash	1.54E+01	mL/g	Distribution coefficient	No containment
	Miscellaneous[c]	4.4	6.43E-02	Mostly fuel-contaminated waste	—	—	—	—	—
Total U-236		100.0	1.45E+00						
U-238	RFO-DOW-16H	51.3	7.62E+01	Depleted uranium (roaster oxide)	Surface wash	1.54E+01	mL/g	Distribution coefficient	Drums
	RFO-DOW-3H	18.8	2.79E+01	Uncemented sludge	Surface wash	1.54E+01	mL/g	Distribution coefficient	Drums
	PDA-RFO-1A	16.8	2.49E+01	Evaporator salt (nitrate) and roaster oxides (depleted uranium) on Pad A	Surface wash	1.54E+01	mL/g	Distribution coefficient	Drums
	LLW—trash	5.0	7.39E+00	2000 through 2009 miscellaneous LLW	Surface wash	1.54E+01	mL/g	Distribution coefficient	No containment
	SMC-628-2	1.5	2.31E+00	Unsolidified slag	Surface wash	1.54E+01	mL/g	Distribution coefficient	11% drums, 89% other
	ARA-627-1H	1.1	1.64E+00	Plastic bags, brick, HEPA filters, scrap, glove boxes, and fuel	Surface wash	1.54E+01	mL/g	Distribution coefficient	No containment
	Miscellaneous[c]	5.5	8.14E+00	Mostly debris, some fuel-contaminated waste, and ingrowth from Rocky Flats Plant Pu-242	—	—	—	—	—
Total U-238		100.0	1.48E+02						

a. Estimates have not been adjusted for inventory removed by the Accelerated Retrieval Project.
b. See Section 4.4 of Anderson and Becker (2006).
c. Miscellaneous indicates numerous waste streams that contribute less than 1% to the total. They are combined for the table, but are explicitly included with the appropriate release mechanism in the release simulations.
d. The annual fractional release rate (1/year) determines the corrosion or dissolution rate. A value of 3.47E-02 1/year originally was calculated as an upper bound for fuel-like materials. However, the reference supporting these calculations is no longer available. Using an available reference, a new value was calculated at 3.15E-02 1/year. Because the original value was considered credible and is still more conservative than the new value, it was used in the modeling.

HEPA = high-efficiency particulate air
LLW = low-level waste

Table 5-3. Rocky Flats Plant plutonium-238, -239, and -240 waste streams, best-estimate inventories (curies) at time of disposal, and baseline source-release information for Operable Unit 7-13/14 modeling.

Contaminant	Waste Type	Portion in Waste Stream (%)	Inventory (Ci)[a]	Waste Stream Description	Release Mechanism[b]	Release Parameter Value[b]	Release Parameter Units	Parameter Description
Pu-238	Graphite	27.8	5.13E+02	Molds, crucibles, and scarfings	Surface wash	2.50E+03	mL/g	Distribution coefficient
	Type III	19.8	3.65E+02	Filters	Surface wash	2.50E+03	mL/g	Distribution coefficient
	Type I and V	18.6	3.43E+02	Debris	Surface wash	2.50E+03	mL/g	Distribution coefficient
	Line-generated waste	15.5	2.86E+02	Line-generated waste (e.g., gloves and glove boxes)	Surface wash	2.50E+03	mL/g	Distribution coefficient
	Series 741	12.3	2.28E+02	Series 741 and 742 sludge (e.g., inorganic first- and second-stage sludge)	Surface wash	2.50E+03	mL/g	Distribution coefficient
	Type I	5.4	1.00E+02	Combustible materials (e.g., paper, rags, plastic, clothing, wood, and polyethylene bottles)	Surface wash	2.50E+03	mL/g	Distribution coefficient
	Series 744	0.3	5.61E+00	Series 744 sludge (special setups)	Surface wash	2.50E+03	mL/g	Distribution coefficient
	Series 743	0.3	4.85E+00	Series 743 sludge (organic)	Surface wash	2.50E+03	mL/g	Distribution coefficient
	Series 745	0.0	1.79E-01	Series 745 nitrate salt	Surface wash	2.50E+03	mL/g	Distribution coefficient
Total Rocky Flats Plant Pu-238		100.0	1.85E+03					
Pu-239	Graphite	26.5	1.67E+04	Molds, crucibles, and scarfings	Subdivided into two fractions (see below)			
	Type III	18.8	1.19E+04	Filters				
	Type I and V	17.7	1.12E+04	Debris				
	Line-generated waste	14.8	9.31E+03	Line-generated waste (e.g., gloves and glove boxes)				
	Series 741	11.8	7.42E+03	Series 741 and 742 sludge (e.g., inorganic first- and second-stage sludge)				
	Type I	5.2	3.26E+03	Combustible materials (e.g., paper, rags, plastic, clothing, wood, and polyethylene bottles)				
	Type II	4.7	2.93E+03	Glass				
	Series 744	0.3	1.83E+02	Series 744 sludge (special setups)				
	Series 743	0.2	1.58E+02	Series 743 sludge (organic)				
	Series 745	0.0	5.82E+00	Series 745 nitrate salt				
Total Rocky Flats Plant Pu-239		100.0	6.30E+04					
	Fraction 0.037		2.33E+03	Simulated mobile fraction	Surface wash	0.00E+00	mL/g	Distribution coefficient
	Fraction 0.963		6.07E+04	Sorbing fraction	Surface wash	2.50E+03	mL/g	Distribution coefficient

Table 5-3. (continued).

Contaminant	Waste Type	Portion in Waste Stream (%)	Inventory (Ci)[a]	Waste Stream Description	Release Mechanism[b]	Release Parameter Value[b]	Release Parameter Units	Parameter Description
Pu-240	Graphite	26.4	3.72E+03	Molds, crucibles, and scarfings	Subdivided into two fractions (see below)			
	Type III	18.8	2.64E+03	Filters				
	Type I and V	17.7	2.50E+03	Debris				
	Line-generated waste	14.8	2.09E+03	Line-generated waste (e.g., gloves and glove boxes)				
	Series 741	11.8	1.66E+03	Series 741 and 742 sludge (e.g., inorganic first- and second-stage sludge)				
	Type I	5.2	7.29E+02	Combustible materials (e.g., paper, rags, plastic, clothing, wood, and polyethylene bottles)				
	Type II	4.7	6.57E+02	Glass				
	Series 744	0.3	4.09E+01	Series 744 sludge (special setups)				
	Series 743	0.3	3.54E+01	Series 743 sludge (organic)				
	Series 745	0.0	3.57E-01	Series 745 nitrate salt				
Total Rocky Flats Plant Pu-240		100.0	1.41E+04					
	Fraction 0.037		5.20E+02	Simulated mobile fraction	Surface wash	0.00E+00	mL/g	Distribution coefficient
	Fraction 0.963		1.35E+04	Sorbing fraction	Surface wash	2.50E+03	mL/g	Distribution coefficient

a. Estimates have not been adjusted for inventory removed by the Accelerated Retrieval Project.
b. See Section 4.4 of Anderson and Becker (2006)

Table 5-4. Nitrate and chromium waste streams, best-estimate inventories (grams) at time of disposal, and baseline source-release information for Operable Unit 7-13/14 modeling.

Contaminant	Waste Stream Code	Portion in Waste Stream (%)	Inventory (g)	Waste Stream Description	Release Mechanism	Release Parameter Value	Release Parameter Units	Parameter Description	Container Type
Nitrate (as nitrogen)	PDA-RFO-1A	51.6	2.35E+08	Evaporator salts	Surface wash	0.00E+00	mL/g	Distribution coefficient	54.8% drums, 45.2% boxes
	RFO-DOW-17H	37.5	1.71E+08	Evaporator salts	Surface wash	0.00E+00	mL/g	Distribution coefficient	Drums
	CPP-601-4H	10.8	4.95E+07	Aqueous chemicals	Surface wash	0.00E+00	mL/g	Distribution coefficient	No container
	Miscellaneous	0.1	2.57E+05	—	—	—	—	—	—
Total nitrate (as nitrogen)		100.0	4.56E+08						
Chromium	PDA-RFO-1A	78.6	1.82E+06	Evaporator salts	Surface wash	1.00E-01	mL/g	Distribution coefficient	54.8% drums, 45.2% boxes
	RFO-DOW-17H	21.4	4.96E+05	Evaporator salts	Surface wash	1.00E-01	mL/g	Distribution coefficient	Drums
	Miscellaneous	0.0	1.05E+03	—	—	—	—	—	—
Total chromium		100.0	2.32E+06						

Table 5-5. Volatile organic compound waste streams, best-estimate inventories (grams) at time of disposal, and baseline source-release information for Operable Unit 7-13/14 modeling.

Contaminant	Waste Stream Code	Portion in Waste Stream (%)	Inventory (g)[a]	Waste Stream Description	Release Mechanism[b]	Release Parameter Value[b]	Release Parameter Units	Parameter Description	Container Type
Carbon tetrachloride	RFO-DOW-15H	99.5	7.86E+08	Series 743 sludge (organic)	Diffusion	2.50E-06	cm^2/second	Diffusion rate	Drums
	Miscellaneous	0.5	3.66E+06	Mostly other Rocky Flats Plant waste	Diffusion	2.50E-06	cm^2/second	Diffusion rate	Mix of drums and boxes
Total carbon tetrachloride		100.0	7.90E+08						
1,4-Dioxane	RFO-DOW-15H	88.2	1.72E+06	Series 743 sludge (organic)	Diffusion	2.50E-06	cm^2/second	Diffusion rate	Drums
	RFO-DOW-4H	7.8	1.52E+05	Equipment (e.g., drill presses, lathes, and pumps)	Diffusion	2.50E-06	cm^2/second	Diffusion rate	70% drums, 30% wooden boxes
	CPP-603-4H	1.9	3.62E+04	Rags	Diffusion	2.50E-06	cm^2/second	Diffusion rate	Fiber boxes
	Miscellaneous	2.1	4.24E+04	Mostly combustible waste	Diffusion	2.50E-06	cm^2/second	Diffusion rate	No containers
Total 1,4-dioxane		100.0	1.95E+06						
Methylene chloride	RFO-DOW-3H	51.2	7.21E+06	Uncemented sludge	Diffusion	2.50E-06	cm^2/second	Diffusion rate	99.8% drums, 0.2% wooden boxes
	RFO-DOW-4H	20.3	2.85E+06	Equipment (e.g., drill presses, lathes, and pumps)	Diffusion	2.50E-06	cm^2/second	Diffusion rate	70% drums, 30% wooden boxes
	RFO-DOW-9H	18.3	2.58E+06	Paper, rags, and plastic	Diffusion	2.50E-06	cm^2/second	Diffusion rate	55% drums, 45% wooden boxes
	RFO-DOW-12H	9.3	1.31E+06	Dirt, sand, concrete, ashes, and soot	Diffusion	2.50E-06	cm^2/second	Diffusion rate	81% drums, 19% wooden boxes
	RFO-DOW-6H	0.9	1.36E+05	Filters	Diffusion	2.50E-06	cm^2/second	Diffusion rate	Wooden or cardboard boxes
Total methylene chloride		100.0	1.41E+07						
Tetrachloroethylene	RFO-DOW-15H	100.0	9.87E+07	Series 743 sludge (organic)	Diffusion	2.00E-06	cm^2/second	Diffusion rate	Drums
Total tetrachloroethylene		100.0	9.87E+07						
Trichloroethylene	RFO-DOW-15H	99.6	8.92E+07	Series 743 sludge (organic)	Diffusion	2.00E-06	cm^2/second	Diffusion rate	Drums
	Miscellaneous	0.4	4.07E+05	Power Burst Facility waste streams	Diffusion	2.00E-06	cm^2/second	Diffusion rate	No containers
Total trichloroethylene		100.0	8.96E+07						

a. Estimates were not adjusted for inventory removed by the Accelerated Retrieval Project.
b. See Section 4.4 of Anderson and Becker (2006).

Table 5-6. Factors used to convert disposal quantity (grams) to amount of contaminant in the total waste stream to nitrate as total nitrogen.

Contaminant	Conversion Factor
Aluminum nitrate nonahydrate	0.20
Copper nitrate	0.15
Mercury nitrate monohydrate	0.09
Nitric acid	0.22
Potassium nitrate	0.14
Sodium nitrate	0.16
Uranyl nitrate	0.07
Sodium dichromate	0.40
Potassium dichromate	0.35

Inventories for one contaminant of potential concern (i.e., nitrate) could not be extracted directly from the Waste Information and Location Database because many compounds contain nitrogen. Table 5-6 lists conversion factors used to estimate disposal inventories for nitrate (listed as total nitrogen). Conversion factors were taken directly from the MERCK Index (Merck 1989) or developed from the chemical formula and atomic weights of the constituent chemicals. Nitrogen-bearing inventories were multiplied by conversion factors in Table 5-6 to determine the amount of nitrate as total nitrogen buried in the SDA.

5.1.2 Container Failure Rates

Distributions were developed to represent failure rates as a function of time for different types of containers (e.g., drums, concrete casks, and metal boxes) (Becker et al. 1996; Becker 1997) and were implemented in the source-term model. Multiple failure rates were assigned to contaminants buried in more than one type of container. For example, if the annual disposal inventory for a particular contaminant included disposals in both drums and cardboard boxes, the relative fraction for each container type was used to model the disposal for that year. For waste streams not buried in containers or cardboard or wooden boxes, container failure time in the model was set at zero.

The majority of containers buried in the SDA were 55-gal metal drums. Historical disposal practices included periods when drums were stacked carefully in the SDA and periods when drums were dumped in the SDA (see Section 3.1). Drums stacked in the SDA provide a barrier to contaminant release until the metal corrodes. Therefore, stacked drums fail at a slower rate compared to drums that were dumped into the pits with no attempt at maintaining structural integrity. A separate study to determine the failure rate of metal drums in the SDA used data gathered during earlier waste-retrieval efforts (Becker 1997). Failure-rate distributions were developed to represent stacked and dumped drums. For stacked drums, a normal distribution was developed with a mean failure time of 31.4 years from the time of disposal and a standard deviation of 14.6 years. Data for dumped drums indicated that 28.5% fail at disposal and that the remaining 71.5% fail in a normal distribution, with a mean failure time of 11.7 years from time of disposal and a standard deviation of 5 years. The fraction of a contaminant in drums was modeled with the distributed failure appropriate for the type of drum disposal (i.e., whether the drums were stacked or dumped).

Assumptions about container failure have changed over time. Becker (1997) made a conservative assumption for container failure to maximize the amount of contaminants released. Nuclear logging of the Type A probes and vapor flux data indicates that a substantial source remains in the waste. Sondrup et al. (2004) attempted to quantify the amount of mass remaining in the source and recommended that 50% of the mass buried be used as the best estimate of the mass remaining in the source at the current time. Visual observations of retrievals from the Operable Unit 7-10 Glovebox Excavator Method Project indicated a substantial amount of organic sludge mass in the waste; this provided partial corroboration for the 50%-remaining estimate. Because diffusion from sludge has been studied in laboratory testing and is well characterized, the drum failure rate used for VOCs was modified to reflect retention of more mass in the drums. Thus, failure parameters used to model drum failure for VOCs is a mean time to failure of 45 years with a standard deviation of 22.5 years. Visual observations in the Operable Unit 7-10 Glovebox Excavator Method Project retrieval indicated that, while many of the drums had corroded, the polyethylene bags within the drums appeared to be intact and provided a barrier to VOC release. The drum failure rate used might be more indicative of an effective rate-of-failure for containers with polyethylene bags. Because no data are available to support the less conservative container failure rate for contaminants other than VOCs, the more conservative failure rate given above was used for other contaminants.

The rate of corrosion for carbon steel was used to determine failure time of metal boxes and canisters. Boxes and canisters were considered to fail when one-half of the wall thickness had corroded.

Each waste stream was evaluated for the type of container used. Many of these containers were wood or other readily degradable boxes, and no delay of contaminant release was assumed for these boxes in the model. Polyethylene bags were not accounted for in container failure modeling. Fifty-five-gal drums, concrete casks, and metal boxes offer barriers to contaminant release; these barriers were accounted for in the source-term model. Waste streams listed as “O” (i.e., other) in the Contaminant Inventory Database for Risk Assessment, or as a combination of container types without a fractional distribution for each type, were modeled as having no container.

5.1.3 Release Mechanisms and Release Rates

The DUST-MS code is a one-dimensional model that has three contaminant-release mechanisms: surface washoff, diffusion, and dissolution. These release mechanisms are modeled as follows:

- Surface-washoff model—estimates release from general laboratory trash and is equivalent to the first-order leach model used in other codes (e.g., GWSCREEN) (Rood 1999)
- Diffusion model—computes diffusional release from different waste geometries (e.g., VOCs from sludge and cement-encased waste) by applying diffusion coefficients for each waste form
- Dissolution-release model—estimates release caused by general corrosion (e.g., release of activated metal) from corrosion of the base metal.

The annual amount of each contaminant was apportioned among the three DUST-MS release mechanisms, based on waste form. The percent of a contaminant in a release mechanism was entered in the DUST-MS code. The total disposal inventory was analyzed to determine the release mechanism and release rate as functions of the waste stream contents buried in any given year.

Because each contaminant has a unique set of information, the amount of each contaminant buried each year was modeled as a separate waste container. The DUST-MS code was used to compute the sum of the results to provide total release over the time interval for use in the transport models. The basis for using individual values is discussed in the following paragraphs.

Waste streams composed primarily of metal were modeled either as dissolution release (i.e., through corrosion of the base metal) or as surface washoff (i.e., contamination on the metal). For actinides and fission products, metal waste streams were modeled as surface-washoff release; activation products are integral to the base metal and are released as metal corrodes.

Nagata and Banaee (1996) assessed the metal buried in the SDA and concluded that the majority is a form of stainless steel or Inconel (nickel-based alloy). Alder Flitton et al. (2001) provided a corrosion rate of 1 mm (0.04 in.) in 4,500 years (2.22E-05 cm/year) for stainless steel in soil at the INL Site with application of a magnesium chloride dust suppressant. For beryllium, the IRA corrosion rate (Becker et al. 1998) was updated for the ABRA and RI/BRA based on results of a long-term corrosion and degradation test (Adler Flitton et al. 2001). Measured results from the test were increased to include the effect of magnesium chloride dust suppressant applied to the surface of the SDA.

For corrosion mechanisms, DUST-MS requires input of an annual fractional release rate, which is equal to the corrosion rate divided by the volume-to-surface area ratio. Review of available data showed the ratio of surface area to volume for typical INL-type nuclear reactor core materials to be 0.535/cm (Oztunali and Roles 1985). Combining the corrosion rate and geometry data provided a fractional release of 1.19E-05/year from stainless steel.

Similarly, the corrosion rate of beryllium blocks was based on the long-term corrosion and degradation test (Adler Flitton et al. 2001). As for stainless steel, measured beryllium corrosion was modified to account for chloride in the dust suppressant. The rate used for corrosion of beryllium blocks was 1 mm (0.04 in.) in 39.37 years (2.54E-03 cm/year). The ratio of surface area to the volume of beryllium blocks is 1.043/cm. Combining geometry data with the corrosion rate provides a fractional release of 2.65E-03/year from the beryllium blocks. In 2004, most of the activated beryllium blocks buried in the SDA were grouted. After grouting, release from the blocks would be reduced. If the blocks were completely encapsulated, the corrosion rate would drop to near zero because water and oxygen would have to diffuse through grout to the blocks for the blocks to continue to corrode, and contaminants would then have to diffuse out of the grout for release into the subsurface. Because complete encapsulation cannot be verified, it was assumed for modeling that the blocks were only 80% encapsulated. This allows corrosion to occur, but at a reduced rate. Corrosion is assumed to occur only at the ungrouted surface area; therefore, the rate was reduced by the same 80%. Monitoring ports have been reinstalled near the blocks in Soil Vault Row (SVR) 20, and long-term monitoring of these ports is expected to show a reduction in release.

The grouting of beryllium reflector blocks from research reactors at the Reactor Technology Complex (formerly called Test Reactor Area) was performed as a non-time-critical removal action (Lopez 2004). Three different reactors had beryllium reflector blocks that were buried in the SDA. Table 5-7 lists the reactor, disposal date, C-14 curies disposed of, whether blocks were grouted, and location of the disposal. The location of the Advanced Test Reactor Core 1 shipment in 1973 and the Advanced Test Reactor Core 2 shipments were not identified before the non-time-critical removal action. Consequently, 86.3 of the 92.4 Ci of C-14 in the beryllium blocks were grouted and credit is taken in the risk model for only grouting the 86.3 Ci. Grout demonstrations have been shown to be highly effective (Loomis et al. 2002), but without an actual field validation, it was conservative to assume that only 80% encapsulation of grouted blocks occurred. Twenty percent of the surface area not encapsulated is assumed to be in contact with water and continues to corrode at the original rate. In effect, the corrosion rate of grouted blocks is reduced to 20% of original ungrouted value. In reality, encapsulation is likely much higher and there is a large amount of grout returns at the surface that would provide an effective barrier to water infiltration. No credit is taken for this barrier. Ungrouted blocks corrode at the original rate.

The previous discussion applies to integral contamination of steel or beryllium. Release of other metal (e.g., lead) into the subsurface depends on chemical properties of soil water and solubility of that metal in INL Site pore-water conditions. Soil water has a high pH, causing many contaminants to have a low solubility (Dicke 1997). To simulate release of metal (e.g., lead), the surface-washoff-release model was used with the appropriate contaminant-specific solubility limit for INL Site soil-water chemistry. Sludge buried in the SDA contains VOCs, radioactive contaminants, and other hazardous constituents. Volatile organic compounds are released from sludge through vapor diffusion (Kudera and Brown 1996). As shown in Table 5-2, release rates can vary by several orders of magnitude. Section 5.3 provides more details specific to modeling of VOCs. Release of metal and radioactive contaminants from sludge occurs through leaching, which was modeled with the surface-washoff-release model.

Table 5-7. Beryllium blocks buried in the Subsurface Disposal Area.

Generator	Date	C-14 (Ci)	Grouted	Location
Materials Testing Reactor Core 1	1977	2.92E+01	Yes	T52 and 58
Engineering Test Reactor Core 1	1970	2.17E+01	Yes	T54
Advanced Test Reactor Core 1	1973	3.00E-01	No	T57
Advanced Test Reactor Core 1	1976	7.51E+00	Yes	T58
Advanced Test Reactor Core 2	1977	5.83E+00	No	SVR 12
Advanced Test Reactor Core 3	1993	1.20E+01	Yes	SVR 20
Advanced Test Reactor outer shim control cylinder	1987	1.59E+01	Yes	SVR 17

SVR = soil vault row
T = trench

A surface-washoff release mechanism was assumed for waste streams that comprise generic laboratory trash. The surface-washoff release mechanism provides the most rapid release rates. Similarly, contaminants identified as surface contamination of a base material (e.g., anticontamination clothing) were modeled with the surface-washoff release model. The surface-washoff release model applies a distribution coefficient to determine release. The soil-to-water distribution coefficient was used as a first approximation.

The surface-washoff release model was used to simulate release from resins. For activation and fission products, using surface-washoff release generates a higher release rate, which is appropriate because these contaminants are generally mobile (low distribution coefficient [K_d]). Resin would sorb the contaminant better than soil. Major changes to source-release modeling from the ABRA include the following (Anderson and Becker 2006):

- Using a K_d specific for resins for mobile fission products (e.g., Tc-99 and I-129) instead of the soil-to-water K_d. This reduces the release of those contaminants.

- Modeling a colloidal fraction for plutonium. This fraction is highly mobile in the source model and produces a much higher release. Plutonium-239 and Pu-240 were simulated with a colloidal fraction, based on the work of Batcheller and Redden (2004), which showed that certain processes at Rocky Flats Plant could produce colloids. The fraction of Rocky Flats Plant plutonium that is mobile is 3.7% for the base case. Plutonium-238 was not simulated with a colloidal fraction because it would have been separated as an impurity and would not have gone through the high-temperature processes that generate colloids.

- Including solubility limits for uranium. The limit that was used matches the measured value in the waste, reducing the release of uranium from the source.

- Changing the distribution coefficient for many of the actinides. For distribution coefficients like plutonium, the K_d decreased, which would increase release. For distribution coefficients like neptunium, the K_d increased, which would reduce release. The changes in assigned values for distribution coefficients were explained in Appendix A of Holdren and Broomfield (2004).

- Increasing the number of source areas. This increase provides better detail in INL Site-generated waste areas and allows better definition for evaluating potential remedial alternatives in the feasibility study.

- Changing the release methodology for biotic modeling. Previously, contaminant mass was considered not available for biotic transport until it had been released from the waste form. However, for some waste types (e.g., sludge), it was realized that biota[a] could penetrate the waste and move contaminants before the contaminants had actually been released from the waste to the subsurface. To be conservative, any contaminant mass that would be released by the surface-washoff release mechanism was assumed to be available for biotic transport. To simplify modeling and be even more conservative, the containers were not accounted for (i.e., all the surface-washoff mass was assumed to be immediately available for release, even if it was drummed waste).

5.1.4 Contaminant Grouping for Modeling

Contaminant release and subsurface transport were simulated for 31 contaminants, which were grouped into 11 groups of contaminants for fate and transport simulation. The modeling groups were based on common decay chain ancestry or on other common chemical or physical characteristics. These groups are shown in Table 5-8. Group 9 includes miscellaneous contaminants that were not actually modeled in DUST-MS for source release. Their release was easily modeled through spreadsheet calculations consistent with the updated biotic modeling assumption that all inventory identified as surface wash is immediately available for uptake. The only exposure pathway available to these contaminants is surface exposure, and the only anticipated risk is through biotic uptake. Four contaminants (i.e., Nb-94, Sr-90, Cs-137, and Th-228) comprised Group 9. Very little Th-228 was in the SDA buried waste inventory; however, Th-228 inventories will increase over time through ingrowth attributable to two anthropogenic predecessor isotopes that are in the SDA inventory. These predecessors are Pu-240 and U-232. Uranium-232 screened out as a risk driver, but its daughter, Th-228, was assessed to be a surface pathway risk and was modeled accordingly. For completeness, contributions from its other predecessor, Pu-240, were included in the risk assessment.

This same grouping was used in source-term simulations to provide a consistent set of inputs for the biotic-uptake model (i.e., DOSTOMAN) and the subsurface model (i.e., TETRAD). Members of a decay-chain are assigned to the same group. Isotopes in the chain with a half-life of more than 1 year were included explicitly in the simulations, while contaminants with shorter half-lives were assumed to be in equilibrium with long-lived parents. Grouping for contaminants of potential concern and long-lived decay-chain members is defined in Table 5-8 as Groups 1 through 5. Some of the long-lived daughter products were not identified as contaminants of potential concern (see Section 3.4), but are included here to confirm that they pose no unacceptable risk and to assess sensitivity and uncertainty. Some of the RI/BRA sensitivity cases reduce the release of the parent nuclide and thus increase the ingrowth of the daughter in the waste zone.

---

a. Biota: the total complement of animals and plants in a particular area.

Table 5-8. Contaminant groups for Operable Unit 7-13/14 simulations.

Simulation Group	Group Name	Contaminants in Group[a]	Description	Basis for Group
1	Am-241	Am-241, Np-237, U-233, and Th-229	Pu-241 decay chain	Neptunium series beginning at Am-241, created by weapons production.
2	Am-243	Am-243, Pu-239, U-235, Pa-231, and Ac-227	Am-243/Pu-239 decay chain	Am-243 to Pu-239, both created primarily by weapons production, to actinium series initiated by U-235.
3	Pu-240	Pu-240, U-236, Th-232, and Ra-228	Pu-240 decay chain	Pu-240 to U-236, created primarily by weapons production, to thorium series initiated by Th-232.
4[b]	Pu-238	Pu-238, U-234, Th-230, Ra-226, and Pb-210	Pu-238 decay chain	Pu-238, created primarily by reactor operations, to U-234 to miduranium series.
5[b]	U-238	U-238, U-234, Th-230, Ra-226, and Pb-210	Uranium decay chain	Uranium series initiated by U-238, primarily from weapons production.
6	Tc-99	Tc-99, I-129, and Cl-36	Mobile activation products	Created by reactor operations.
8[c]	C-14	C-14	Mobile, dual-phase[d] activation product	Requires dual-phase simulation. Created by reactor operations.
9	Nb-94	Nb-94, Sr-90, Cs-137, and Th-228	Fission and activation products	Surface pathways only. Created by reactor operations.[e]
10	Nitrate	Nitrate (as nitrogen) and chromium	Toxic chemicals	Nonvolatile (single-phase), nonradioactive chemicals. Nitrate is contained primarily in Series 745 sludge from Rocky Flats Plant. Mobile with no decay. Chromium is a possible model performance indicator.
11	Volatile organic compound	Carbon tetrachloride, 1,4-dioxane methylene chloride, tetrachloroethylene, and trichloroethylene[f]	Toxic, dual-phase[d] chemicals in organic sludge	Volatile (dual-phase) nonradioactive chemicals. Scaled Interim Risk Assessment results in the Ancillary Basis for Risk Analysis.

a. Simulations include contaminants that are not contaminants of potential concern. These additional contaminants are decay-chain products or are useful for other reasons (e.g., comparison to performance assessment modeling and interpreting model performance and uncertainty).
b. Groups 4 and 5 both contain U-234, Th-230, Ra-226, and Pb-210.
c. Group 7 was reserved for tritium, which was dropped as a model performance indicator.
d. Dual-phase refers to simultaneous transport in both vapor and liquid phases.
e. Th-232 is not directly created by reactor operations, but is a progeny in two decay chains for isotopes that are produced in a reactor (i.e., Pu-240 and U-232).
f. Simulations for trichloroethylene will be part of the feasibility study.

5.1.5 Simulated Source Areas

The SDA was divided into 18 source areas to represent disposal locations for modeling contaminant release and transport for radionuclides and chemicals, except for C-14. Carbon-14 used nine source areas. Because of the influence of beryllium blocks on C-14 risk, a separate design was chosen to represent the blocks for C-14 modeling, which resulted in the difference in source area representation for C-14 from the rest of the contaminants. These source areas are listed in Tables 5-9 and 5-10. Each source area is represented in the subsurface model grid, as illustrated in Figures 5-2 and 5-3. Because DUST-MS is a one-dimensional model, multiple simulations were implemented for each contaminant group to simulate release from each source area individually. Then results were combined for input into subsurface-transport and biotic uptake simulations.

Tables 5-11, 5-12, and 5-13 provide the contaminant masses assigned to each source area from each contaminant group. The bases used for assigning contaminants within the SDA to source areas follow.

Beryllium disposals were assumed to have occurred when reactor cores were changed out in the Materials Test Reactor in 1968, the Engineering Test Reactor in 1970, and the Advanced Test Reactor in 1972, 1977, 1986, and 1987.

Inventory is assigned based on inventory evaluations and disposal location records in the Waste Information and Location Database. For some contaminants, the inventory evaluation calculated the inventory on a shipment basis. For other contaminants, assumptions are made that allow the inventory to be distributed to the individual shipments. The individual shipment inventory is then summed by disposal location and year to determine yearly input for each source area. Table 5-11 provides the inventory for each of the 18 source areas for all radionuclides, except C-14. Table 5-12 provides the inventory for each of the 18 source areas for the chemicals assessed. Table 5-13 provides the inventory for each of the nine source areas for C-14. Tables 5-14 and 5-15 show inventories for Group 6 (i.e., Tc-99, I-129, and Cl-36) and Group 8 (i.e., C-14), respectively, as they remain at milestones associated with grouting. These inventories are used to restart source-release modeling with altered conditions. The inventories consist of grouted and nongrouted portions after grouting was completed in 2004, and the remaining grouted inventory when grout fails after 1,038 years in Calendar Year 3042. Tables 5-16 and 5-17 show the inventory of radionuclides and nonradionuclides, respectively, remaining in Pit 4 in 2005 before retrieval. They also show the inventory remaining in Pit 4 after completion of the Accelerated Retrieval Project if 80% of the targeted waste is removed.

Table 5-9. Source areas in the Subsurface Disposal Area implemented in the source-release model for all contaminants, except carbon-14.

Source Area Abbreviation	Description	Average Depth (m)	Surface Area (m^2)
T1-10	Trenches 1–10	3.60	17,419
Acid_Pit	Acid Pit	1.43	2,903
P1–2&T11–15	Pits 1–2 and Trenches 11–15	2.99	26,129
T16-41	Trenches 16–41	2.38	7,258
P3	Pit 3	1.25	5,806
P4	Pit 4	3.90	11,613
P5	Pit 5	2.65	10,161
T42-58	Trenches 42–58	2.19	27,581
P6	Pit 6	5.46	4,355
P8	Pit 8	2.50	4,355
P7&9	Pits 7 and 9	2.01	5,806
P10-12	Pits 10–12	3.69	13,064
P13	Pit 13	3.66	1,452
Pad_A[a]	Pad A	0.49	4,355
P14-16	Pits 14–16	1.43	11,613
SVRs	Soil vault rows	3.38	15,968
P17-20	LLW Pits 17–20	7.47	13,064
LLW_proj	Projected LLW Pits 17–20	7.50	10,161

a. Pad A waste includes part of the waste originally buried in Pits 11 and 12. Residual inventory in Pits 11 and 12 was assigned to the Pad A source area.

LLW = low-level waste

Table 5-10. Carbon-14 source areas in the Subsurface Disposal Area implemented in the source-release model.

Source Area Abbreviation	Description	Average Depth (m)	Surface Area (m^2)
Pre-60	Pre-1960, C-14	3.90	4,355
60-66	1960–1966, C-14	3.51	7,258
67-83	1967–1983, C-14	2.26	8,710
Post-83	Post-1983, C-14	5.52	14,516
TR52	Trench 52, C-14 (beryllium)	1.49	4,355
TR58	Trench 58, C-14 (beryllium)	2.80	2,903
SVR12	Soil Vault Row 12, C-14 (beryllium)	2.71	1,452
SVR17	Soil Vault Row 17, C-14 (beryllium)	4.48	2,903
SVR20	Soil Vault Row 20, C-14 (beryllium)	2.01	1,452

Figure 5-2. Eighteen source areas simulated for all contaminants, except carbon-14, in the source-release model and specifically represented in the subsurface model domain.

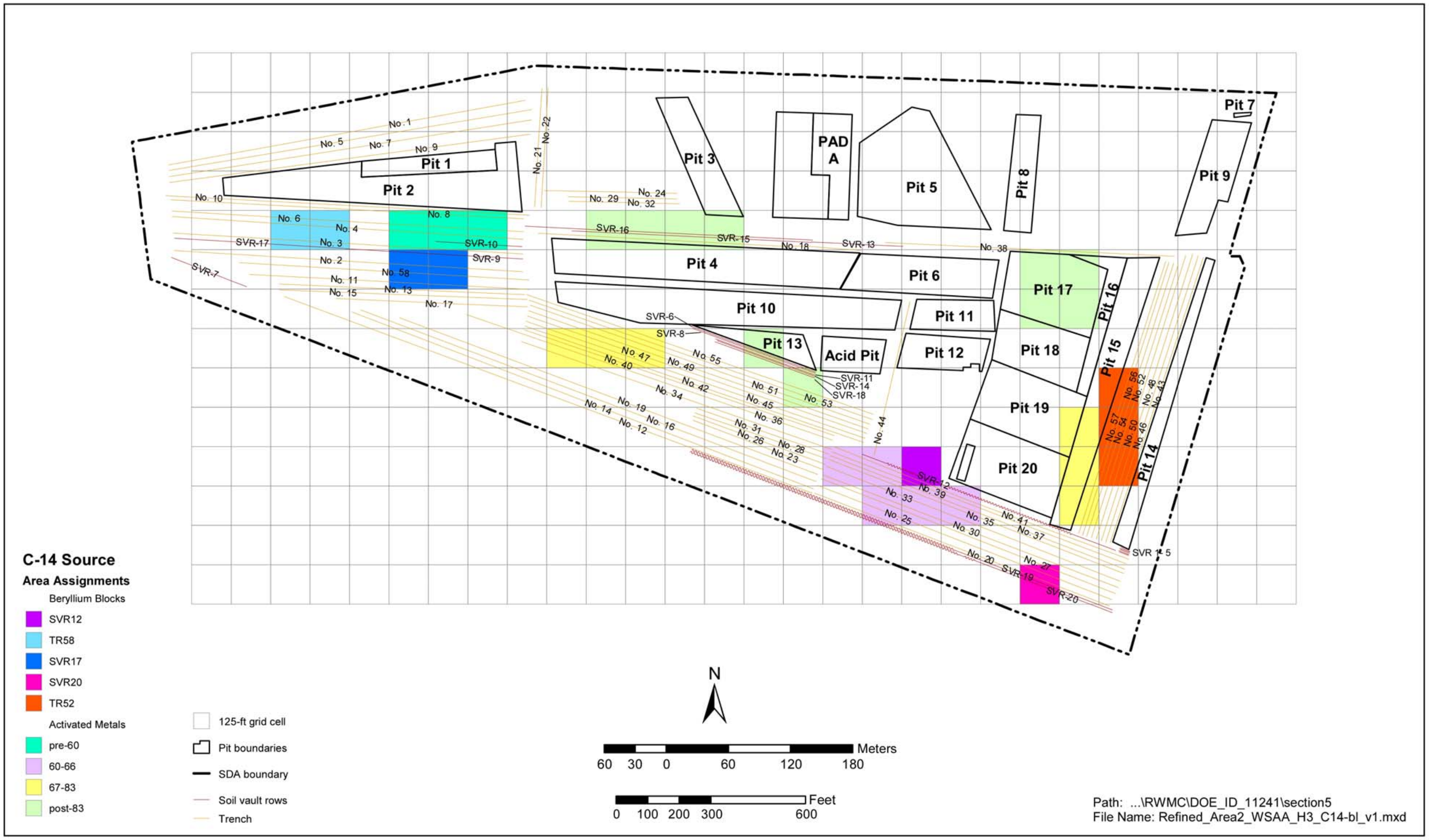

Figure 5-3. Nine carbon-14 source areas simulated in the source-release model and specifically represented in the subsurface model domain.

Table 5-11. Activity (curies) of radionuclides (Groups 1 through 6 and 9) buried in the 18 simulated source areas, by simulation groups and waste stream types, for Subsurface Disposal Area modeling.

Group	Radionuclide	Total	T1–10	Acid Pit	P1-2 and T11–15	T16–41	P3	P4	P5	T42–58	P6	P8	P7 and 9	P10–12	P13	Pad A	P14–16	SVRs	P17–20	LLW_proj
1	Am-241	**2.43E+05**	2.08E+04	4.14E-04	7.71E+04	4.36E+02	2.15E+03	5.15E+04	2.88E+04	1.18E+02	1.19E+04	5.11E-02	1.02E+04	3.98E+04	6.99E-01	5.34E+01	2.68E+00	4.12E+00	2.95E+00	1.19E+00
	Np-237	**1.41E-01**	2.30E-03	2.79E-07	1.40E-04	4.96E-02	2.71E-05	2.61E-05	8.59E-05	2.35E-02	9.79E-07	1.59E-05	1.68E-06	1.01E-03	1.47E-03	3.73E-07	8.55E-03	2.20E-02	9.89E-03	2.28E-02
	U-233	**2.12E+00**	9.52E-07	6.39E-11	7.77E-07	5.51E-01	3.25E-03	7.94E-09	4.59E-01	6.48E-01	8.15E-02	3.74E-09	4.29E-09	2.46E-08	3.84E-07	3.55E-14	1.13E-05	8.33E-05	3.56E-01	1.74E-02
	Th-229	**7.14E-06**	3.21E-09	6.49E-13	2.06E-10	2.07E-09	4.98E-12	1.75E-12	3.82E-12	4.80E-07	2.99E-13	4.79E-12	9.00E-13	6.35E-11	2.79E-10	4.87E-22	9.43E-09	1.07E-07	6.54E-06	0.00E+00
2	Am-243	**1.18E-01**	1.14E-02	2.18E-06	7.51E-04	4.57E-03	1.92E-05	1.84E-05	9.26E-06	5.97E-02	1.33E-06	2.20E-05	3.16E-06	2.25E-04	1.02E-03	6.94E-11	1.28E-02	2.44E-02	1.11E-03	1.88E-03
	Pu-239[a]	**2.33E+03**	2.42E+01	0.00E+00	7.26E+02	2.12E+00	1.23E+02	4.77E+02	1.56E+02	0.00E+00	1.27E+02	0.00E+00	1.10E+02	5.85E+02	0.00E+00	1.16E+00	0.00E+00	0.00E+00	0.00E+00	0.00E+00
	Pu-239	**6.18E+04**	6.30E+02	5.38E-05	1.92E+04	9.02E+01	3.21E+03	1.26E+04	4.07E+03	3.97E+02	3.31E+03	8.43E-02	2.85E+03	1.52E+04	2.44E+01	3.03E+01	2.47E+01	8.87E+01	4.49E+00	5.07E-01
	U-235	**4.88E+00**	1.01E+00	2.32E-03	7.23E-01	4.41E-01	7.45E-02	2.91E-01	3.28E-01	9.77E-02	2.19E-01	2.42E-05	3.74E-02	3.35E-01	1.65E-02	2.99E-01	5.99E-01	3.85E-02	3.23E-01	3.82E-02
	Pa-231	**8.61E-04**	3.90E-07	7.48E-11	2.56E-08	5.56E-07	6.37E-10	4.48E-10	2.69E-10	1.15E-06	4.11E-11	6.77E-10	1.09E-10	7.71E-09	3.42E-08	1.35E-15	7.08E-07	3.94E-07	8.58E-04	0.00E+00
	Ac-227	**4.29E-06**	3.90E-07	7.48E-11	2.56E-08	5.56E-07	6.37E-10	4.48E-10	2.69E-10	1.15E-06	4.11E-11	6.77E-10	1.09E-10	7.71E-09	3.42E-08	1.35E-15	7.08E-07	3.94E-07	1.02E-06	0.00E+00
3	Pu-240[a]	**5.22E+02**	5.41E+00	0.00E+00	1.63E+02	4.74E-01	2.76E+01	1.05E+02	3.52E+01	0.00E+00	2.91E+01	0.00E+00	2.51E+01	1.32E+02	0.00E+00	1.86E-01	0.00E+00	0.00E+00	0.00E+00	0.00E+00
	Pu-240	**1.41E+04**	1.41E+02	4.13E-05	4.52E+03	1.85E+01	7.19E+02	2.88E+03	9.17E+02	4.31E+01	7.58E+02	2.03E-02	6.54E+02	3.43E+03	4.90E-01	5.06E+00	8.53E-01	2.22E+00	4.74E-01	1.83E-01
	U-236	**1.45E+00**	3.52E-01	4.44E-08	1.52E-01	1.38E-01	4.89E-03	1.43E-01	1.56E-01	9.94E-02	6.21E-02	4.56E-05	1.90E-02	1.43E-01	6.29E-03	1.42E-02	1.54E-02	6.80E-02	5.95E-02	1.75E-02
	Th-232	**3.51E+00**	1.06E-11	2.03E-15	1.08E+00	9.36E-01	4.06E-08	2.28E-01	2.36E-07	1.05E+00	1.09E-15	7.39E-08	2.81E-08	4.35E-05	3.79E-05	2.81E-05	1.18E-02	1.50E-01	2.58E-02	2.75E-02
	Ra-228	**3.66E-05**	2.27E-10	4.36E-14	1.48E-11	6.84E-11	3.65E-13	1.24E-13	1.54E-13	1.17E-07	2.07E-14	3.36E-13	6.32E-14	4.49E-12	2.01E-11	1.38E-24	2.59E-10	3.20E-08	1.07E-05	2.57E-05
4	Pu-238[b]	**2.08E+03**	4.06E+01	3.45E-03	6.04E+02	1.02E+02	1.03E+02	3.90E+02	1.26E+02	4.13E+01	1.03E+02	4.89E-02	8.72E+01	4.12E+02	4.06E+00	9.67E-01	2.00E+01	4.44E+01	2.05E+00	4.91E-01
5	U-238	**1.48E+02**	6.06E+00	9.90E-02	1.63E+01	2.61E+00	6.25E-01	2.63E+01	2.01E+01	2.51E+00	1.28E+01	6.46E-05	1.45E+00	2.40E+01	1.39E-02	2.21E+01	2.00E+00	5.61E-02	3.95E+00	7.39E+00
	U-234	**6.26E+01**	6.05E+00	6.59E-02	1.18E+01	7.89E+00	6.78E-01	3.91E+00	4.85E+00	3.25E+00	4.31E+00	7.61E-04	1.95E+00	6.87E+00	1.52E-01	4.21E+00	1.85E+00	7.51E-01	3.62E+00	4.07E-01
	Th-230	**5.77E-02**	1.22E-09	5.68E-06	4.08E-07	9.23E-05	1.05E-08	4.53E-08	6.16E-09	4.15E-05	1.52E-09	2.41E-08	1.58E-09	1.14E-07	5.41E-07	1.79E-02	6.15E-05	1.51E-05	1.34E-02	2.62E-02
	Ra-226	**6.51E+01**	3.24E-10	1.50E-06	2.42E+01	3.76E+01	3.90E-03	2.74E+00	1.09E-09	4.30E-02	1.38E-10	2.27E-09	4.29E-10	4.27E-08	1.41E-07	1.72E-02	2.00E-01	1.02E-06	7.91E-02	1.91E-01
	Pb-210	**5.59E-07**	2.27E-12	1.06E-08	6.75E-10	5.04E-09	1.47E-11	5.76E-12	6.94E-12	1.00E-08	9.62E-13	1.23E-11	2.93E-12	2.09E-10	9.25E-10	0.00E+00	1.38E-08	7.11E-09	5.10E-07	0.00E+00
6	Tc-99[c]	**1.50E+01**	1.56E-03	0.00E+00	4.35E-03	3.32E-01	1.65E-04	2.06E-03	5.65E-03	2.12E-01	7.73E-05	1.40E-05	2.46E-05	1.27E-03	4.05E-05	0.00E+00	1.52E-01	1.43E+01	8.73E-04	3.46E-03
	I-129[c]	**7.44E-04**	1.20E-06	0.00E+00	5.79E-06	5.53E-04	3.01E-07	4.33E-06	9.50E-06	1.54E-04	1.40E-07	1.95E-07	4.04E-08	4.70E-07	6.64E-08	0.00E+00	2.96E-06	1.20E-05	1.20E-06	0.00E+00
	Cl-36[c]	**7.52E-01**	2.14E-04	0.00E+00	3.67E-04	4.84E-02	6.72E-09	1.72E-12	6.30E-10	1.07E-01	2.54E-12	2.35E-08	2.74E-12	1.51E-07	4.72E-09	0.00E+00	9.90E-04	5.73E-02	4.92E-07	5.38E-01
	Tc-99[d]	**1.20E-02**	0.00E+00	0.00E+00	0.00E+00	0.00E+00	0.00E+00	0.00E+00	0.00E+00	8.51E-03	0.00E+00	0.00E+00	0.00E+00	0.00E+00	0.00E+00	0.00E+00	0.00E+00	3.46E-03	0.00E+00	0.00E+00
	I-129[d]	**9.91E-05**	0.00E+00	0.00E+00	0.00E+00	0.00E+00	0.00E+00	0.00E+00	0.00E+00	7.19E-05	0.00E+00	0.00E+00	0.00E+00	0.00E+00	0.00E+00	0.00E+00	0.00E+00	2.73E-05	0.00E+00	0.00E+00
	Cl-36[d]	**8.83E-01**	0.00E+00	0.00E+00	0.00E+00	0.00E+00	0.00E+00	0.00E+00	0.00E+00	6.41E-01	0.00E+00	0.00E+00	0.00E+00	0.00E+00	0.00E+00	0.00E+00	0.00E+00	2.41E-01	0.00E+00	0.00E+00
	Tc-99[e]	**4.24E+00**	2.61E-02	0.00E+00	0.00E+00	1.15E+00	0.00E+00	2.89E-04	1.26E-04	2.14E+00	6.26E-07	8.26E-05	0.00E+00	1.42E-01	5.00E-02	5.65E-05	1.06E-01	6.20E-01	0.00E+00	0.00E+00
	I-129[e]	**9.18E-03**	4.52E-05	0.00E+00	0.00E+00	1.99E-03	0.00E+00	0.00E+00	0.00E+00	5.25E-03	0.00E+00	7.49E-11	3.60E-10	2.92E-04	1.03E-04	1.16E-07	2.21E-04	1.28E-03	0.00E+00	0.00E+00
	Cl-36[e]	**1.49E-03**	0.00E+00	0.00E+00	0.00E+00	2.63E-04	0.00E+00	0.00E+00	0.00E+00	1.20E-03	0.00E+00	1.23E-12	0.00E+00	4.78E-06	1.68E-06	1.91E-09	3.56E-06	2.09E-05	0.00E+00	0.00E+00
	Tc-99[f]	**6.26E+00**	4.63E-04	0.00E+00	0.00E+00	6.70E-01	0.00E+00	8.81E-06	5.66E-08	9.27E-01	0.00E+00	0.00E+00	1.18E-05	5.34E-05	1.18E-01	0.00E+00	1.71E+00	0.00E+00	7.90E-01	2.05E+00
	I-129[f]	**1.33E-01**	1.76E-06	0.00E+00	7.41E-08	1.66E-02	0.00E+00	3.48E-08	2.23E-10	2.39E-02	0.00E+00	0.00E+00	4.64E-08	2.11E-07	2.94E-03	0.00E+00	2.34E-02	0.00E+00	1.96E-02	4.65E-02
	Cl-36[f]	**0.00E+00**	0.00E+00	0.00E+00	0.00E+00	0.00E+00	0.00E+00	0.00E+00	0.00E+00	0.00E+00	0.00E+00	0.00E+00	0.00E+00	0.00E+00	0.00E+00	0.00E+00	0.00E+00	0.00E+00	0.00E+00	0.00E+00
	Tc-99[g]	**6.67E+00**	0.00E+00	0.00E+00	0.00E+00	0.00E+00	0.00E+00	0.00E+00	0.00E+00	6.67E+00	0.00E+00	0.00E+00	0.00E+00	0.00E+00	0.00E+00	0.00E+00	0.00E+00	0.00E+00	0.00E+00	0.00E+00
	I-129[g]	**1.80E-02**	0.00E+00	0.00E+00	0.00E+00	0.00E+00	0.00E+00	0.00E+00	0.00E+00	1.80E-02	0.00E+00	0.00E+00	0.00E+00	0.00E+00	0.00E+00	0.00E+00	0.00E+00	0.00E+00	0.00E+00	0.00E+00
	Cl-36[g]	**0.00E+00**	0.00E+00	0.00E+00	0.00E+00	0.00E+00	0.00E+00	0.00E+00	0.00E+00	0.00E+00	0.00E+00	0.00E+00	0.00E+00	0.00E+00	0.00E+00	0.00E+00	0.00E+00	0.00E+00	0.00E+00	0.00E+00
	Tc-99[h]	**1.07E+01**	8.14E-01	1.64E-04	5.22E-02	4.01E+00	2.94E-03	7.77E-04	1.91E-03	2.48E+00	7.61E-05	2.83E-03	3.69E-04	2.26E-02	2.19E-01	1.94E-07	9.53E-01	1.92E+00	2.11E-01	3.67E-02
	I-129[h]	**2.38E-02**	1.30E-03	2.50E-07	8.52E-05	9.41E-03	5.24E-06	1.40E-06	3.17E-06	4.70E-03	1.26E-07	4.53E-06	6.61E-07	3.93E-05	4.15E-04	3.98E-10	1.55E-03	3.14E-03	3.93E-04	2.71E-03
	Cl-36[h]	**6.72E-03**	1.86E-10	0.00E+00	4.12E-06	9.00E-06	6.64E-09	8.97E-07	3.76E-08	3.83E-03	2.51E-15	1.18E-08	4.47E-09	2.18E-07	4.33E-06	6.10E-12	1.33E-03	1.44E-03	9.67E-05	0.00E+00

Table 5-11. (continued).

Group	Radionuclide	Total	T1–10	Acid Pit	P1-2 and T11–15	T16–41	P3	P4	P5	T42–58	P6	P8	P7 and 9	P10–12	P13	Pad A	P14–16	SVRs	P17–20	LLW_proj
9	Nb-94	**8.38E+01**	1.55E+00	0.00E+00	7.29E-02	4.44E+01	1.45E-04	0.00E+00	3.01E-02	1.01E+01	1.21E-04	7.86E-05	1.31E-04	1.79E+00	4.42E-04	2.55E-07	4.18E-01	2.20E+01	5.75E-01	2.83E+00
	Sr-90	**2.76E+04**	1.93E+02	0.00E+00	1.05E+03	9.84E+03	1.49E+00	0.00E+00	3.82E+01	1.08E+04	4.91E-01	6.64E-01	1.65E-01	8.40E+02	2.96E+02	3.34E-01	6.54E+02	3.67E+03	5.13E+00	0.00E+00
	Totals		**2.18E+04**	**1.71E-01**	**1.03E+05**	**1.06E+04**	**6.34E+03**	**6.80E+04**	**3.42E+04**	**1.14E+04**	**1.63E+04**	**8.72E-01**	**1.39E+04**	**6.04E+04**	**3.26E+02**	**1.18E+02**	**7.10E+02**	**3.85E+03**	**2.51E+01**	**1.60E+01**

a. Colloidal or mobile portion of plutonium.
b. Inventories for Group 4 daughter products (i.e., U-234, Th-230, Ra-226, and Pb-210) are included in Group 5.
c. Associated with activated metal (called C-14A in the model).
d. Associated with beryllium blocks (called C-14B in the model).
e. Associated with fuel-like materials (called C-14F in the model).
f. Associated with resins (called C-14R in the model).
g. Associated with Vycor glass (called C-14V in the model).
h. Subject to surface wash (called C-14W in the model).

Table 5-12. Mass (grams) of volatile organic compounds and nonradionuclides (Groups 10 and 11) buried in the 18 simulated source areas, by simulation groups, for Subsurface Disposal Area modeling.

Group	Contaminant	Total	T1–10	Acid Pit	P1-2 and T11–15	T16–41	P3	P4	P5	T42–58	P6	P8	P7 and 9	P10–12	P13	Pad A	P14–16	SVRs	P17–20	LLW_proj
10	Nitrate	**4.56E+08**	0.00E+00	4.97E+07	1.52E+04	4.02E+01	7.80E+03	0.00E+00	0.00E+00	0.00E+00	5.16E+07	0.00E+00	6.89E+06	1.08E+08	0.00E+00	2.35E+08	0.00E+00	0.00E+00	0.00E+00	0.00E+00
	Chromium[a]	**2.31E+06**	0.00E+00	0.00E+00	0.00E+00	0.00E+00	0.00E+00	0.00E+00	0.00E+00	0.00E+00	1.49E+05	0.00E+00	1.99E+04	3.16E+05	0.00E+00	1.82E+06	0.00E+00	0.00E+00	0.00E+00	0.00E+00
11	Carbon tetrachloride	**7.86E+08**	0.00E+00	0.00E+00	0.00E+00	0.00E+00	0.00E+00	3.48E+08	3.45E+06	0.00E+00	2.36E+08	0.00E+00	1.03E+08	9.57E+07	0.00E+00	0.00E+00	0.00E+00	0.00E+00	0.00E+00	0.00E+00
	1,4-Dioxane	**3.90E+06**	8.62E+03	0.00E+00	3.41E+04	9.64E+02	4.01E+03	7.90E+05	3.00E+04	2.67E+03	5.20E+05	1.58E+02	2.28E+05	2.99E+05	1.43E+02	0.00E+00	3.37E+04	2.39E-01	2.39E+00	0.00E+00
	Methylene chloride	**1.41E+07**	7.05E+05	0.00E+00	2.62E+06	1.58E+04	1.02E+05	3.19E+06	1.61E+06	0.00E+00	1.15E+06	0.00E+00	9.79E+05	3.71E+06	0.00E+00	0.00E+00	0.00E+00	0.00E+00	0.00E+00	0.00E+00
	Tetrachloroethylene	**9.87E+07**	0.00E+00	0.00E+00	0.00E+00	0.00E+00	0.00E+00	4.33E+07	5.37E+05	0.00E+00	2.91E+07	0.00E+00	1.26E+07	1.31E+07	0.00E+00	0.00E+00	0.00E+00	0.00E+00	0.00E+00	0.00E+00
	Trichloroethylene[b]	—	—	—	—	—	—	—	—	—	—	—	—	—	—	—	—	—	—	—
	Totals		**7.14E+05**	**4.97E+07**	**2.67E+06**	**1.68E+04**	**1.14E+05**	**3.95E+08**	**5.63E+06**	**2.67E+03**	**3.19E+08**	**1.58E+02**	**1.24E+08**	**2.21E+08**	**1.43E+02**	**2.37E+08**	**3.37E+04**	**2.39E-01**	**2.39E+00**	**0.00E+00**

a. For modeling performance assessment only.
b. Simulations for trichloroethylene will be part of the feasibility study; value not yet computed.

Table 5-13. Revised modeled activity (curies) of carbon-14 (Group 8) in beryllium blocks at time of grouting and at time of grout failure.

Group	Radionuclide	Total	TR58	SVR12	SVR17	SVR20	TR52	Pre-60	60–66	67–83	Post-83
8	C-14[a]	**6.76E+00**	1.30E+00	5.46E+00	0.00E+00	0.00E+00	0.00E+00	0.00E+00	0.00E+00	0.00E+00	0.00E+00
	C-14[b]	**7.91E+01**	3.25E+01	0.00E+00	1.51E+01	1.16E+01	1.99E+01	0.00E+00	0.00E+00	0.00E+00	0.00E+00
	C-14[c]	**3.14E+01**	1.29E+01	0.00E+00	6.00E+00	4.59E+00	7.88E+00	0.00E+00	0.00E+00	0.00E+00	0.00E+00

a. Portion that was not grouted after grouting was completed in 2004 (called C-14N in the model)
b. Portion that was grouted in 2004 (called C-14G in the model). The release mechanism is corrosion of the beryllium. The grout reduces the surface area in contact with infiltrating water and reduces the corrosion rate.
c. Remaining after grout has failed (called C-14E in the model, for the end state). Grout is expected to remain effective for a minimum of 1,038 years (Calendar Year 3042) (Hanson et al. 2004).

Table 5-14. Revised modeled activity (curies) of radionuclides (Group 6) at time of grouting and at time of grout failure.

Group	Radionuclide	Total	T1–10	Acid Pit	P1-2 and T11–15	T16–41	P3	P4	P5	T42–58	P6	P8	P7 and 9	P10–12	P13	Pad A	P14–16	SVRs	P17–20	LLW_proj
6	Tc-99[a]	**7.52E-04**	0.00E+00	0.00E+00	0.00E+00	0.00E+00	0.00E+00	0.00E+00	0.00E+00	3.65E-05	0.00E+00	0.00E+00	0.00E+00	0.00E+00	0.00E+00	0.00E+00	0.00E+00	7.15E-04	0.00E+00	0.00E+00
	I-129[a]	**5.82E-06**	0.00E+00	0.00E+00	0.00E+00	0.00E+00	0.00E+00	0.00E+00	0.00E+00	2.86E-07	0.00E+00	0.00E+00	0.00E+00	0.00E+00	0.00E+00	0.00E+00	0.00E+00	5.53E-06	0.00E+00	0.00E+00
	Cl-36[a]	**4.90E-02**	0.00E+00	0.00E+00	0.00E+00	0.00E+00	0.00E+00	0.00E+00	0.00E+00	2.36E-03	0.00E+00	0.00E+00	0.00E+00	0.00E+00	0.00E+00	0.00E+00	0.00E+00	4.66E-02	0.00E+00	0.00E+00
	Tc-99[b]	**1.05E-02**	0.00E+00	0.00E+00	0.00E+00	0.00E+00	0.00E+00	0.00E+00	0.00E+00	7.93E-03	0.00E+00	0.00E+00	0.00E+00	0.00E+00	0.00E+00	0.00E+00	0.00E+00	2.58E-03	0.00E+00	0.00E+00
	I-129[b]	**9.33E-05**	0.00E+00	0.00E+00	0.00E+00	0.00E+00	0.00E+00	0.00E+00	0.00E+00	7.16E-05	0.00E+00	0.00E+00	0.00E+00	0.00E+00	0.00E+00	0.00E+00	0.00E+00	2.18E-05	0.00E+00	0.00E+00
	Cl-36[b]	**7.80E-01**	0.00E+00	0.00E+00	0.00E+00	0.00E+00	0.00E+00	0.00E+00	0.00E+00	5.97E-01	0.00E+00	0.00E+00	0.00E+00	0.00E+00	0.00E+00	0.00E+00	0.00E+00	1.83E-01	0.00E+00	0.00E+00
	Tc-99[c]	**4.71E-03**	0.00E+00	0.00E+00	0.00E+00	0.00E+00	0.00E+00	0.00E+00	0.00E+00	3.55E-03	0.00E+00	0.00E+00	0.00E+00	0.00E+00	0.00E+00	0.00E+00	0.00E+00	1.16E-03	0.00E+00	0.00E+00
	I-129[c]	**4.03E-03**	0.00E+00	0.00E+00	0.00E+00	0.00E+00	0.00E+00	0.00E+00	0.00E+00	3.09E-03	0.00E+00	0.00E+00	0.00E+00	0.00E+00	0.00E+00	0.00E+00	0.00E+00	9.39E-04	0.00E+00	0.00E+00
	Cl-36[c]	**1.80E-01**	0.00E+00	0.00E+00	0.00E+00	0.00E+00	0.00E+00	0.00E+00	0.00E+00	1.38E-01	0.00E+00	0.00E+00	0.00E+00	0.00E+00	0.00E+00	0.00E+00	0.00E+00	4.23E-02	0.00E+00	0.00E+00

a. Portion that was not grouted after grouting was completed in 2004 (called Tc-99N, I-129N, and Cl-36N in the model).
b. Portion that was grouted in 2004 (called Tc-99G, I-129G, and Cl-36G in the model). The release mechanism is corrosion of the beryllium. The grout reduces the surface area in contact with infiltrating water and reduces the corrosion rate.
c. Remaining after grout has failed (called Tc-99E, I-129E, and Cl-36E in the model, for the end state). Grout is expected to remain effective for a minimum of 1,038 years (Calendar Year 3042) (Hanson et al. 2004).

Table 5-15. Activity (curies) of tritium and carbon-14 (Group 8) in beryllium blocks buried in the nine simulated source areas, by simulation groups, for Subsurface Disposal Area modeling.

Group	Radionuclide	Total	TR58	SVR12	SVR17	SVR20	TR52	Pre-60	60–66	67–83	Post-83
8	C-14[a]	**5.02E+02**	0.00E+00	0.00E+00	0.00E+00	0.00E+00	0.00E+00	1.15E+01	2.31E+02	1.52E+02	1.07E+02
	C-14[b]	**9.24E+01**	3.67E+01	5.83E+00	1.59E+01	1.20E+01	2.20E+01	0.00E+00	0.00E+00	0.00E+00	0.00E+00
	C-14[c]	**6.57E+00**	0.00E+00	0.00E+00	0.00E+00	0.00E+00	0.00E+00	2.16E-07	6.50E+00	5.73E-02	1.42E-02
	C-14[d]	**2.61E+01**	0.00E+00	0.00E+00	0.00E+00	0.00E+00	0.00E+00	3.00E-01	2.87E+00	1.36E+01	9.34E+00
	C-14[e]	**1.04E+02**	0.00E+00	0.00E+00	0.00E+00	0.00E+00	0.00E+00	6.06E-02	5.77E+01	3.99E+01	5.95E+00
	Totals		**3.67E+01**	**5.83E+00**	**1.59E+01**	**1.20E+01**	**2.20E+01**	**1.19E+01**	**2.98E+02**	**2.06E+02**	**1.22E+02**

a. Associated with activated metal (called C-14A in the model).
b. Associated with beryllium blocks (called C-14A in the model).
c. Associated with fuel-like materials (called C-14F in the model).
d. Associated with resins (called C-14R in the model).
e. Associated with surface wash (called C-14W in the model).

Table 5-16. Activity (curies) of radionuclides (Groups 1 through 6 and 9) in Pit 4 before and after the Accelerated Retrieval Project retrieval.

Group	Radionuclide	Immediately Before Retrieval (2004) (Ci)	Immediately After Retrieval (2004) (Ci)
1	Am-241	4.83E+04	3.32E+04
	Np-237	6.04E-01	6.04E-01
	U-233	4.90E-05	4.90E-05
	Th-229	5.78E-08	5.78E-08
2	Am-243	1.76E-05	1.76E-05
	Pu-239 (mobile/colloidal)	1.26E+02	9.24E+01
	Pu-239	1.26E+04	9.23E+03
	U-235	2.90E-01	2.90E-01
	Pa-231	2.16E-04	2.16E-04
	Ac-227	8.99E-05	8.99E-05
3	Pu-240 (mobile/colloidal)	2.73E+01	2.08E+01
	Pu-240	2.87E+03	2.19E+03
	U-236	1.21E-01	1.21E-01
	Th-232	2.25E-01	2.25E-01
	Ra-228	2.10E-01	2.10E-01
4	Pu-238[a]	2.85E+02	2.12E+02
5	U-238	2.63E+01	1.43E+01
	U-234	3.94E+00	2.12E+00
	Th-230	1.38E-03	1.38E-03
	Ra-226	2.66E+00	2.66E+00
	Pb-210	1.90E+00	1.90E+00
6	Tc-99[b]	2.06E-03	2.06E-03
	I-129[b]	4.33E-06	4.33E-06
	Cl-36[b]	1.72E-12	1.72E-12
	Tc-99[c]	0.00E+00	0.00E+00
	I-129[c]	0.00E+00	0.00E+00
	Cl-36[c]	0.00E+00	0.00E+00
	Tc-99[d]	2.89E-04	2.89E-04
	I-129[d]	0.00E+00	0.00E+00
	Cl-36[d]	0.00E+00	0.00E+00
	Tc-99[e]	8.81E-06	8.81E-06
	I-129[e]	3.48E-08	3.48E-08
	Cl-36[e]	0.00E+00	0.00E+00
	Tc-99[f]	0.00E+00	0.00E+00
	I-129[f]	0.00E+00	0.00E+00
	Cl-36[f]	0.00E+00	0.00E+00
	Tc-99[g]	7.77E-04	7.77E-04
	I-129[g]	1.40E-06	1.40E-06
	Cl-36[g]	8.97E-07	8.97E-07

Table 5-16. (continued).

Group	Radionuclide	Immediately Before Retrieval (2004) (Ci)	Immediately After Retrieval (2004) (Ci)
9	Nb-94	8.21E-05	8.21E-05
	Sr-90	2.09E+02	2.09E+02

a. Inventories for Group 4 daughter products (i.e., U-234, Th-230, Ra-226, and Pb-210) are included in Group 5.
b. Associated with activated metal (called C-14A in the model).
c. Associated with beryllium blocks (called C-14B in the model).
d. Associated with fuel-like materials (called C-14F in the model).
e. Associated with resins (called C-14R in the model).
f. Associated with Vycor glass (called C-14V in the model).
g. Subject to surface wash (called C-14W in the model).

Table 5-17. Mass (grams) of volatile organic compounds and nonradionuclides (Groups 10 and 11) in Pit 4 before and after the Accelerated Retrieval Project retrieval.

Group	Contaminant	Immediately Before Retrieval (g)	Immediately After Retrieval (g)
10	Nitrate	4.49E+06	4.49E+06
	Chromium	1.12E+04	1.12E+04
11	Carbon tetrachloride	4.40E+07	8.80E+06
	1,4-Dioxane	3.96E+04	8.37E+03
	Methylene chloride	6.31E+05	6.31E+05
	Tetrachloroethylene	5.52E+06	1.10E+06
	Trichloroethylene	NA[a]	NA[a]

a. Simulations for trichloroethylene will be part of the feasibility study; value not yet computed.

5.1.6 Infiltration Rates

Site-specific infiltration rates were developed for the SDA. The infiltration rate assigned to each of the source areas (18 for radionuclides and nine for VOCs) was based on the assignment of infiltration in corresponding gridblocks in the subsurface flow and transport model. Infiltration rates applied to the gridblocks of the subsurface flow and transport model, with the source areas, are presented in Figures 5-4, 5-5, and 5-6. Infiltration assigned to individual gridblocks in the subsurface model was averaged over those gridblocks representing each source area. The resulting averages are shown at the bottom of the figures. The basis for infiltration rates is discussed in Section 5.2.

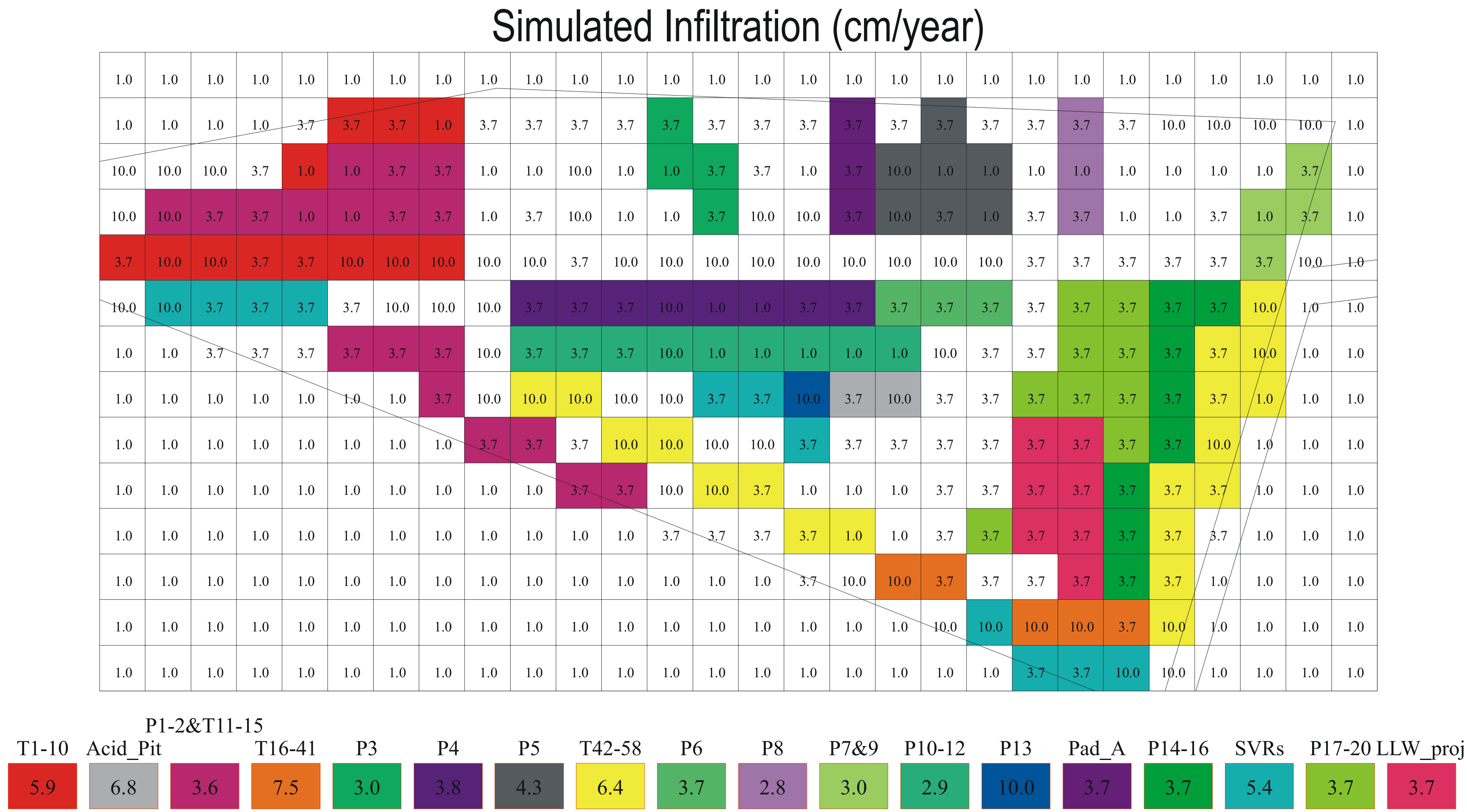

Figure 5-4. Infiltration rates with averages by source area for dissolved-phase contaminants.

Simulated Infiltration (cm/year)

1.0	1.0	1.0	1.0	1.0	1.0	1.0	1.0	1.0	1.0	1.0	1.0	1.0	1.0	1.0	1.0	1.0	1.0	1.0	1.0	1.0	1.0	1.0	1.0	1.0	1.0	1.0	1.0
1.0	1.0	1.0	1.0	3.7	3.7	3.7	1.0	3.7	3.7	3.7	3.7	3.7	3.7	3.7	3.7	3.7	3.7	3.7	3.7	3.7	3.7	3.7	10.0	10.0	10.0	10.0	1.0
10.0	10.0	10.0	3.7	1.0	1.0	3.7	3.7	1.0	1.0	10.0	1.0	1.0	3.7	3.7	1.0	3.7	10.0	1.0	1.0	1.0	1.0	1.0	1.0	1.0	1.0	3.7	1.0
10.0	10.0	3.7	3.7	1.0	1.0	3.7	3.7	1.0	3.7	10.0	1.0	1.0	3.7	10.0	10.0	3.7	10.0	3.7	1.0	3.7	3.7	1.0	1.0	3.7	1.0	3.7	1.0
3.7	10.0	10.0	3.7	3.7	10.0	10.0	10.0	10.0	10.0	3.7	10.0	10.0	10.0	10.0	10.0	10.0	10.0	10.0	10.0	3.7	3.7	3.7	3.7	3.7	3.7	10.0	1.0
10.0	10.0	3.7	3.7	3.7	3.7	10.0	10.0	10.0	3.7	3.7	3.7	10.0	1.0	1.0	3.7	3.7	3.7	3.7	3.7	3.7	3.7	3.7	3.7	3.7	10.0	1.0	1.0
1.0	1.0	3.7	3.7	3.7	3.7	3.7	3.7	10.0	3.7	3.7	3.7	10.0	1.0	1.0	1.0	1.0	1.0	10.0	3.7	3.7	3.7	3.7	3.7	3.7	10.0	1.0	1.0
1.0	1.0	1.0	1.0	1.0	1.0	1.0	3.7	10.0	10.0	10.0	10.0	10.0	3.7	3.7	10.0	3.7	10.0	3.7	3.7	3.7	3.7	3.7	3.7	3.7	1.0	1.0	1.0
1.0	1.0	1.0	1.0	1.0	1.0	1.0	1.0	3.7	3.7	3.7	10.0	10.0	10.0	10.0	3.7	3.7	3.7	3.7	3.7	3.7	3.7	3.7	3.7	10.0	1.0	1.0	1.0
1.0	1.0	1.0	1.0	1.0	1.0	1.0	1.0	1.0	1.0	3.7	3.7	10.0	10.0	3.7	1.0	1.0	1.0	3.7	3.7	3.7	3.7	3.7	3.7	3.7	1.0	1.0	1.0
1.0	1.0	1.0	1.0	1.0	1.0	1.0	1.0	1.0	1.0	1.0	1.0	3.7	3.7	3.7	3.7	1.0	1.0	3.7	3.7	3.7	3.7	3.7	3.7	3.7	1.0	1.0	1.0
1.0	1.0	1.0	1.0	1.0	1.0	1.0	1.0	1.0	1.0	1.0	1.0	1.0	1.0	1.0	3.7	10.0	10.0	3.7	3.7	3.7	3.7	3.7	3.7	1.0	1.0	1.0	1.0
1.0	1.0	1.0	1.0	1.0	1.0	1.0	1.0	1.0	1.0	1.0	1.0	1.0	1.0	1.0	1.0	1.0	1.0	10.0	10.0	10.0	10.0	3.7	10.0	1.0	1.0	1.0	1.0
1.0	1.0	1.0	1.0	1.0	1.0	1.0	1.0	1.0	1.0	1.0	1.0	1.0	1.0	1.0	1.0	1.0	1.0	1.0	1.0	3.7	3.7	10.0	10.0	1.0	1.0	1.0	1.0

SVR12	TR58	SVR17	SVR20	TR52	pre-60	60-66	67-83	post-83
3.7	6.8	6.8	3.7	3.7	10.0	3.9	6.8	5.6

Figure 5-5. Infiltration rates with averages by source area for carbon-14.

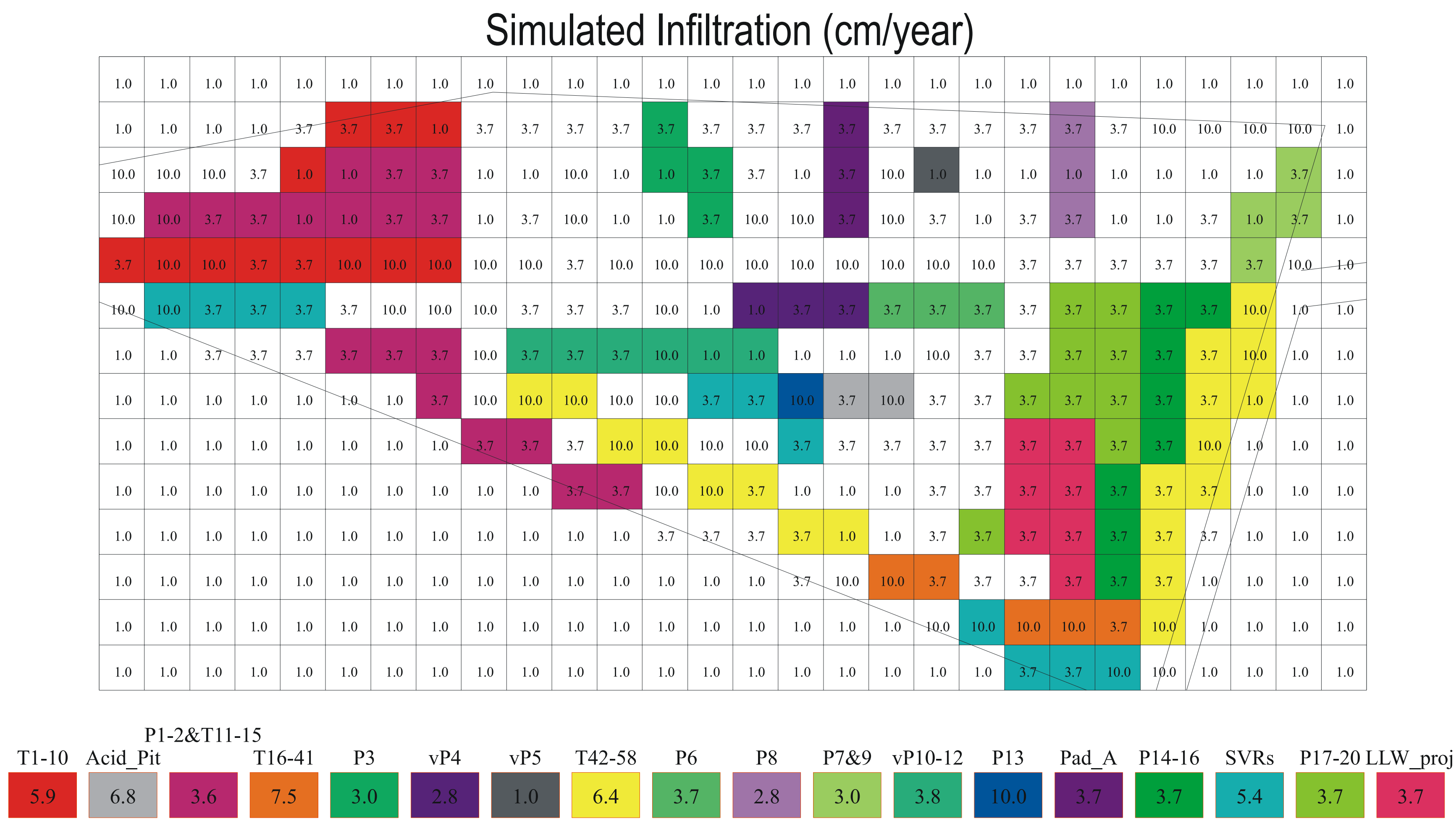

Figure 5-6. Infiltration rates with averages by source area for volatile organic compounds.

5.1.7 Source-Term Model Calibration

Data from monitoring in and immediately proximal to buried waste are required to calibrate the source-term model. Data taken from directly beneath the waste are limited, and time histories have not been developed. For purposes of the RI/BRA, currently available data are insufficient to attempt source-term model calibration. Monitoring of the vadose zone and comparisons to predicted vadose zone concentrations (see Section 5.2) indirectly corroborate the source-release model.

Source-release modeling for the SDA has been an iterative process. Changes in inventories and disposal locations have been made based on improved process knowledge. This improved knowledge has also resulted in refinement of the assigned locations in the vadose zone model where the source-release model results are implemented. Some changes in the inventory were direct results of previous source-release modeling. As an example, Becker et al. (1998) showed that the buried carbon tetrachloride inventory was not sufficient to match observed results of carbon tetrachloride monitoring in the vadose zone. Subsequent evaluation of the carbon tetrachloride inventory resulted in a seven-fold increase in buried carbon tetrachloride (Miller and Varvel 2005) from that initially used for IRA (Becker et al. 1998) modeling.

Different types of probes were installed in the waste, as described in Section 3.6. The Geologic and Environmental Probe System probes (i.e., second generation Type B probes) have improved the capability for collecting leachate within the waste zone and show promise in providing results to compare against the source-release model. Continued monitoring and evaluation of the data could allow validation of the values used in the RI/BRA source-release modeling and provide data sets for calibrating any future source-release modeling.

5.2 Dissolved-Phase Transport Modeling

Contaminant fate and transport simulations performed for dissolved or aqueous-phase contaminants of potential concern are discussed in this section. Volatile organic compound modeling is addressed in Section 5.3. Modeling for dual-phase radionuclides (i.e., radionuclides that partition from the aqueous phase into the gaseous phase) is discussed in Section 5.4. The model developed and implemented to represent movement of water and contaminants in the subsurface, called the remedial investigation and feasibility study (RI/FS) model, was derived from the model presented in the ABRA, referred to as the ABRA model. The predecessor model for the IRA, presented by Magnuson and Sondrup (1998), will be referred to as the IRA model.

The RI/FS model was improved to represent the current best interpretation of water movement and contaminant transport in the subsurface. The numerical model described in this section was developed and implemented to represent movement of subsurface water and contaminants after those contaminants are released from their disposal locations. This section presents a summary of the conceptual model, improvements compared to the ABRA model, the basis for parameters of the numerical model, and results of the numerical model in terms of moisture distributions and resulting contaminant concentrations. Complete details of the derivation of the model and supporting simulations that show the comparability of the model to observations of water movement and contaminant transport are provided by Magnuson and Sondrup (2006).

5.2.1 Dissolved-Phase Flow and Transport Conceptual Model

The general conceptual flow model treated water movement as though subsurface sediment were a heterogeneous, isotropic, porous medium. Net infiltration of meteoric water into the subsurface was described in the model by three constant rates representing areas of low, medium, and high infiltration

(Martian 1995). Surficial sediment and sedimentary interbeds were simulated with varying thicknesses and upper-surface elevations (Leecaster 2004). Only the three uppermost interbeds were considered in the conceptual model. These were the A-B, B-C, and C-D interbeds. Interbeds deeper than the C-D interbed, though present in reality, were not included in the simulations. The deeper interbeds are also discontinuous, based on the fewer number of wells to this depth, and it is conservative to neglect them.

For strictly dissolved-phase contaminant transport, flow in the fractured basalt portion of the subsurface was considered as occurring only in the fracture network to emulate an anisotropic medium with a low effective porosity and a high permeability. For contaminants that also partition into the gaseous phase, both the exchange of water between the fracture network and the basalt matrix, and flow within the basalt matrix were assumed to affect flow and transport.

Sources of water were considered to be constant, allowing steady-state assignment of boundary conditions. The exception was including three transient events to represent historical flooding of the SDA. Transient infiltration events in response to changes in daily and seasonal meteorological conditions were evaluated in the IRA model, and as long as an assumption of equilibrium reversible sorption was included, these transient simulations showed no difference from the steady-state simulation at depth in the vadose zone.

Water that infiltrates into the subsurface but does not contact buried waste serves primarily to dilute groundwater-pathway concentrations. Therefore, the effect of water migrating laterally at depth in the vadose zone from either Spreading Area A or B, or from the Big Lost River, was not included in the conceptual model. These additional sources of water were evaluated in the ABRA model and were found, primarily, to result in additional dilution for strictly dissolved-phase contaminants.

Movement of water in the aquifer was considered controlled by regional flow in the aquifer. Permeabilities were considered to be uniform vertically, and pressures in the aquifer were considered to be in hydrostatic equilibrium, implying predominantly horizontal flow in the aquifer. Because of the long simulation time durations of hundreds to thousands of years, movement of water within the Snake River Plain Aquifer was considered steady state. Neglecting transient influences in the aquifer, such as those that might occur from the spreading areas, is conservative because temporary changes in the direction of water velocity would result in additional dilution.

Movement of water and contaminants within the aquifer was considered controlled by the regional flow in the aquifer. Because of the long durations of hundreds to thousands of years simulated, movement of water within the Snake River Plain Aquifer was considered steady state.

The effective thickness of the Snake River Plain Aquifer was assumed to be 76 m (250 ft). Robertson, Schoen, and Barraclough (1974) derived this estimate from the depth where tritium was observed in wells downgradient of the injection well at the Idaho Nuclear Technology and Engineering Center. More recent evaluations of temperature profiles indicate that the effective thickness is greater (Smith 2002). With predominantly horizontal flow, using a thinner aquifer thickness is conservative because less dilution occurs.

Locally, groundwater flow was affected by a region of low permeability in the aquifer (Wylie and Hubbell 1994). This region has been identified in wells immediately south of the SDA. This low-permeability region may extend underneath the SDA, as evidenced by the estimated transmissivity from a recent pumping test in Well M17S, located centrally inside the SDA. Low velocities in the aquifer, as a result of including this low-permeability region, impact model results. As contaminants enter the aquifer from the vadose zone, less dilution occurs in gridblocks with low aquifer velocities, and simulated contaminant concentrations are higher than they would be if the aquifer velocity were greater.

The general conceptual transport model for dissolved-phase transport considered advection, dispersion, diffusion, radioactive chain decay and ingrowth, and sorption in the sediment portions of the simulation domain.

In the fracture network within the basalt and basalt-matrix portions of the simulations, no sorption was assumed. Sorption in surficial and interbed sediment was assumed to follow linear reversible isotherms that could be described by use of K_ds. Sediment K_ds were assigned based on best-estimate values rather than conservative screening values. A set of best-estimate K_ds from Holden and Broomfield (2004) was used in this application.

Facilitated transport mechanisms (e.g., colloidal transport) may affect contaminant migration in the SDA subsurface. Studies conducted of SDA interbed sediments have shown that very small fractions of plutonium and americium may move in a facilitated manner in the SDA. Grossman et al. (2001) showed that a very low mobile fraction forming from natural colloids in the soil (i.e., much less than 1%) was possible. Batcheller and Redden (2004) considered colloid formation from high-temperature processes and estimated that 3.7% of the waste stream could form colloids. This higher fraction is used for transport of Pu-239 and Pu-240 in the RI/BRA base case. Facilitated transport for Pu-239 and -240 was considered to occur in the source zone and through the surficial sediment and A-B interbeds. The deeper B-C and C-D interbeds were considered as not allowing this facilitated transport to continue downward through the vadose zone because the B-C and C-D interbeds were treated as continuous in the model. This resulted in mechanical filtration for these two isotopes at this depth (Batcheller and Redden 2004) because water velocities are assumed to slow at the interbeds. Several locations can be found where gaps in the B-C interbed exist inside the SDA (see Section 5.2.4.3.2), but the interpolation process (Leecaster 2004) results in nonzero thickness given the 76.2 × 76.2-m (250 × 250-ft) dimension of gridblocks for the B-C interbed. A sensitivity case is evaluated in Section 5.2.6 where the entire B-C interbed is neglected to bound the potential effects on transport of gaps in the B-C interbed.

Single isolated detections of contaminants in the aquifer have occurred in the SDA during monitoring of subsurface contaminants. Though these isolated detections may be indicative of contaminant transport, it is not feasible with the current modeling approach to try to emulate each one. Instead, the subsurface-transport model attempts to mimic the large-scale overall behavior of contaminants in the subsurface. This approach directs the model to emulate contaminants that are consistently present in a distributed manner in the subsurface. Contaminant monitoring in some locations in the vadose zone has identified likely trends in uranium, Tc-99, and nitrate. While not distributed adequately to be useful for calibration, these trends are compared against simulation results in this section.

Evaluation of aquifer contamination from upgradient sources in Section 2.3.4 concluded upgradient facilities may influence contaminant concentrations in the aquifer. The aquifer model ignores this possible influence and only considers regional background concentrations when making comparisons between simulated and observed results. Potential impacts from commingling plumes are the scope of the Operable Unit 10-08 Groundwater Modeling Project (DOE-ID 2004b).

5.2.2 Predecessor Models

The RI/FS model represents the culmination of a sequence of iterative modeling studies. The two previous iterations of three-dimensional modeling are the IRA model (Magnuson and Sondrup 1998) and the ABRA model (Holdren et al. 2002). Both are described briefly to provide context for the RI/FS model.

5.2.2.1 Interim Risk Assessment Model. The IRA model represented the first attempt to simulate flow and transport through the entire vadose zone and aquifer domains for an extensive suite of contaminants of potential concern. Calibration of vadose zone perched water behavior and an interpreted contribution to nitrate concentrations in the aquifer were attempted for the IRA model. Results were termed limited in their degree of success in emulating observed behavior. Attempts to improve calibration were hindered by lack of a widespread, well-behaved, identifiable plume in the vadose zone attributed strictly to dissolved-phase transport. Typically, contaminants in the vadose zone beneath the SDA (see Section 4) are either not detected or are detected at very low concentrations with no stable temporal trends; therefore, monitoring data that could be used to demonstrate transport of a dissolved-phase nonsorbing contaminant were extremely sparse. The IRA model was used to make a series of 10,000-year predictive aquifer simulations for 52 contaminants. Results of that modeling formed the basis for risk estimates in the IRA (Becker et al. 1998) and were used to screen contaminants for the ABRA.

Waste management personnel at the INL Site also used the IRA model to update both the Performance Assessment (Case et al. 2000) and Composite Analysis (McCarthy et al. 2000). The IRA model development, implementation, and results have undergone extensive review by Fabryka-Martin, Gee, and Flint (1999) and the U.S. Geological Survey (USGS) (Rousseau et al. 2005). Though reviews of the IRA model were generally complimentary, none concluded that the IRA model was satisfactory for developing conclusive predictions of the fate and transport of contaminants in the subsurface. The USGS review was by far the most extensive. The main comments from Rousseau et al. (2005) about modeling flow and transport of radionuclides at RWMC follow:

- Modeling performed for the IRA cannot necessarily be shown to be conservative
- Spatial variability of hydrologic and transport properties of the sedimentary interbeds should be evaluated, and impact of including this spatial variability into the IRA model should be assessed
- Impacts of additional sources of vadose zone water from the Big Lost River system on predicted contaminant concentrations should be evaluated
- Selected K_d values used in the IRA cannot be shown to be conservative because they do not account for (1) colloidal transport, (2) the enhanced actinide mobility fraction observed in column studies, (3) variations in mineralogy, (4) nonlinearity of isotherms, and (5) fluctuations in pore-water chemistry. Furthermore, K_d values taken from the literature cannot be shown to be representative of the SDA.

5.2.2.2 Ancillary Basis for Risk Analysis Model. The ABRA model was developed to respond to each of the USGS review observations, particularly the second and third bullets (Rousseau et al. 2005). The vadose zone and aquifer portions of the simulation domain were separated, allowing increased discretization in the vadose zone model. This improved discretization included a gridding method that used variable gridblock thicknesses to better conform to the topography of the interbeds. The lithologic selections included interpretations from 22 additional wells drilled in 1999. Sediment cores were collected from the B-C and C-D interbeds and analyzed for hydrologic and transport properties. These analyses allowed a spatial description of the hydrologic properties to be implemented in the ABRA model. The aquifer model was further calibrated to take advantage of seven new wells completed since publication of the IRA model.

Additional refinement in the vadose zone model allowed an improved resolution of waste streams in the source-release model, with a closer match between the infiltration rates assigned in the vadose zone model and those assigned in the source-release model. Twenty-four contaminants, which were all radionuclides with the exception of nitrate, were simulated with the ABRA model. Volatile organic compounds were not simulated with the ABRA model.

5.2.3 Overview of Improvements to the Ancillary Basis for Risk Analysis Model

Improvements on the ABRA model that are implemented in the RI/FS model are summarized in the following subsections. These improvements include corrections to the ABRA model, as well as refinements.

5.2.3.1 Corrections to the Ancillary Basis for Risk Analysis Model. Three errors in the ABRA model were discovered since publication of the ABRA report. These errors have been corrected in the RI/FS model and are discussed individually.

5.2.3.1.1 Vadose Zone Vertical Grid Extension—The bottom 27.4 m (90 ft) of the vadose zone simulation domain was inadvertently omitted from the ABRA. This 27.4-m (90-ft) portion represents fractured basalt and would, therefore, have had minimal impact on the simulation results because fractured basalt hydrologic-property parameterization ensures rapid water movement. Because only dissolved-phase transport was simulated in the ABRA, this rapid water movement also ensured rapid dissolved-phase transport. There would not have been any noticeable increase in contaminant travel times through the vadose zone if the 27.4 m (90 ft) had been included.

Because the RI/FS model includes vapor-phase transport, the missing 27.4 m (90 ft) would be potentially more important; therefore, the RI/FS model domain now correctly extends down to the bottom of the vadose zone, requiring additional gridblocks in the base vadose zone domain and slightly adds to the computational requirements for the RI/FS model.

5.2.3.1.2 Spatially Variable Interbed Porosity and Permeability—Kriged B-C and C-D interbed porosities and permeabilities were used in the ABRA. A row versus column indexing inconsistency in the assignment of permeabilities resulted in an incorrect permeability field for both the B-C and C-D interbeds. The kriged permeability fields from Leecaster (2002) are now correctly implemented in the RI/FS model. This error was also corrected. Additionally, Leecaster (2002) used minimum instead of average porosities from each location where core samples were evaluated for the B-C interbed evaluation. The spatial variability analysis and kriging of porosities onto the vadose zone model domains for the B-C and C-D interbed was reanalyzed for the RI/FS model with slightly higher averaged B-C interbed porosities. Magnuson and Sondrup (2006) include the reanalysis as an appendix. Neither of these errors was substantive in affecting simulation results presented in the ABRA.

5.2.3.1.3 Interface Between Source-Release and Vadose Zone Models—The source-release model requires a count of the number of gridblocks into which contaminant mass was loaded. In the ABRA, this number of gridblocks was slightly increased, but the information provided to the source-release model was not updated. The result was to slightly increase the mass input to the vadose zone model above what should have been applied.

An additional check was added to the software interface between the source-release and vadose zone models. This interface program processes source-release results into the format necessary for input to the vadose zone flow and transport model. The additional check ensures consistency between the numbers of gridblocks in both models and thereby verifies that mass out of the source model equals mass into the vadose zone model.

5.2.3.2 Aquifer Domain Extension. The 1E-05 risk isopleth at the time of maximum overall risk for a spatially-consistent receptor was not closed in the ABRA aquifer model domain (see Figure 6-31 in Holdren et al. 2002). Instead, this risk isopleth extended south of the INL Site boundary. For the RI/FS, the aquifer domain was extended southward and westward to ensure the 1E-05 risk isopleth would be closed. This task required adopting permeabilities from the Operable Unit 10-08 aquifer model[b] (McCarthy et al. 1995) for extended portions of the domain and interpolating new boundary conditions from Calendar Year 2000 water level data (i.e., the same that were used for the ABRA aquifer model calibration). Extension of the aquifer model domain is explained in detail in Appendix C of the Subsurface Flow and Transport Modeling report (Magnuson and Sondrup 2006).

5.2.3.3 Lithology Database Quality Assessment. An extensive effort to document selected lithologic contacts between sediment and basalt in the vadose zone and the thickness of the surficial sediment and sedimentary interbeds was conducted in support of the RI/FS modeling. Results of this effort are documented in the Updated Stratigraphic Selections for the SDA Wells (Ansley, Helm-Clark, and Magnuson 2004). During this effort, the previous stratigraphic selections by Anderson et al. (1996) were verified to be correctly entered into the data files used for the RI/FS spatial variability and kriging analysis. The primarily effort, however, was in reevaluating the lithologic selections for each well drilled since 1995, and in making new selections for wells drilled since publication of the ABRA report through March 2003. The basis for the lithologic selection for each well was reviewed and reinterpreted, as necessary, using suites of geophysical logs as the primary basis and driller lithologic logs as a last resort. This prioritization method resulted in several occurrences where nonzero thickness locations used for the ABRA became zero thickness locations for the RI/FS model and vice versa. These occurrences are highlighted in Table A-1 of Ansley, Helm-Clark, and Magnuson (2004). After lithologic selections were finalized, the spatial variability analysis and kriged surfaces and thicknesses of the sedimentary features were updated (Leecaster 2004) for the Operable Unit 7-13/14 vadose zone RI/FS model.

5.2.3.4 No Spreading Area Influence in the Vadose Zone. The ABRA model included a steady-state influence of additional water above the C-D interbed to emulate the effect of the spreading areas. Sensitivity simulations, without this additional water, presented in the ABRA showed that the effect of the additional water was to dilute the resulting aquifer concentrations for contaminants that underwent dissolved-phase transport. This finding was most applicable for contaminants with long half-lives that do not undergo substantial decay during transit of the vadose zone. Since short-lived contaminants, such as Sr-90 and Cs-139, are not evaluated for groundwater pathway in the RI/FS, it is appropriate that the RI/FS model does not include this additional spreading-area water above the C-D interbed.

5.2.3.5 Reduction of Infiltration Rate Assigned inside the Subsurface Disposal Area. Three infiltration rates were assigned to different regions inside the SDA in the ABRA model. These rates represented low-, medium-, and high-infiltration rates and were based on inverse modeling to neutron probe access tube measurements documented in the UNSAT-H Infiltration Model Calibration report (Martian 1995). The high infiltration rate of 24.1 cm/year (9.5 in./year) was based on results from three locations that had extremely high infiltration rates due to the neutron-probe access tubes being located in areas of low topography (e.g., near ditches). Excluding these three infiltration rates from the Martian (1995) estimates resulted in an upper-bound or high infiltration rate of 10.0 cm/year (3.9 in./year), which was judged more appropriate for an upper bound on infiltration through the waste.

---

b. The updated INL Site-wide aquifer model, in preparation for Operable Unit 10-08, will maintain consistency with simulated SDA-vicinity water velocities from the Operable Unit 7-13/14 RI/FS model in accordance with the INL Groundwater Model Work Plan (DOE-ID 2004b).

5.2.3.6 Facilitated Transport of Plutonium-239 and Plutonium-240. Facilitated transport mechanisms (e.g., colloidal transport) may affect contaminant migration in the SDA subsurface. In the ABRA, facilitated transport was considered only as a sensitivity case. As recommended by Batcheller and Redden (2004), facilitated transport for a portion of the Pu-239 and -240 inventory in the buried waste was adopted in the base-case model by assigning a K_d of 0 mL/g for the source zone, surficial sediment, and the A-B interbed. Batcheller and Redden (2004) further concluded that plutonium would sorb to the deeper B-C and C-D interbeds, inhibiting continued downward transport through the vadose zone.

5.2.3.7 Revision of Sediment Distribution Coefficients. Distribution coefficient values used in the RI/FS model were reassessed. In the methodology used for the batch tests (Fjeld, Coates, and Elzerman 2000), on which several of the values in the ABRA were based, the fraction of soil samples that were greater than 250 μm was removed before testing. Using only finer sediment particles in the batch tests introduced a bias in the results that overestimated the distribution coefficients. Using a weight ratio of the sieved fraction to the estimated total sample weight, an Environmental Protection Agency recommended method (EPA 1999) was used to adjust distribution coefficients downward for actinium, americium, plutonium, and thorium. Distribution coefficients for uranium and neptunium were revised upward based on the results of batch tests measured on soil cores from wells drilled in Fiscal Year (FY) 2003 (Leecaster and Hull 2004). The complete list of final distribution coefficients for the RI/FS modeling appears in Section 5.2.4.4.2.

5.2.3.8 Gaseous-Phase Simulation of Carbon-14 and Volatile Organic Compounds. Carbon-14 was simulated as a purely dissolved-phase contaminant in the ABRA, resulting in overestimated groundwater-pathway transport because two processes were neglected that allowed C-14 to escape the vadose zone through land surface. These processes were (1) partitioning of C-14 into the gaseous phase, which allows part of the C-14 mass to diffuse through the upper land surface boundary, and (2) gaseous-phase advection through that same boundary in response to changes in barometric pressure. In addition to simulating dissolved-phase movement of C-14, the RI/FS model also includes partitioning of C-14 into the gaseous phase, which accounts for these losses to the atmosphere.

Volatile organic compounds were not simulated for the ABRA. Instead, VOCs were estimated by scaling the IRA (Becker et al. 1998) model results by the ratio of an updated inventory to the previous inventory. Current inventories were used for the RI/FS model, and the updated RI/FS model was used to simulate VOC transport. Calibration was performed using carbon tetrachloride measurements from the extensive vadose zone gas-port monitoring network and data from the groundwater monitoring network. The calibration was performed primarily by adjusting tortuosity values, but much of the information gained from calibrating the IRA model was used in the RI/FS model. Another calibration parameter was the fractured basalt permeability horizontal-to-vertical anisotropy ratio. This ratio was changed from 30:1 used in the ABRA model to 300:1. This change helped to match the observed spreading of carbon tetrachloride in the vadose zone, and demonstrated the link between the flow model and the transport model for carbon tetrachloride. The VOC transport model also included the effects of air drilling and vapor vacuum extraction.

5.2.4 Baseline Model Development and Description

Development and parameterization of models used to simulate flow and transport in the subsurface are described in this section, which also includes a complete list of assumptions. The vadose zone model is described first, followed by the aquifer model.

5.2.4.1 Assumptions. This section lists all assumptions that resulted from the conceptual model (discussed previously) or that were necessary to develop the subsurface model. Assumptions are divided into flow and transport categories. Most of these assumptions were the same as those used in developing the ABRA model. These assumptions were applied only to modeling dissolved-phase subsurface flow and transport. Assumptions relative to source-term modeling and VOC modeling are included in Sections 5.1 and 5.3, respectively.

5.2.4.1.1 Flow-Modeling Assumptions

- Infiltration is spatially variable inside the SDA and is greater than infiltration that occurs outside the SDA because of disturbed soil profiles with reduced vegetation inside the SDA.

- The spatially variable infiltration description from Martian (1995), adapted for the ABRA model, is adequate for base-case modeling.

- The higher infiltration rates, beginning in 1952, are implemented as though they were effective across the SDA.

- The background infiltration rate outside the SDA, through undisturbed vegetated sediment, is 1 cm/year (0.4 in./year).

- Initial conditions obtained from simulating a background infiltration rate of 1 cm/year (0.4 in./year) for 300,000 days (approximately 820 years) are adequate for representing the vadose zone beneath the SDA.

- The amount of water entering the SDA from the three historical floods is adequately estimated by Vigil (1988).

- Duration of infiltration from each of the historical flooding events is 10 days.

- Infiltration patterns in the SDA will remain the same indefinitely into the future for the base-case simulations and will be revised for feasibility study cases to reflect the impact of an infiltration-reducing cover.

- The high-infiltration rate assigned over parts of the SDA by Martian (1995) is sufficient to account for occasional flooding of the SDA that may occur in the future for the base-case simulations.

- The surficial sediment and sedimentary interbeds have spatially variable lithologic surfaces and thicknesses that influence water and contaminant movement.

- Interbeds below the C-D interbed are thin and discontinuous and do not significantly affect flow and transport near the SDA. Neglecting these deeper interbeds is conservative with respect to maximizing the groundwater-pathway concentrations.

- Hydrologic properties in the surficial sediment and A-B interbed are homogeneous. Hydrologic properties in the B-C and C-D interbeds are heterogeneous and varied spatially.

- The B-C and C-D interbeds have a low-porosity, low-permeability feature at their upper surface, which indicates either sediment within the interbed or the effect of fracture infilling by fine-grained sediment in the low-permeability basalt immediately above the interbed. (Though this feature was included in the subsurface model and discussed in detail in the IRA and ABRA modeling text, it was not specifically identified as an assumption.)

- Waste has the same hydrologic properties as the surficial sediment.

- Flow in fractured porous basalt is controlled by the fracture network and is adequately represented as an anisotropic high-permeability, low-porosity, equivalent-porous continuum using a Darcian description.

- The field-scale hydraulic properties for fractured basalt were adequately described through inverse modeling by Magnuson (1995) for the large-scale infiltration test.

- Any effect of water from the Big Lost River discharged to the spreading areas, on water movement in the vadose zone beneath the SDA, is neglected. (In the ABRA, the effect of this influence was shown to primarily dilute concentrations for contaminants with long half-lives in the vadose zone and the aquifer. Not including the spreading area influence is conservative with respect to maximizing the groundwater-pathway concentrations.)

- Water movement in the aquifer is treated as steady state. Possible influences of discharges from the Big Lost River to the spreading areas do not influence flow in the aquifer in the immediate vicinity of the SDA.

- Water levels corrected for borehole deviations from FY 2003 are adequate for calibrating the Snake River Plain Aquifer model and are representative of long-term, steady-state conditions.

- Within the aquifer, pressure is in hydrostatic equilibrium and water movement is predominantly horizontal.

- A continuous region of low permeability exists locally in the aquifer, south and southwest of the SDA, that affects local flow directions.

- The effective thickness of the Snake River Plain Aquifer is 76 m (250 ft) (Robertson, Schoen, and Barraclough 1974).

5.2.4.1.2 Transport Modeling Assumptions

- Field-measured concentrations of contaminants are generally representative and valid, based on data quality requirements associated with sampling activities. Single, isolated detections of contaminants are anomalous and not representative because contaminants are not consistently present.

- Advection, dispersion, diffusion, sorption, and radioactive decay are the only processes that influence dissolved-phase contaminant movement in the subsurface beneath the SDA.

- A linear equilibrium reversible distribution coefficient is representative of all geochemical processes that occur between contaminants dissolved in water and sediment. All available site-specific information was used to determine appropriate contaminant-distribution coefficients.

- Aqueous-phase concentrations remain at low environmental levels and preclude competition between contaminants for sorption sites.

- Distribution coefficients are homogeneous in the interbeds.

- Sorption does not occur in fractured basalt portions of the vadose zone and aquifer.

- Facilitated transport occurs in the vadose zone above the B-C interbed for Pu-239 and Pu-240. These isotopes undergo sorption within the B-C and C-D interbeds (Batcheller and Redden 2004).

- No upgradient INL Site facilities influence aquifer contaminant concentrations near the SDA, with the exception of nitrate, which has an estimated local background concentration of 1.4 mg/L.

- Feasibility study remedial alternatives will address (1) all estimated contamination retained in the waste at the time of treatment and (2) all contamination previously released that is still within the surficial sediment portion of the vadose zone model.

5.2.4.2 Simulation Code. The TETRAD computer code (Vinsome and Shook 1993), Version 12.7 ms, was used for the RI/FS to simulate flow and transport. The TETRAD code has complete multiphase, multicomponent simulation capabilities and can mimic the behavior of any number of components in aqueous, gaseous, oleic, and solid phases. The TETRAD code has dual-permeability capabilities, which allow movement of components in a coupled fracture-matrix system. When dual permeability is invoked, water and contaminants move in both the aqueous and gaseous phases in both the fracture network and the basalt matrix. This dual-permeability feature was used in the RI/FS model to simulate movement of VOCs and C-14.

The TETRAD Version 12.7 code previously was used for the IRA and ABRA models. Before conducting modeling for the RI/FS, an evaluation exercise was performed to determine whether TETRAD was still the most appropriate code to use. This exercise resulted in a recommendation to continue using TETRAD for groundwater-pathway simulations for the RI/FS (Appendix C of Holdren and Broomfield 2004).

The TETRAD 12.7 ms simulator is a proprietary code, and its use constitutes an off-the-shelf application by modeling staff from the INL Site. Quality control for these types of simulations consists of ensuring that results are reproducible. This requires archiving the version of the simulator, the model inputs, model outputs, and processing codes used to create the inputs and outputs. An extensive searchable electronic archive is maintained by the Operable Unit 7-13/14 Project for this purpose. A description of this archive is contained in Appendix B of Magnuson and Sondrup (2006).

5.2.4.3 Vadose Zone Flow Model

5.2.4.3.1 Horizontal Domain Extent and Discretization—The same vadose zone horizontal domain and discretization was used in the RI/FS model as was used in the ABRA model. The extent of the vadose zone domain is shown in Figure 5-7. This horizontal extent was judged adequate to simulate flow and transport without undue influence from horizontal no-flux boundaries.

Horizontal gridding for the final vadose zone domain is shown in Figure 5-8. Two concentric levels of refinement are used to obtain adequate grid resolution in the SDA. The largest horizontal grids are 152.4 m (500 ft) on a side, and the smallest gridblocks are 38.1 m (125 ft) on a side. Selection of the grid domain required a balance between the objectives of maximizing the extent of the domain so that outlying wells (e.g., Wells M7S, M15S, and M16S) could be included, while still obtaining sufficient resolution in the SDA for representing disposal locations and geologic and hydrologic features. Some outlying wells were not encompassed in the vadose zone simulation domain. The final domain extent was adequate to simulate transport without undue influence from the horizontal no-flux boundaries, which would otherwise truncate further horizontal spreading of water and contaminants in the vadose zone.

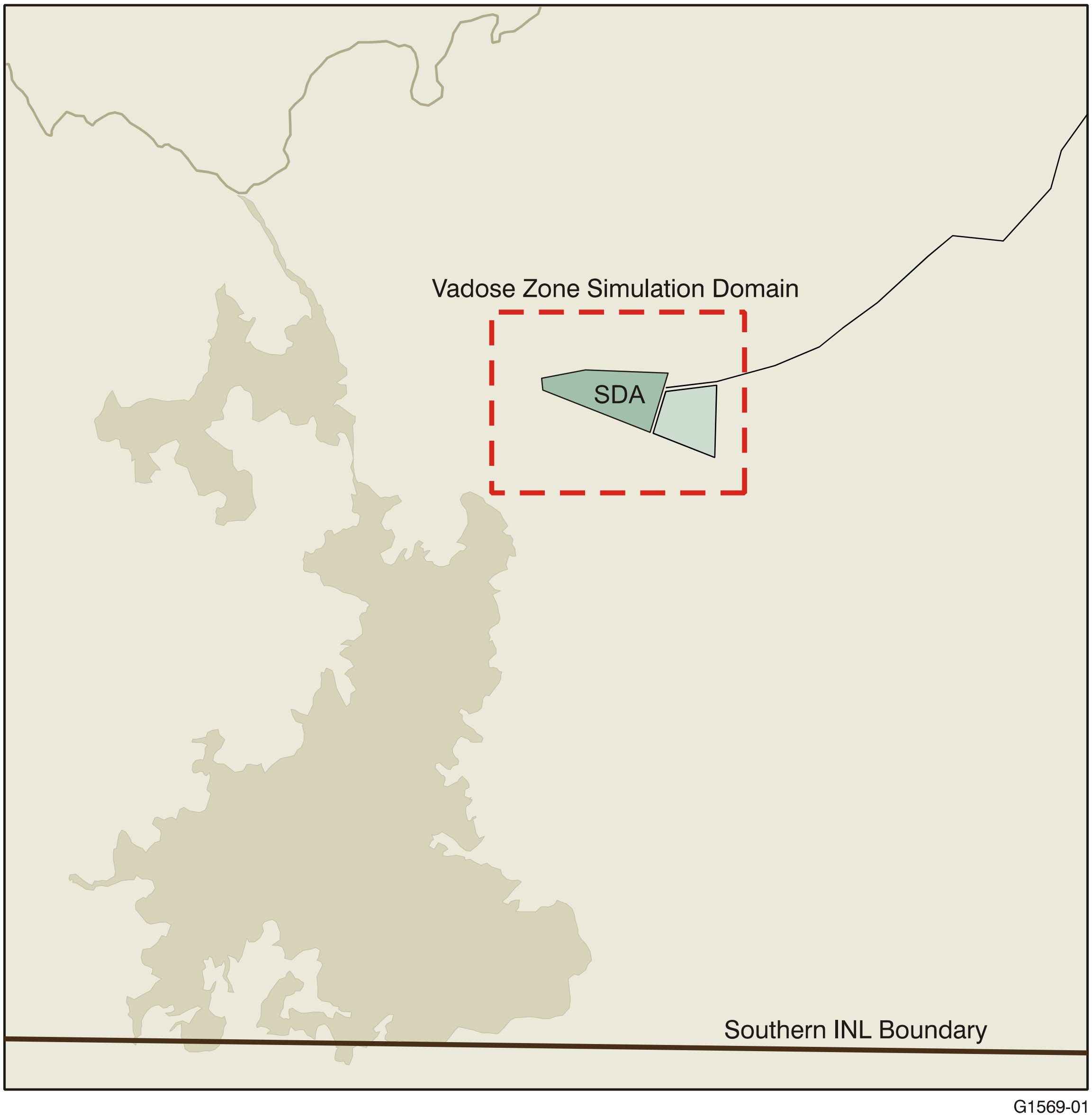

Figure 5-7. Horizontal domain for remedial investigation and feasibility study vadose zone flow and transport.

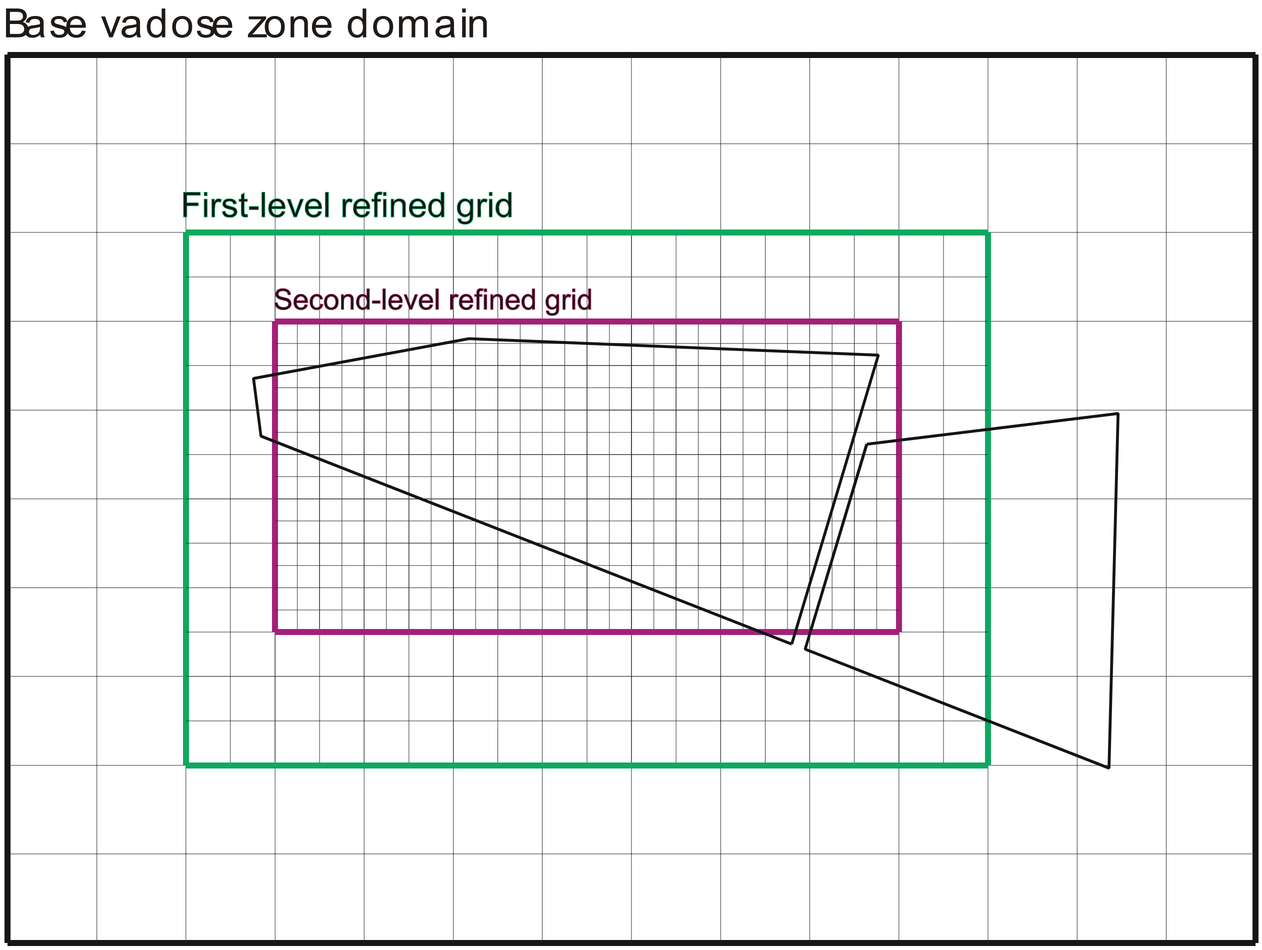

Figure 5-8. Horizontal discretization for the vadose zone model domain.

5.2.4.3.2 Lithologic Assignment—An extensive effort to document selected lithologic contacts between sediment and basalt in the vadose zone and the thickness of the surficial sediment and sedimentary interbeds was conducted in support of the RI/FS model. The results of this effort are documented in Ansley, Helm-Clark, and Magnuson (2004). During this effort, previous interpretations by Anderson et al. (1996) were verified to be correctly entered into the data files used for the spatial variability and kriging analysis. The primary effort, however, was in reevaluating lithologic selections for each well drilled since 1995 and in making new selections for wells drilled since publication of the ABRA through March 2003. The basis for the lithologic selection at each well was reviewed and reinterpreted as necessary using suites of geophysical logs as the primary basis and driller lithologic logs as a last resort. Table B-1 in Ansley, Helm-Clark, and Magnuson (2004) is the stratigraphic database for 134 wells deeper than the surficial sediment; this database is the foundation from which the RI/FS vadose zone model lithology is derived.

After lithologic selections were finalized, the spatial variability analysis and kriged surfaces and thicknesses of the sedimentary features were updated for the Operable Unit 7-13/14 vadose zone model (Leecaster 2004). Surfaces and thicknesses for surficial sediment and the A-B, B-C, and C-D interbeds were kriged for the base and refined grids. The kriged surfaces and thicknesses are shown in Figures 5-9 through 5-16. The kriged results generally honor the data, with limited exceptions where both zero and nonzero thickness observations exist within a single grid. This is a result of single values being estimated for each grid and the smoothing that results from kriging. All lithologic selections were used in the

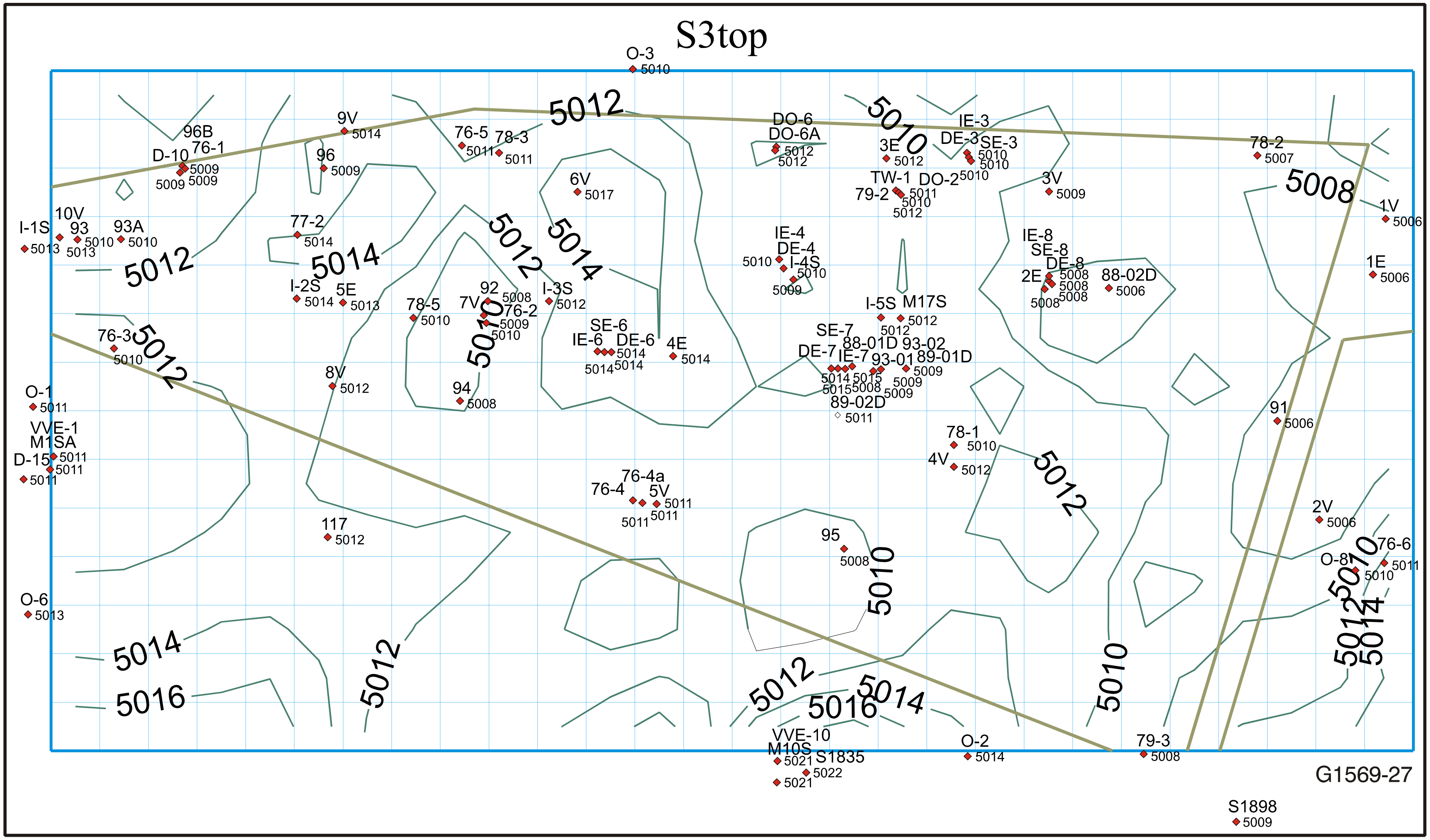

Figure 5-9. Kriged ground surface elevation (feet above mean sea level) for the second-level refined grid.

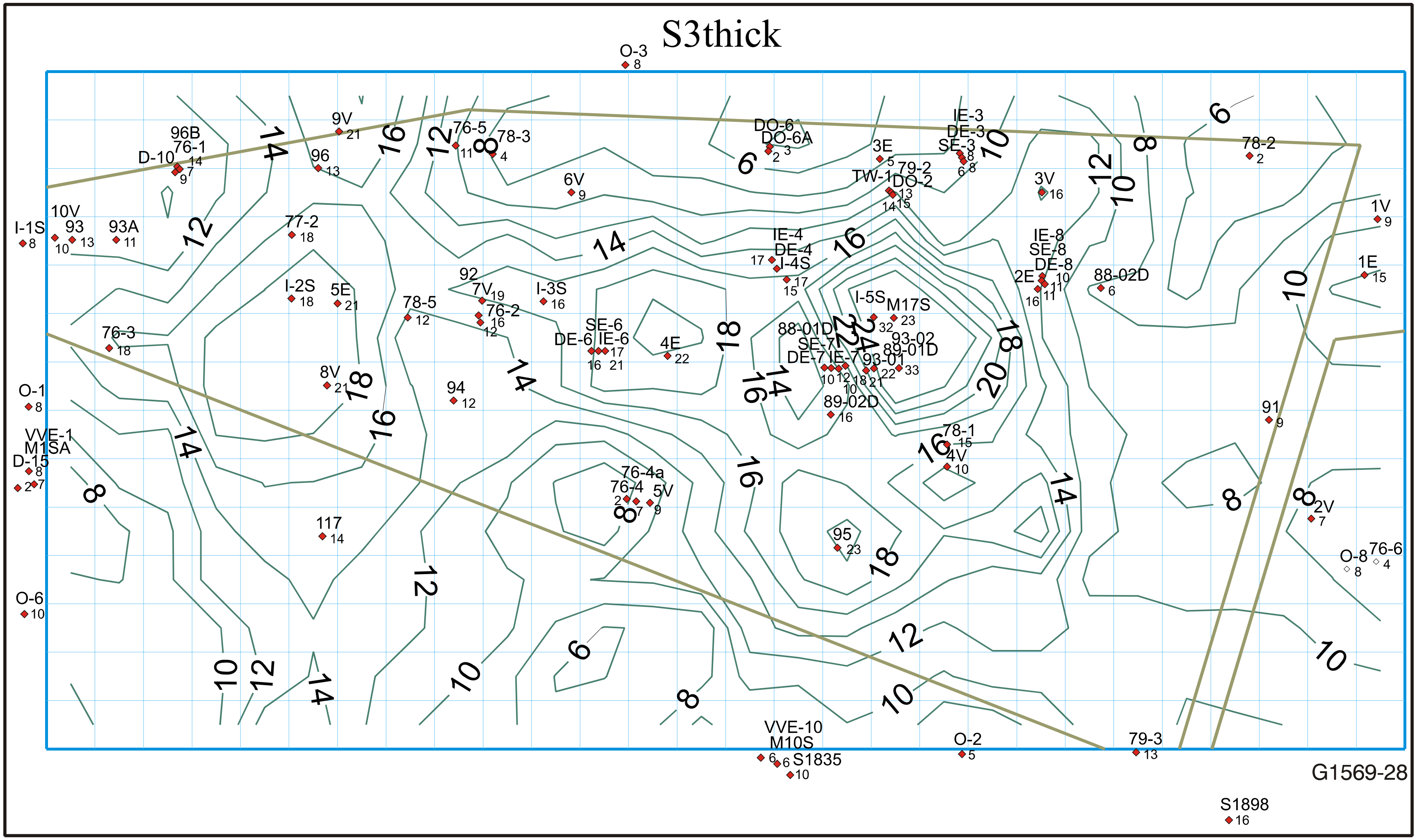

Figure 5-10. Kriged thickness (feet) of surficial sediment for the second-level refined grid.

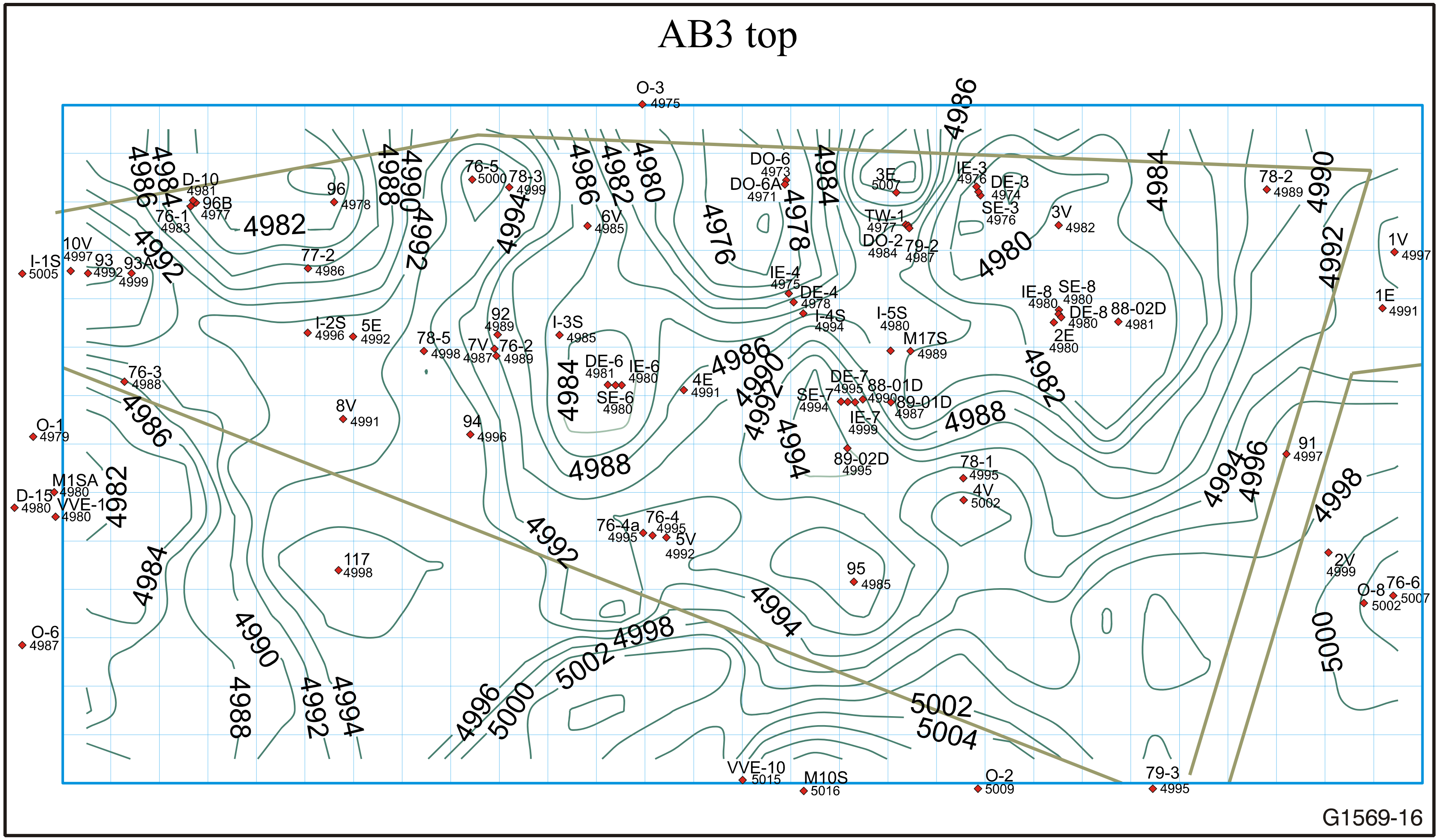

Figure 5-11. Kriged surface (feet above mean sea level) of the A-B interbed for the second-level refined grid.

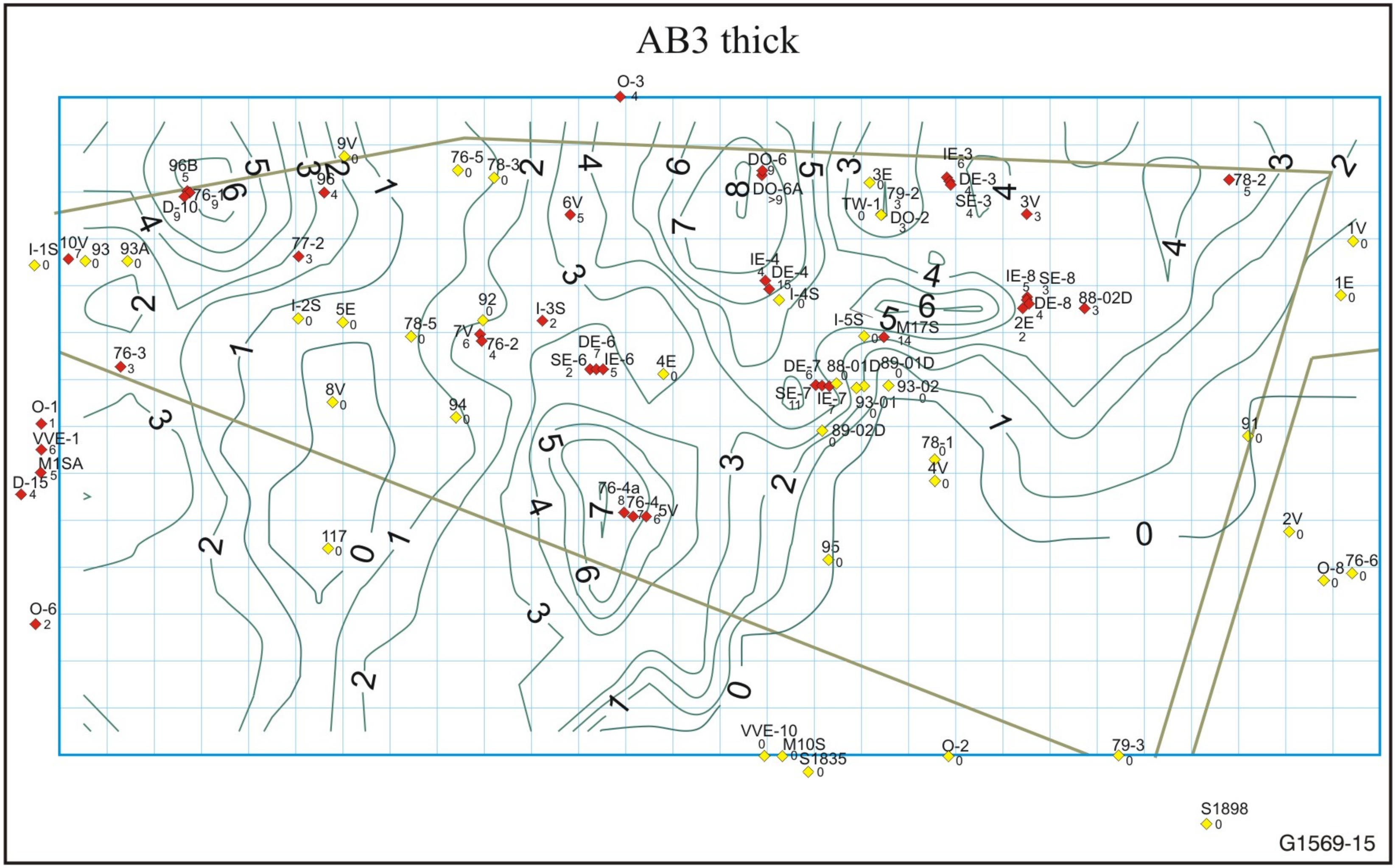

Figure 5-12. Kriged thickness (feet) of the A-B interbed for the second-level refined grid. Yellow symbols mark the locations where the A-B interbed is absent.

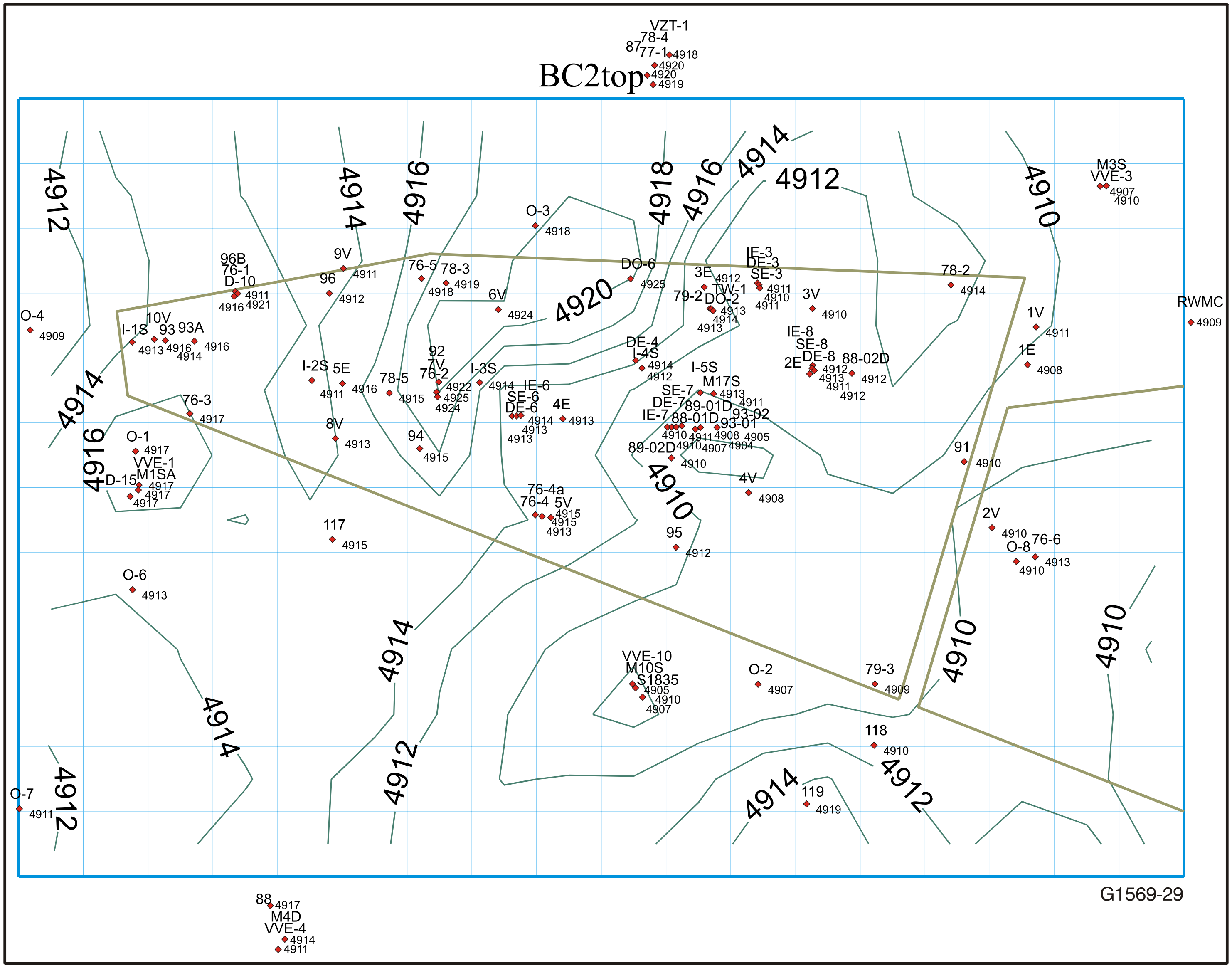

Figure 5-13. Kriged surface (feet above mean sea level) of the B-C interbed for the first-level refined grid.

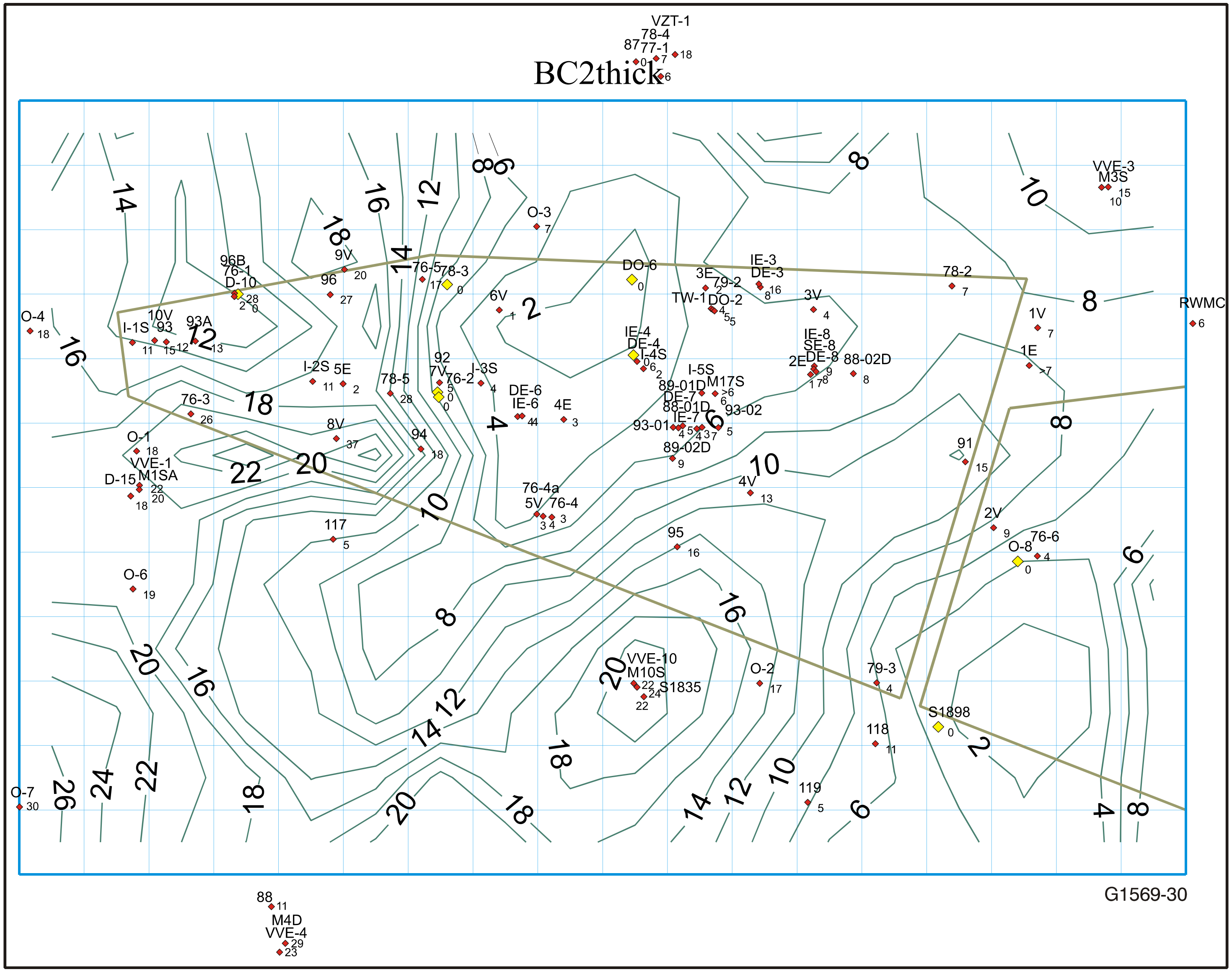

Figure 5-14. Kriged thickness (feet) of the B-C interbed for the first-level refined grid. Yellow symbols mark the locations where the B-C interbed is absent.

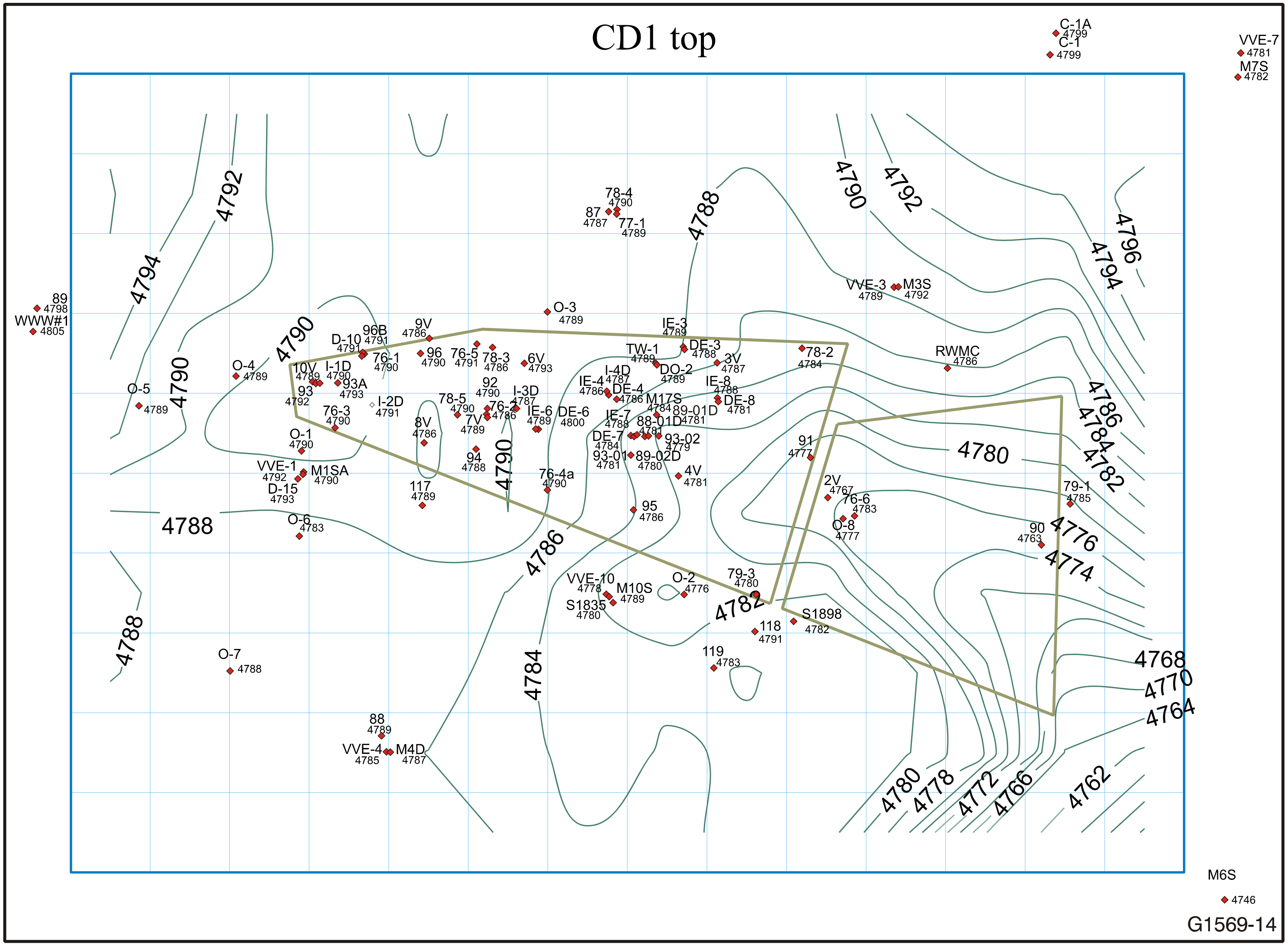

Figure 5-15. Kriged surface (feet above mean sea level) of the C-D interbed for the base grid. Note the trough leading southeasterly from the Subsurface Disposal Area toward Well M6S.

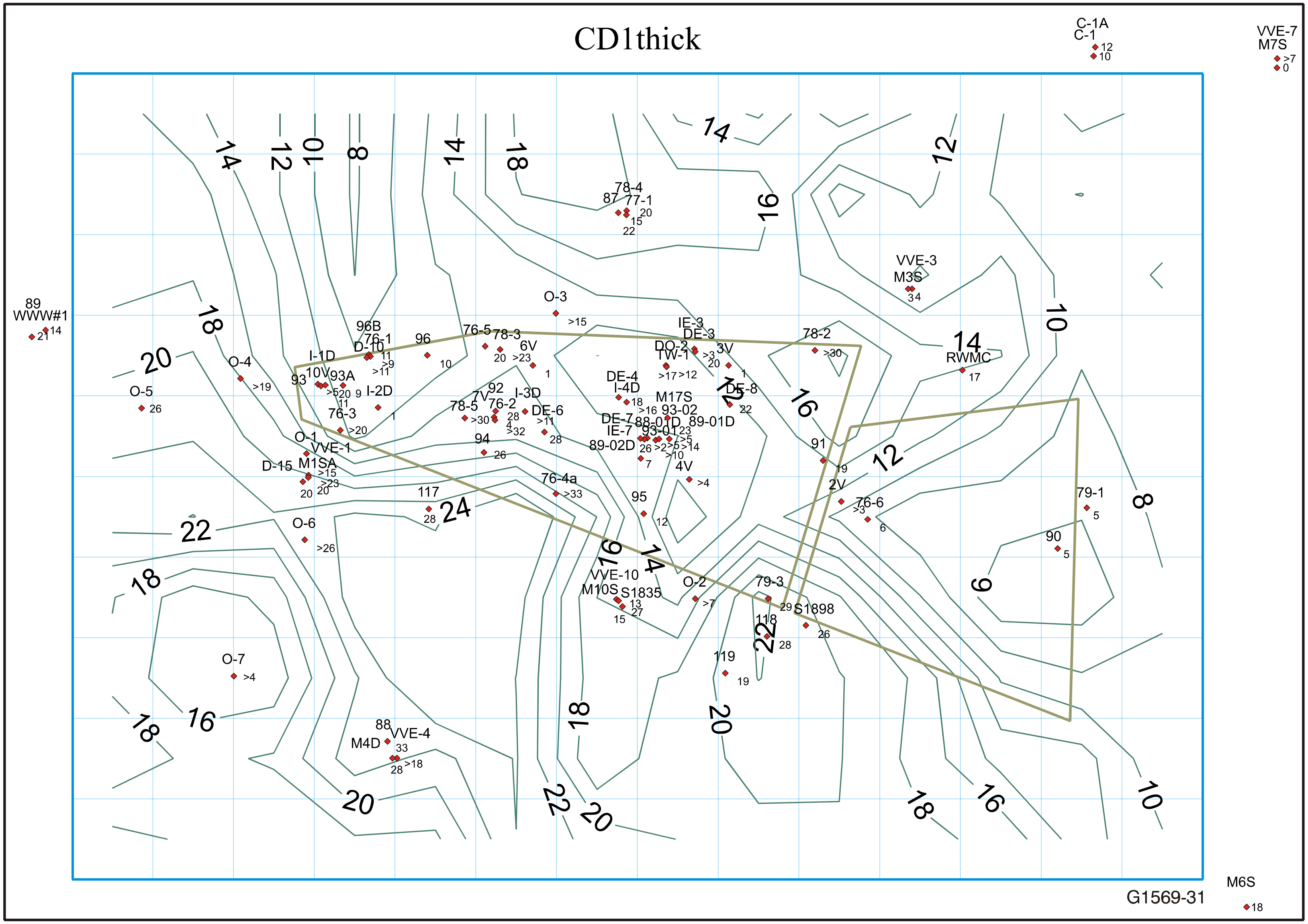

Figure 5-16. Kriged thickness (feet) of the C-D interbed for the base grid.

kriging process without introducing bias by selectively removing locations with nonzero thickness when zero thickness locations were nearby. The A-B interbed has two extensive contiguous regions of gridblocks where the kriged thickness was zero, which are indicated by the zero contour line in Figure 5-12. These regions persist through the kriging because of the large number of wells with strictly zero thickness. Although it may be confusing to see an interpreted upper surface of the A-B interbed when that interbed is interpreted to be absent (compare Figure 5-11 to Figure 5-12), no A-B interbed is found in model gridblocks inside the zero contour line indicated in Figure 5-12. The upper surface appears contiguous and nonzero everywhere in Figure 5-11 because the lithologic database (Ansley, Helm-Clark, and Magnuson 2004) contains information on contact between the A and B basalt flows and treats the contact as the upper surface of the A-B interbed where it is not present.

Both surface shape and thickness of each of the sedimentary features impact movement of water and contaminants through the subsurface. In particular, an interpreted trough or channel in the upper surface of the C-D interbed—that develops in the eastern half of the SDA and then extends to the southeastern corner of the domain—influences water and contaminant movement above and through the C-D interbed.

5.2.4.3.3 Vertical Conformable Gridding—The next step in development of the RI/FS vadose zone model was vertical discretization of the base simulation domain. The kriged lithologic surfaces from Leecaster (2004) were used in conjunction with the horizontally discretized domains to create a conformable vertical grid. A minimum vertical grid size, maximum vertical grid size, and geometric factor for increasing vertically adjacent gridblocks were assigned for each lithologic unit in the base vadose zone domain. Minimum grid size was 0.5 m (1.6 ft) for each of the sediment and basalt units, except for the A-B interbed, where a minimum grid size of 0.4 m (1 ft) was assigned. The geometric factor for the ratio between successive vertical gridblocks was a maximum of 1.5, which is a commonly used ratio to ensure numerical accuracy. Maximum vertical gridblock size was 3 m (9.8 ft) in the sediment units and 10 m (33 ft) in the basalt. Logic for adjusting vertical gridblock sizes was applied vertically at each horizontal gridblock location to allow for an optimum match of the gridblock interfaces to the kriged surface elevations. By having the same minimum gridblock size specified for both sediment and basalt features, uniformity of gridblock sizes was ensured across lithologic interfaces. The total number of vertical gridblocks determined through this process was 80 at each horizontal location for the base vadose zone simulation domain. The upper surface of the vadose zone simulation domain was variable and was determined from the kriged elevation for the surficial sediment. The lower surface of the vadose zone simulation domain was assigned as a flat plane at the water table. As discussed previously, this assignment was correctly implemented for the RI/FS model as opposed to the ABRA model, where the plane was assigned at an elevation 27.5 m (90 ft) above the aquifer.

The logic for vertical grid discretization was different for the refined areas. Vertical discretization for the base domain was not adjusted further, based on the kriged elevations in the refined grids. Rather, the kriged elevations for the refined grids were compared to the conformable vertical discretization determined from the base grid, and then, as necessary, the material properties assigned in the refined domains were adjusted. This process resulted in smooth grid interfaces in the base domain and some degree of stair stepping in the refined grids. This can be seen in Figure 5-17, which shows three-dimensional views of resulting grids, starting with the base grid and ending with the second-level grid refinement. The A-B interbed appears black in the base grid as a result of fine vertical discretization. These three-dimensional views are distorted both horizontally and vertically because the software (Visual Numerics 2001) that produces the views projects onto a cube. The outline of the SDA is shown in each case projected just above the cube.

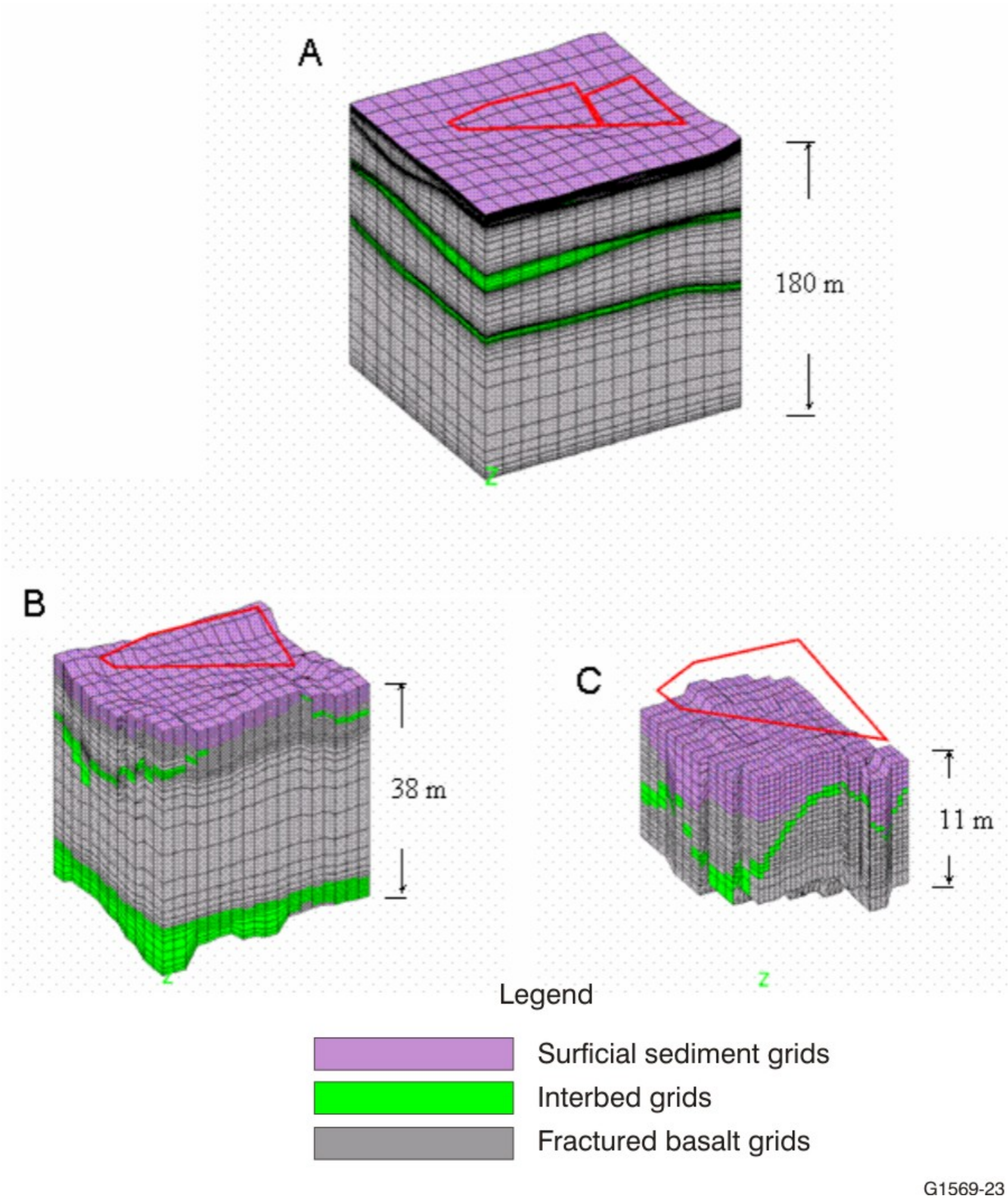

Figure 5-17. Southwest views of base grid (A), first-level refined grid (B), and second-level refined grid (C) beneath the Subsurface Disposal Area showing vertical conformable gridding. The A-B interbed appears black in the base grid as a result of fine vertical discretization.

One special-case modification was made to lithologic assignments once the conformable grid was built. At a subset of grid locations in the second-level refined grid that represented the LLW pits (i.e., contiguous Pits 17 through 20), the region assigned as surficial sediment was extended downward 9.1 m (30 ft) from the top of the model to represent the approximate depth of these pits.

5.2.4.3.4 Hydrologic Property Assignment—Hydrologic properties for porosity and permeability of the surficial sediment and the A-B interbed were assigned the same properties as the ABRA model (see Table 5-18) because no new information was available for these units. The fractured basalt porosity and vertical permeability were the same as the ABRA. The fractured basalt horizontal permeability was increased one order of magnitude from the value used in the ABRA and is now assigned a value of 90,000 mD. This increase was identified as part of the carbon tetrachloride transport calibration (see Section 5.3).

Table 5-18. Parameterization of hydrologic properties and source of parameters for surficial sediment, A-B interbed, and fractured basalt.

Parameter	Permeability	Porosity	Source of Parameters
Surficial sediment	680 mD, isotropic	0.50 cm^3/cm^3 (Martian 1995)	Average of calibrated properties in Martian (1995)
A-B interbed	4 mD	0.57 cm^3/cm^3 (Magnuson and McElroy 1993)	Waste Area Group 3 modeling in Rodriguez et al. (1997)
Fractured basalt	300 mD vertical and 90,000 mD horizontal	0.05 cm^3/cm^3 (Magnuson 1995)	Magnuson (1995)

Parameters assigned for the van Genuchten moisture characteristic curve were based on the average of four SDA surficial sediment samples that were hydraulically characterized and reported in Baca et al. (1992) and McElroy and Hubbell (1990). The values for residual moisture content, van Genuchten alpha, and van Genuchten N were 0.142 cm^3/cm^3, 1.066 m^{-1}, and 1.523 (dimensionless), respectively. These values were the same as those used in the ABRA model. In the TETRAD model, the residual water saturation is entered rather than the residual water content. The residual water saturation calculated from the GWSCREEN defaults is 0.292, and this value was used in the RI/FS model for all sediment features. The appropriateness of assigned hydraulic properties was evaluated by Magnuson and Sondrup (2006) by comparing simulated water potentials to observed water potentials in the B-C and C-D interbeds for a range of van Genuchten N parameters. The simulated values showed good agreement to the measured distribution of water potentials.

Moisture characteristic curve parameters for fractured basalt in the RI/FS model were slightly different from those used for the IRA and ABRA models. Two parameters in the analytic expression used for relative permeability of the fractured basalt portions of the simulation domain are the residual water saturation and a parameter that controls the amount of curvature. For the ABRA, the values for residual water saturation and the amount of curvature were 0.0 and 1.001, respectively. In the RI/FS model, these two parameters are assigned values of 0.01 and 2.0, respectively. The reason for the change was to take advantage of faster simulations that resulted from different parameters. Either parameterization results in rapid movement of water down through the fractured basalt, as discussed by Magnuson and Sondrup (2006). The simulation speedup from this change, approximately a factor of 2, resulted from less numerical overshoot and undershoot behavior for gridblocks near saturation in the iterative solution. The nearly linear slope of the water saturation relative-permeability curve—with the amount-of-curvature parameter set to 1.001—resulted in the iterative solution overshooting and then undershooting the correct solution when water saturation approached unity. These overshoots resulted in additional iterations to obtain a mass-convergent solution.

Kriged permeability fields for the B-C and C-D interbeds are shown in Figure 5-18. The kriged porosity fields for the B-C and C-D interbeds are shown in Figure 5-19. Only the most refined grid for each interbed is shown, although kriging results were provided in Leecaster (2002) for all base and refined grids. For these grids, the average of the kriged porosities for the B-C and C-D interbeds were 0.354 and 0.428, respectively, for these grids.

Similar to the ABRA and IRA models, a low-permeability value of 1 mD and a low-porosity value of 0.05 were assigned to the top gridblocks representing both the B-C and C-D interbeds. This was accomplished by identifying the uppermost gridblock representing these interbeds in the grid with the greatest level of refinement, and then assigning the low-porosity and low-permeability value to that gridblock and the next two interbed gridblocks beneath it for a total of three low-permeability, low-porosity gridblocks. The three low-permeability, low-porosity gridblocks were used to emulate the thicker, single low-permeability low-porosity gridblock used in the IRA model, and was necessary for the RI/FS model carbon tetrachloride calibration (see Section 5.3). This low-permeability feature represents either a low-permeability sedimentary feature at the top of the interbeds or, more likely, a low-permeability feature caused by fine sediment infilling of fractures in the basalt immediately above the interbed. The latter occurs from deposition of entrained sediment fines as infiltration continues to occur through overlying basalt emplaced after formation of the interbeds. Inclusion of this low-permeability, low-porosity feature was necessary to achieve simulated conditions close to saturation at locations within the interbeds and to facilitate spreading of carbon tetrachloride in the vadose zone as part of the transport calibration.

An artifact of this assignment of low-permeability, low-porosity gridblocks is shown in Figure 5-20, which portrays the maximum simulated porosity for the first level of grid refinement for the B-C interbed. A variable number of vertical gridblocks represent the B-C interbed at each location. In Figure 5-20, the actual maximum simulated porosity, after the low-permeability, low-porosity gridblocks were implemented, was queried at each horizontal location. These values are posted in Figure 5-20 within each gridblock. Then these maximums values are contoured using the same intervals as in Figure 5-19. Two thinner regions of the B-C interbed show up in this plot. These are regions where the maximum porosity is 0.05 and occurs because the number of vertical gridblocks in these regions was three or less and therefore, the entire interbed thickness was assigned the low-permeability, low-porosity value. Also posted in Figure 5-20 are the average value of the maximums (i.e., 0.32) and the overall average of all the B-C interbed (i.e., 0.21). These values show the effect of the assigned low-permeability, low-porosity gridblocks in lowering porosity. For clarification, although hydrologic properties were assigned differently in the low-permeability, low-porosity portions of the interbeds, distribution coefficients were assigned to these portions consistently with the rest of the interbeds.

5.2.4.3.5 Boundary and Initial Conditions—Aqueous-phase surface boundary conditions for the vadose zone model primarily consist of assigning surface water fluxes. Two types of water fluxes were imposed on the simulation domain representing steady-state conditions and historical flooding conditions. Gaseous-phase boundary conditions of atmospheric pressure were also applied across the upper surface of the domain to prevent pressure building up in the subsurface during infiltration events.

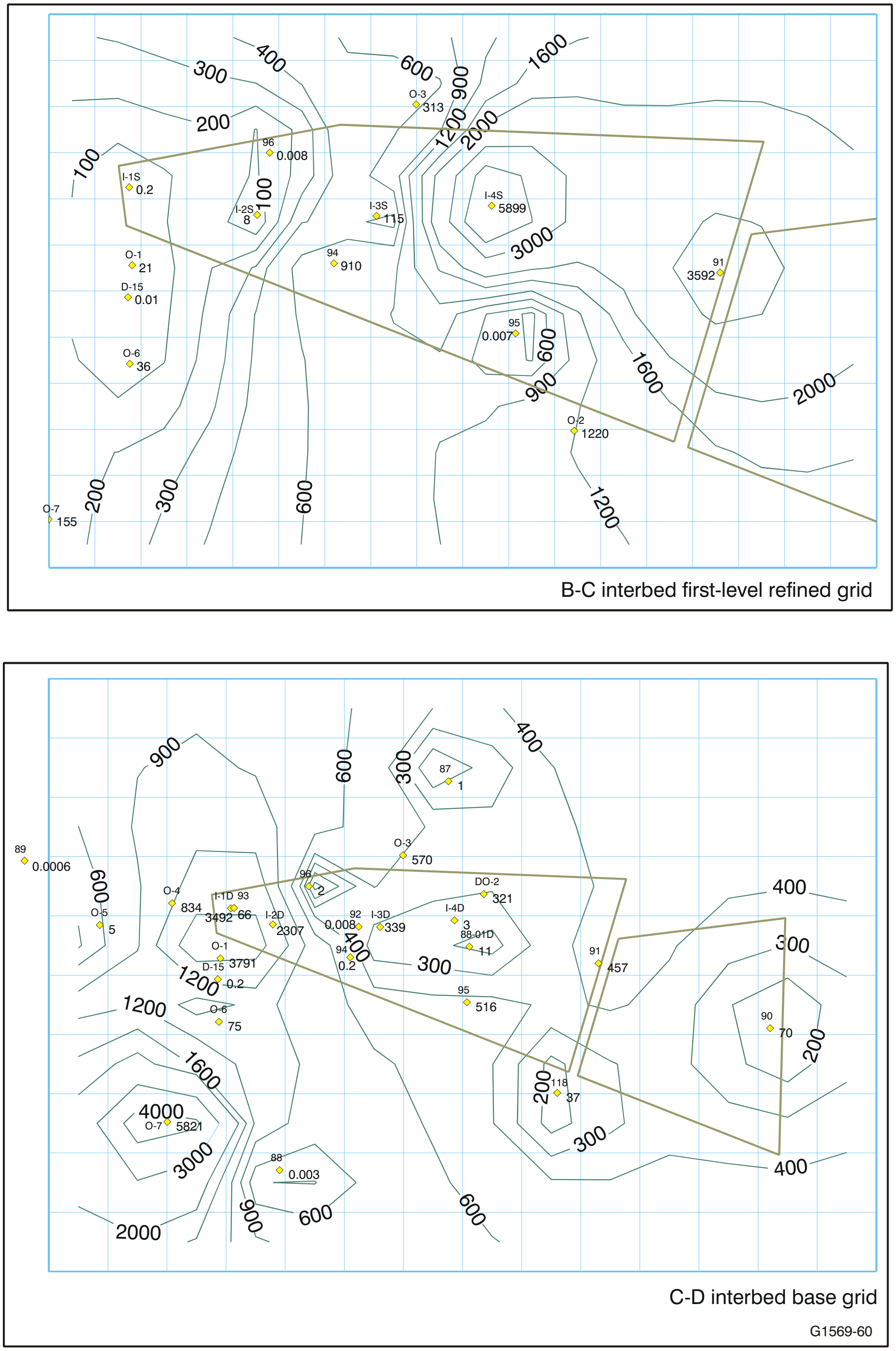

Figure 5-18. Kriged permeability (millidarcy) for the B-C and C-D interbeds. Measured values from core samples are indicated at their respective locations.

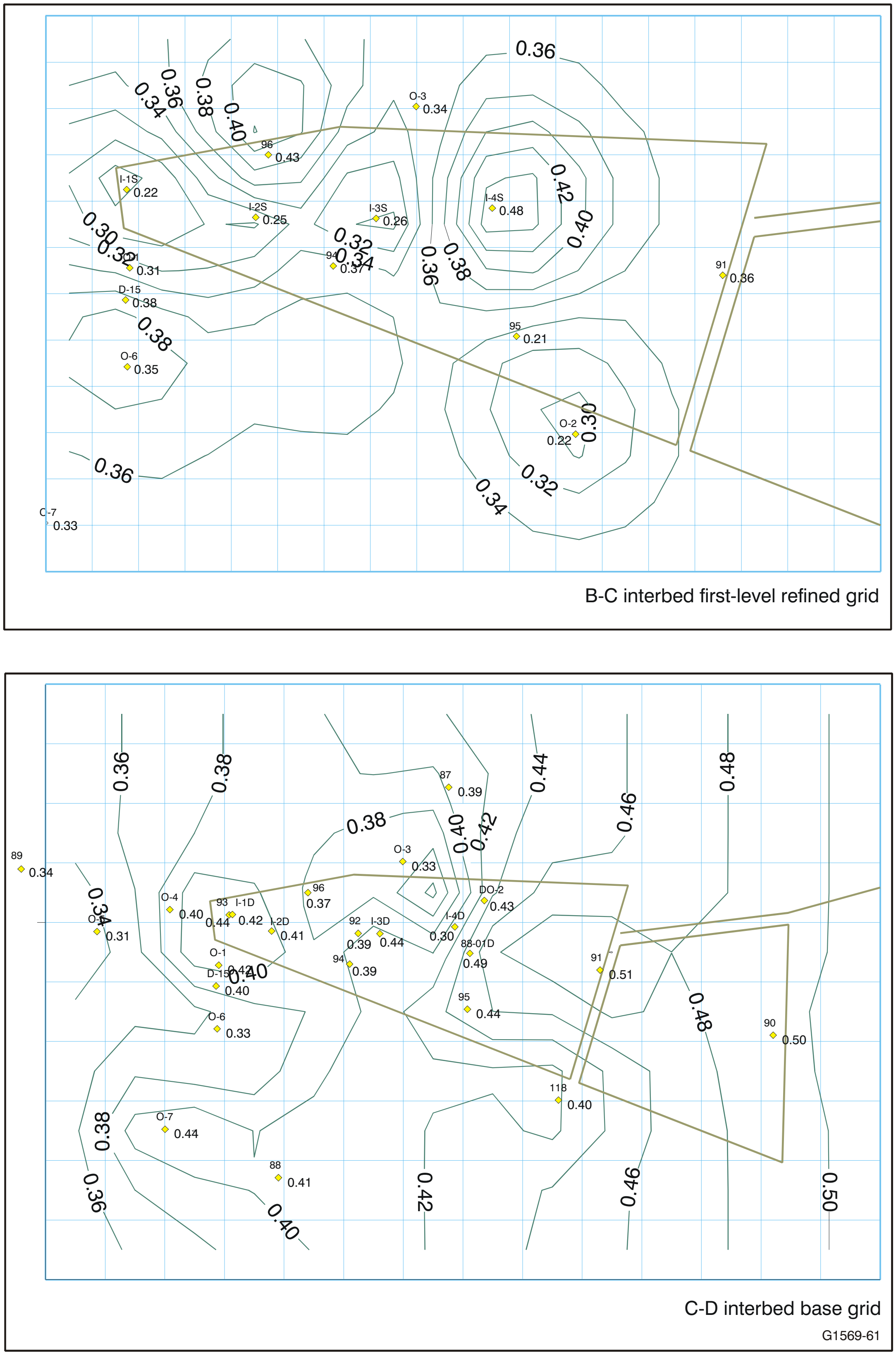

Figure 5-19. Kriged porosity for the B-C and C-D interbeds. Measured values from core samples are indicated at their respective locations.

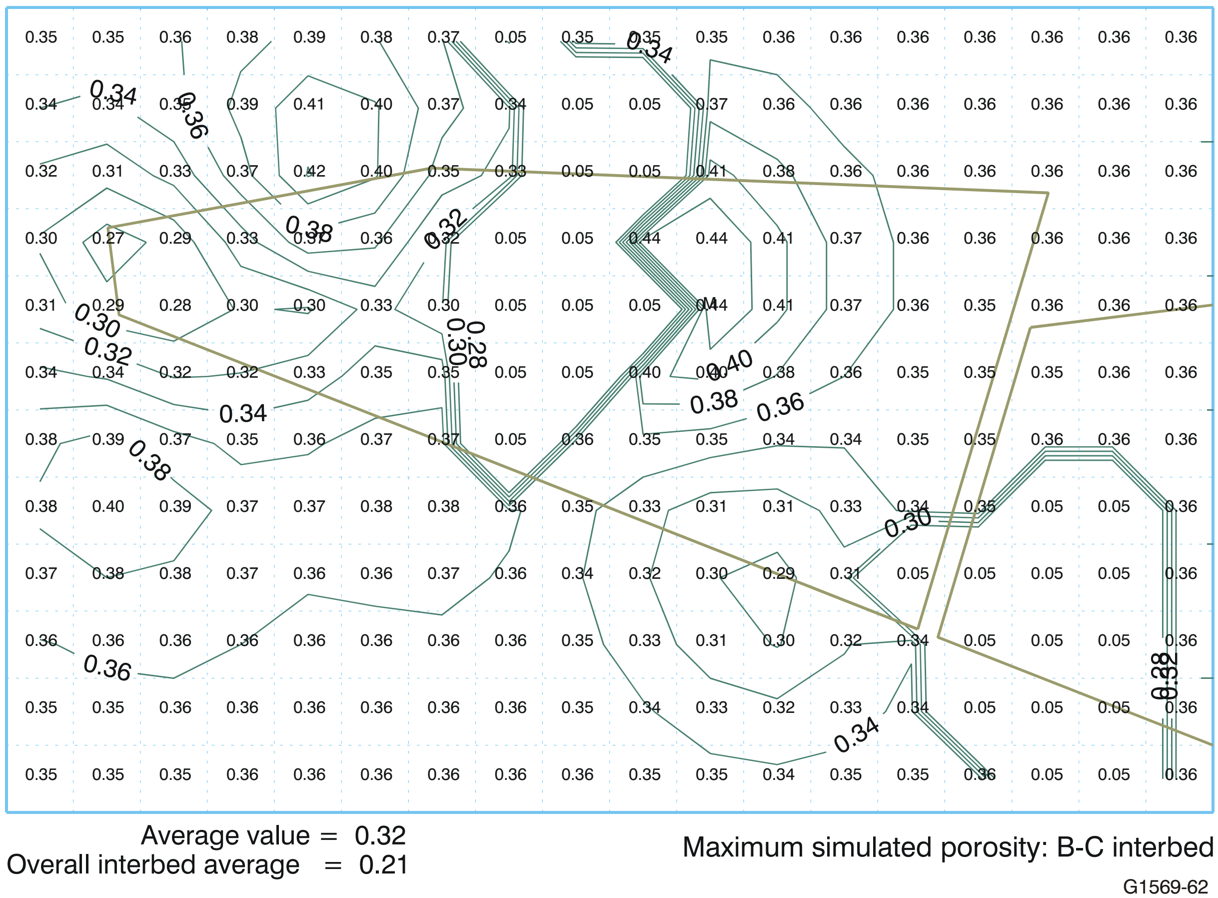

Figure 5-20. Maximum simulated porosity for the B-C interbed.

As with the ABRA model, three infiltration rates were assigned to different regions inside the SDA for the RI/FS model. These rates represented low-, medium-, and high-infiltration rates and were based on inverse modeling to neutron probe access tube measurements from Martian (1995). The spatial assignment was modified slightly, based on preliminary inverse modeling of moisture contents from Type B probes within the waste. The modeling is termed preliminary because it was determined the moisture content results were impacted by thermal influences and were not finalized. Despite the preliminary and qualitative nature of the inverse-modeling infiltration estimates, the infiltration values for the gridblocks containing Type B soil moisture, resistivity, and temperature Probes Pit5-TW1, MM2-3, and 741-08 were changed to the high-infiltration rate. Figure 5-21 shows the resulting distribution of the three assigned infiltration rates across the SDA.

In the RI/FS, the value assigned for the high-infiltration rate was changed to 10.0 cm/year (3.9 in./year), rather than the 24.1-cm/year (9.4-in./year) value used in the ABRA model. The high ABRA infiltration rate of 24.1 cm/year included the effect of three locations that had extremely high-infiltration rates due to the neutron probe access tubes being located in areas of low topography (e.g., ditches) (Martian 1995). Excluding these elevated infiltration rates resulted in a high-infiltration rate of 10.0 cm/year (3.9 in./year), which was judged more representative of upper-bound water infiltration through waste in the SDA. The change in the high-infiltration rate from 24.1 to 10.0 cm/year (9.4 to 3.9 in/year) resulted in a reduction in the overall average assigned infiltration across the SDA from 8.5 cm/year (3.3 in./year) in the ABRA model to 5.0 cm/year (1.9 in./year) in the RI/FS model.

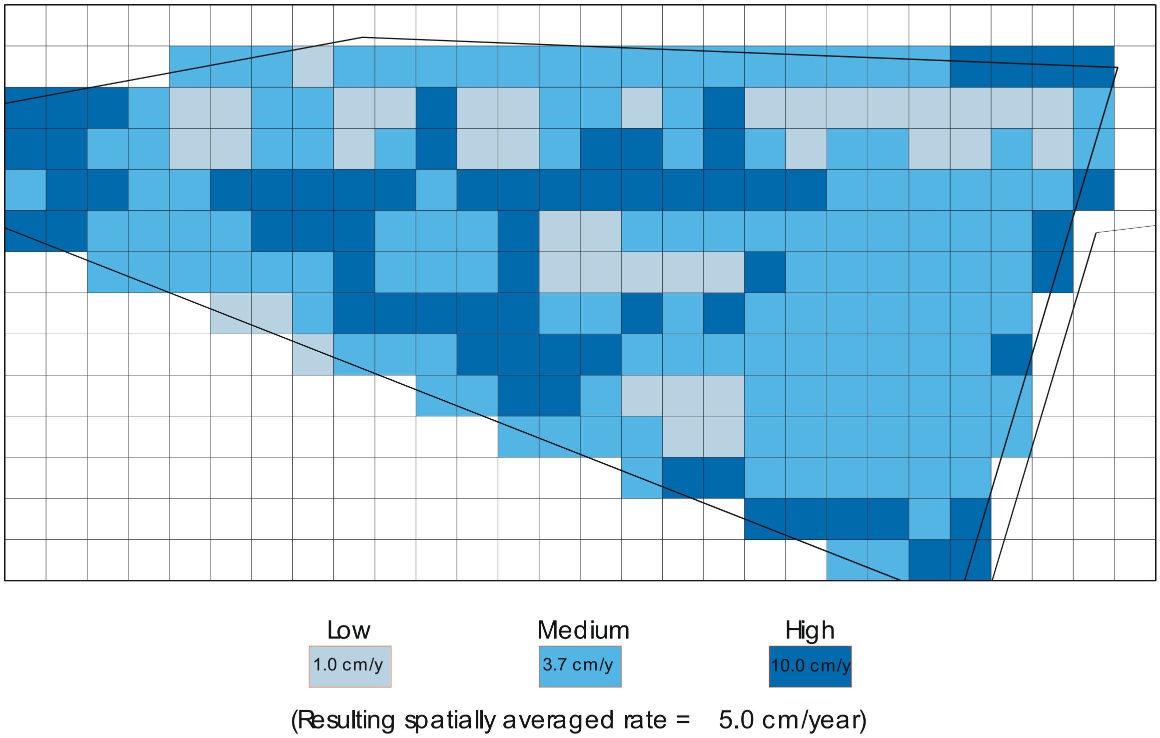

Figure 5-21. Spatially variable infiltration assignment for the model domain inside the Subsurface Disposal Area.

The horizontal discretization of the SDA in the RI/FS model limits the extent that infiltration can be assigned on a site-specific basis. High infiltration through ditches or temporary collapse features that focus infiltration are beyond the scope of the modeling. When considering transport from buried waste, the infiltration rates need to be assigned based on what infiltration is likely to be through the waste, rather than infiltration through ditches near roads.

Outside the SDA, surface infiltration was assigned the same rate of 1 cm/year (0.4 in./year) that was used in the ABRA modeling, based on Cecil et al. (1992).[c]

Three historical flooding events have occurred in the SDA (see Section 2.2.8) and were included in the RI/FS model, essentially using the same method as the IRA model, but with slight differences caused by differences in gridding. Figure 5-22 shows locations where additional water was imposed at the surface for the 1962, 1969, and 1982 floods, respectively. Estimates of the amount of water that entered the SDA for each of the floods were taken from Vigil (1988) and are shown in Table 5-19. Each flood was assumed to last 10 days. The locations selected for the 1962 flood exclude the gridblocks representing Pit 3, which was open and flooded in 1962 (see Section 2.2.8). However, because the source-release model does not include the effect of the floods, this omission has no substantial effect.

The lower boundary of the vadose zone domain was assigned a vapor-static atmospheric pressure to emulate a water table condition. Water and tracer components (i.e., contaminants) in the water could freely advect out through the bottom boundary of the simulation domain.

---

c. This surface-infiltration-rate estimate is expected to decrease based on an ongoing reevaluation by INL Site scientists.

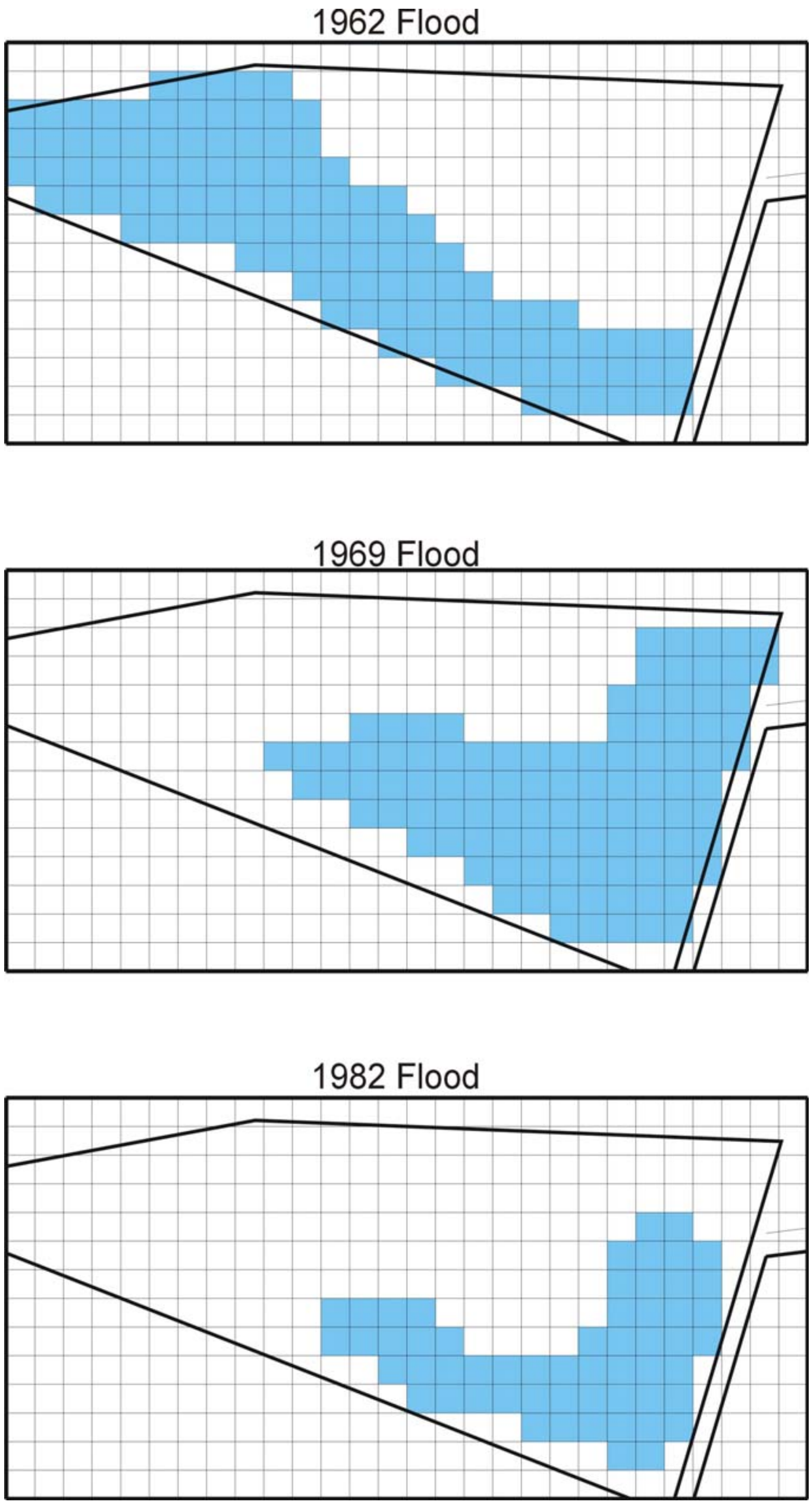

Figure 5-22. Locations of additional water supplied by the 1962, 1969, and 1982 flooding events in the Subsurface Disposal Area in the second-level refined grid.

Table 5-19. Historical flooding volumes and application rates at the Subsurface Disposal Area.

Year	Estimated Volume (acre-ft)	Infiltration Rate (m/day)
1962	30	2.26×10^{-2}
1969	20	1.68×10^{-2}
1982	8.3	1.24×10^{-2}

Default no-flux boundaries were allowed for all horizontal or lateral sides of the simulation domain. This was different from the ABRA, because no influence from the spreading areas was included at the western boundary above the C-D interbed. Although the USGS tracer test (Nimmo et al. 2001) showed that there can be an influence above the C-D interbed, when that influence was included in the ABRA model, it only served to dilute simulated groundwater-pathway concentrations for long half-life radioactive contaminants that migrated strictly as dissolved in the aqueous phase. Therefore, the influence of the spreading areas was not included in the RI/FS modeling.

Initial conditions for all simulations were obtained by assigning an initial water saturation of 50% to the entire simulation domain. Then the simulation was run for 300,000 days (approximately 820 years) to let the system come into equilibrium. Water saturation in the C-D interbed was monitored to determine whether equilibrium had been obtained. Figure 5-23 shows the simulated time history of water saturation at a location at the top of the C-D interbed, located centrally beneath the SDA. Initially, this gridblock wets up as excess water in the fractured basalt from above the interbed moves into and through the interbed. After the first approximate 50 years, change in saturation was negligible, indicating that steady-state conditions had been achieved.

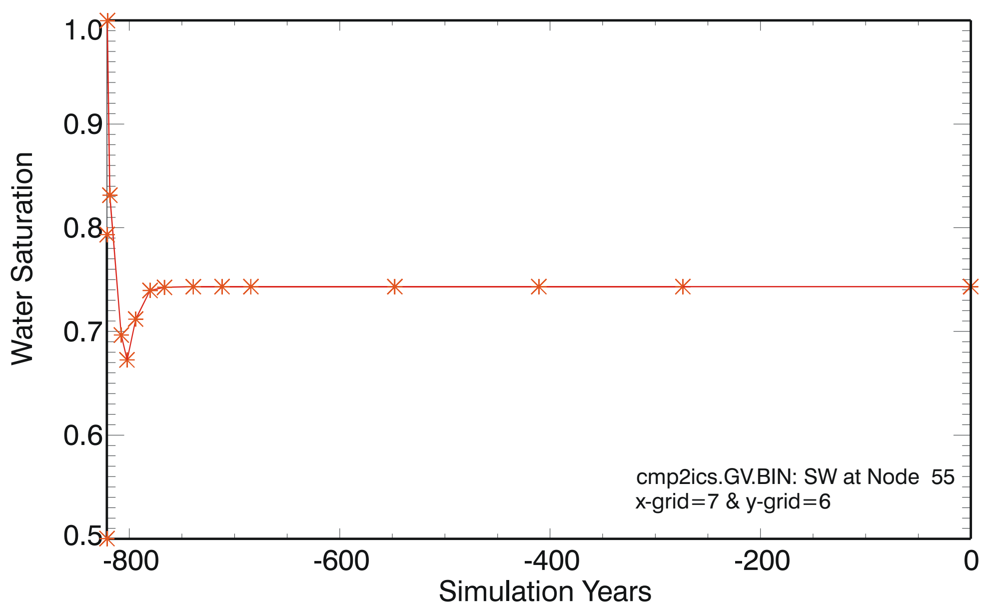

Figure 5-23. Initial-condition simulation showing the time history of water saturation in the C-D interbed beneath the Subsurface Disposal Area.

5.2.4.3.6 Results of the Vadose Zone Flow Model Simulation— This section provides selected results from the vadose zone flow model for moisture contents and vertical water fluxes. Results are presented as plan views for the B-C and C-D interbeds to illustrate the spatial distribution of simulated interbed saturations and water fluxes. Comparisons of simulated water potentials to measurements are provided by Magnuson and Sondrup (2006).

Figure 5-24 shows the RI/BRA base-case maximum simulated water saturation in 2001 for the B-C and C-D interbeds for the first-level refined grid and base grid, respectively. The simulation results for 2001 reflect steady-state saturations well after the 1982 flood. The wettest simulated regions with water saturation greater than 0.9 are shaded. Figure 5-24 was generated by reviewing, sequentially, each horizontal gridblock location and determining the maximum value—water saturation in this case—vertically in all gridblocks representing an interbed. These maximums are then contoured. The minimum and maximum from these maximum values, the average of these maximum values, and an overall average of the entire interbed also are posted at the bottom of Figure 5-24.

All well locations in these two interbeds, where perched water has been detected at least once, are shown in red for comparison (see Figure 5-24). At least one simulated area of elevated moisture content agrees with known perched water locations. Simulation results were not calibrated to improve the agreement with the areas that show perching. Rather, the results are compared to perched water locations to show that simulation results represent the character in the observed spatial variability in observed perched water where discrete locations with perched water and also locations without exist. Caution must be used in interpreting the locations with perched water because the wells were not all drilled at the same time. Wells 92, 93, and 96 were drilled in 1972; Well D-10 was drilled in 1987; and Wells 9V and 10V were drilled in 1994. The remaining indicated wells conveniently use the construction year as the first part of the well name. Wells 93 and 96 were abandoned shortly after drilling because their only purpose was for characterization. Thus, no indication is available as to whether perched water is ephemeral or constant at these locations. No strict correlation exists between when the wells that resulted in perched water were drilled and the amount of precipitation that was received in the year before drilling. Some wells were drilled during periods of normal or above-average precipitation, and some were drilled in periods of below-average precipitation. Not shown on Figure 5-24 is the larger number of wells for which perched water was not observed. These are not shown, partially because in many cases the method of drilling may have precluded observing perched water.

As with the ABRA model, less-than-obvious control is exerted by the presence or absence of the A-B interbed. The A-B interbed is largely absent in the southeastern portion of the SDA, and this is the most extensive region of elevated water saturation in the simulation results. This region continues farther down in the vadose zone in the C-D interbed but is shifted southeasterly due to the slope of the C-D interbed. The effect of the trough or channel in the upper surface of the C-D interbed is reflected in the extreme southeastern corner where saturated conditions develop, in the simulation, due to water accumulating in that gridblock when the lateral no-flow boundaries are encountered. One other interesting occurrence of near-saturated conditions occurs at the western boundary in the B-C interbed. This region of elevated saturation occurs also as a result of the A-B interbed. However, instead of the A-B interbed being absent above this region, two pronounced depressions in the topography of the A-B interbed focus flow from the extreme western part of the SDA. Some less-pronounced depressions also are in the B-C interbed and further serve to focus water movement at this western extreme. Lastly, perched water has been observed continuously in Well 92 since it was drilled in 1972. In the RI/BRA simulation results, the location containing Well 92 is still in a region of lower water content.

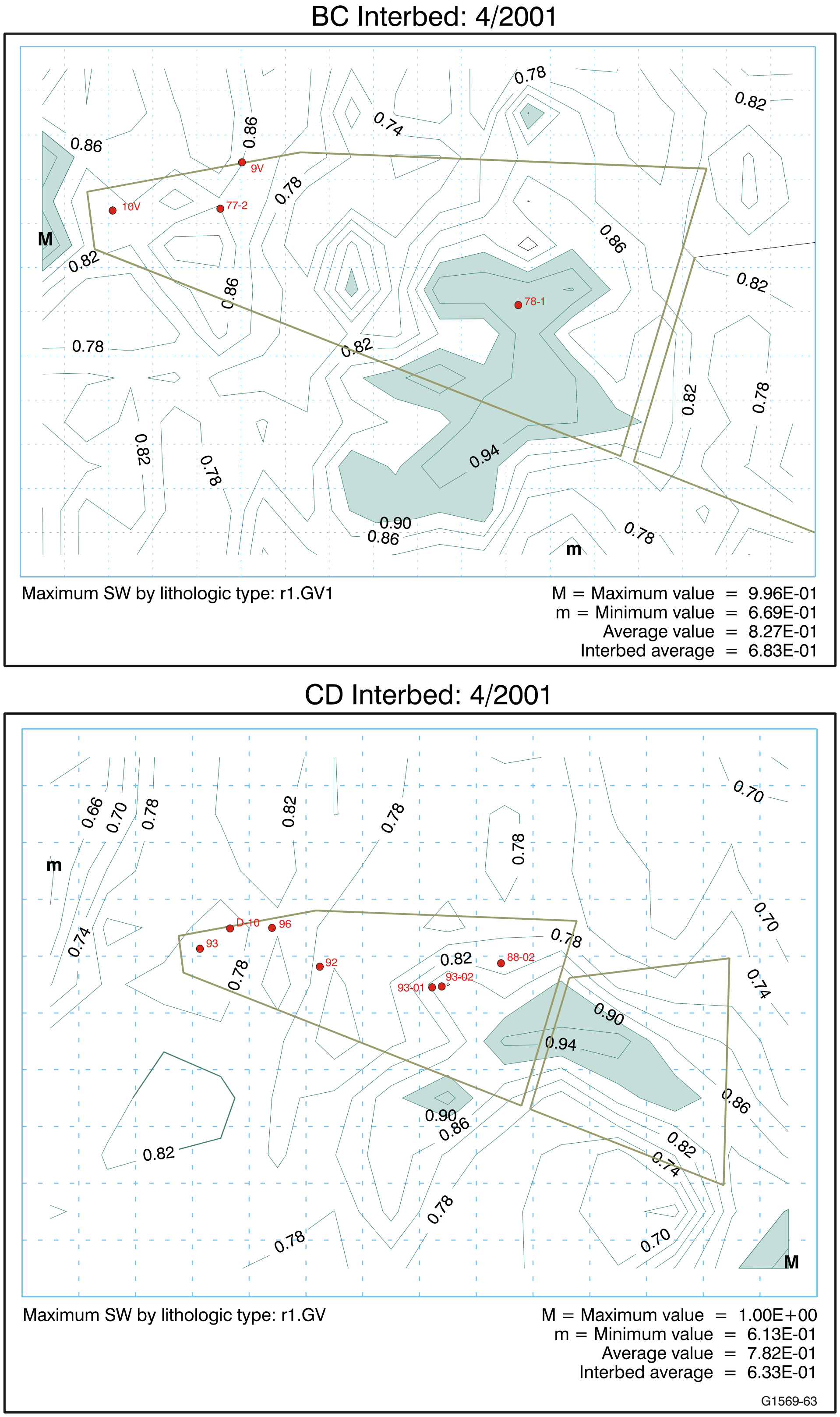

Figure 5-24. Maximum interbed water saturations for the base-case remedial investigation and feasibility study model. Red symbols indicate well locations where perched water was observed at least once.

Because water velocities control contaminant movement, the simulated maximum water flux at each location across the B-C and C-D interbeds is shown in Figure 5-25. An irregular contour interval set of 0.5, 1, 3, 5, 7, 10, 15, 20, and 25 cm/year (0.2, 0.4, 1.2, 1.9, 2.7, 3.9, 5.9, 7.8 and 9.8 in./year) is used to show adequate detail in the contour lines. These results provide insight into the effect of simulated velocities on transport. The degree of focusing on water movement by simulated variable topography and the presence and absence of the the A-B interbed is notable. The spatial average of the assigned infiltration inside the SDA is 5 cm/year (1.9 in./year). By the depth of the B-C interbed, a large portion of the western half of the SDA is at a deficit relative to this value. West of the SDA boundary, there is a zone of increased vertical water flux primarily due to depressions in the upper surface of both the A-B and B-C interbeds. In the eastern half of the SDA, there is a large area of increased water flux that extends southward past the southern SDA boundary. By the depth of the C-D interbed, there is no zone of increased water flux west of the SDA boundary. The zone of increased flux through the B-C interbed has dissipated. The zone of elevated water flux in the eastern half of the SDA persists through the C-D interbed, although it is shifted toward the east–southeast due to the topography of the top of the C-D interbed. The interpolated channel in the upper surface of the C-D interbed, leading east–southeast beneath the Transuranic Storage Area, does capture some water and direct it all the way to the southeast corner of the model domain, where it is forced to go through the C-D interbed due to the horizontal no-flux boundaries.

These zones of increased water flux exert influence on where simulated contaminants migrate through the vadose zone. For comparison purposes, estimated steady-state vertical Darcian fluxes at the deep tensiometer monitoring locations from Hubbell et al. (2004) are shown in Figure 5-25. These estimated values are based on the averaged matric potentials from McElroy and Hubbell (2003), the use of a unit-gradient assumption, and hydraulic characterization of saturated and unsaturated properties of collocated core samples. Comparability of the simulated and estimated fluxes varies. In the B-C interbed, the simulated high-infiltration region west of the SDA is partially supported by estimated values for Wells O4 and I4. The low value at Well O1, south of the western SDA boundary, agrees with the simulated flux through this region. The two extremely high-infiltration estimates at Wells I2S and I4S are so out of range that there is no comparison in the simulated results. The low estimated flux at Well 03, closer to the center of the SDA, agrees well. Elevated values at Wells I5S and 02 show decent agreement with the simulated region of elevated flux in the eastern half of the SDA. In the C-D interbed, there is less agreement, partly caused by coarser discretization. The simulated water flux across the western part of the SDA does not vary much from 1 cm/year (0.4 in./year), while the estimated values range from 7.8 to 213 cm/year (3 to 83.8 in./year). Note that if the spreading area water source were still included in these simulations, the simulated flux would show better agreement. As previously discussed, the spreading area influence was not included in the RI/FS model because it primarily diluted the simulated groundwater-pathway concentrations since the spreading area water was introduced laterally at depth in the model and did not contact emplaced waste.

5.2.4.4 Vadose Zone Transport Model. This section describes development and implementation of the dissolved-phase transport model for the vadose zone. General mechanisms included in the transport model were advection, mechanical dispersion, diffusion, sorption, radioactive decay, buoyancy, and facilitated transport. Each is discussed in the following subsections.

5.2.4.4.1 Interface from the Source Release Model into the Vadose Zone Model—The vadose zone model implements the temporal source-term release (see Section 5.1) spatially in an automated fashion, using the PV-Wave program. PV-Wave is a commercial visual data analysis software program that was used for pre and post-processing model results. In addition to being spatially distributed, the source release is also distributed vertically at each assigned location based on the number of gridblocks within the surficial sediment at that location. Once released, the contaminants are allowed to migrate with the simulated water movement.

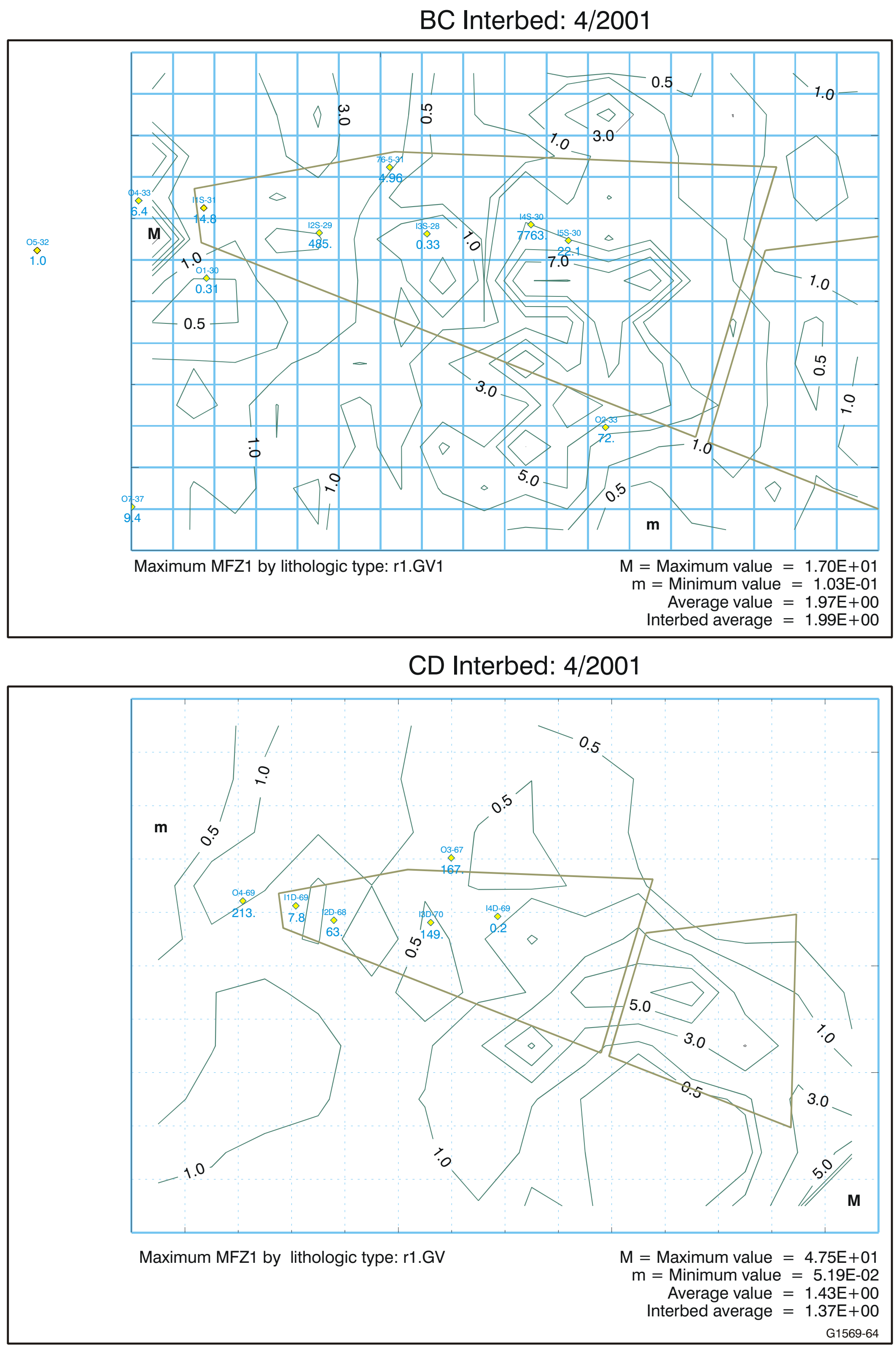

Figure 5-25. Maximum interbed vertical water flux (cm/year) for the base-case remedial investigation and feasibility study model. Blue symbols indicate well locations with estimated vertical water fluxes derived from deep tensiometer monitoring.

The general methodology for distributing contaminant release vertically at each location was to:

1. Start release in the first gridblock that was at a depth of greater than 1.5 m (4.9 ft) below the top surface. This was equivalent to maintaining a clean overburden thickness of 1.5 m (4.9 ft).

2. End release one gridblock above the bottommost surficial sediment gridblock. This maintained a clean underburden thickness of at least 0.5 m (1.6 ft).

Two exceptions were implemented to these general rules. First, the Pad A releases were assigned to the second gridblock beneath the surface for the three gridblock locations representing Pad A. The reason for this assignment is that Pad A waste is actually buried above grade, and the second gridblock down was the closest approximation that could be made in the model; the uppermost gridblock was used to assign infiltration rates. Second, Acid Pit sources were assigned at the bottommost gridblock to approximate burial at the bottom of an open pit. The LLW Pit is not listed as an exception for waste zone thickness assignments. As discussed previously (see Section 5.2.4.3.3), the surficial sediment at grid locations representing the LLW disposal pits was deepened to 9.1 m (30 ft) when the lithologic assignments for the gridblocks were made. With this approach, the general methodology correctly assigned waste for the LLW waste streams that went into the active pit.

5.2.4.4.2 Distribution Coefficient—Sorption was considered to follow linear, reversible isotherms that could be described using distribution coefficients, or K_ds. A K_d lumps all possible geochemical interactions into a single parameter. Because sorption was assumed not to occur within the fractured basalt portions of either the vadose zone or the aquifer, only sediment K_d values were necessary in the RI/FS model.

Table 5-20 gives the K_ds used in the RI/FS model that were defined for use in Holdren and Broomfield (2004). Values for Ac-227, Am-241, Am-243, Pu-238, Pu-239, and Pu-240 were decreased from those used in the IRA and ABRA models to account for sieving of interbed material (Hull 2003). Values for Np-237 and uranium isotopes were increased based on additional batch equilibrium measurements from interbed cores (Leecaster and Hull 2004). The value for C-14 is different than the value in Holdren and Broomfield (2004). The C-14 value of 0.4 mL/g was selected from the conservative end of the range presented in Plummer, Hull, and Fox (2004). The value for chromium also is different than the value in Holdren and Broomfield (2004). Chromium was simulated in both the IRA and ABRA models with a K_d of 0.1 mL/g. This same value is used in the RI/FS model. The derivation of VOC K_ds is described in Section 5.3.

5.2.4.4.3 Facilitated Transport—Plutonium mobility in the RI/FS model was based on research by Batcheller and Redden (2004). The source-term model accounts for the mobile fraction leaving the waste form. In the vadose zone model, this released mobile fraction of plutonium is then allowed to migrate with a 0 K_d through the surficial sediment and A-B interbed. The B-C and C-D interbeds are assigned the sediment K_d value of 2,500 mL/g from Table 5-20. Facilitated transport is considered for Pu-239 and Pu-240, but not for Pu-238. As discussed in Section 5.1.1, Pu-238 is not simulated with a colloidal fraction.

5.2.4.4.4 Other Transport Parameters—A variety of additional parameters were required to implement the vadose zone transport model. These additional parameters were particle density, diffusion coefficients, tortuosity, and decay half-lives. Particle density was assigned the typical value of 2,700 kg/m^3 for sediment (Freeze and Cherry 1979). This was the same value assigned in the ABRA model. Because sorption was assumed not to occur in fractured basalt, the grain density assigned for that portion of the simulation domain did not matter.

Table 5-20. Sediment distribution coefficients for Operable Unit 7-13/14 remedial investigation and feasibility study simulations.

Contaminant	Distribution Coefficient (mL/g)
Ac-227	2.25E+02
Am-241	2.25E+02
Am-243	2.25E+02
C-14	4.00E-01
Cl-36	0.00E+00
I-129	0.00E+00
Nb-94	5.00E+02
Np-237	2.30E+01
Pa-231	8.00E+00
Pb-210	2.70E+02
Pu-238	2.50E+03
Pu-239	0.00E+00[a] and 2.50E+03[b,c]
Pu-240	0.00E+00[a] and 2.50E+03[b,c]
Ra-226	5.75E+02
Sr-90	6.00E+01
Tc-99	0.00E+00
Th-229	5.00E+02
Th-230	5.00E+02
Th-232	5.00E+02
U-233	1.54E+01
U-234	1.54E+01
U-235	1.54E+01
U-236	1.54E+01
U-238	1.54E+01
Chromium	1.00E-01
Nitrate	0.00E+00
Carbon tetrachloride	2.20E-01
1,4-Dioxane	6.15E-04
Methylene chloride	4.40E-03
Tetrachloroethylene	1.82E-01

a. Mobile fraction source release, surficial sediment, and A-B interbed.
b. Mobile fraction in B-C and C-D interbeds.
c. Nonmobile fraction source release, surface sediment, and interbeds.

Diffusion of contaminants within the aqueous phase was assigned the common literature value of 1×10^{-5} cm^2/second (Freeze and Cherry 1979). This was the same value assigned in the ABRA model. The restriction of diffusion caused by tortuosity also was included, based on a relationship from Lerman (1988) that was used to describe diffusion, as shown in Equation (5-1):

$$D = D_o \theta_w^2 \tag{5-1}$$

where

D	=	diffusion in the porous medium (length^2/time)
D_o	=	free-water diffusion coefficient (length^2/time)
θ_w	=	volumetric moisture content (unitless).

Various formulations of diffusion and tortuosity are implemented in different simulators. In the TETRAD simulator, diffusion within the aqueous phase is treated, as shown in Equation (5-2):

$$D_{eff} = \frac{\theta_w D_o}{\tau_w} \tag{5-2}$$

where

D_{eff}	=	effective diffusion coefficient (length^2/time)
τ_w	=	aqueous-phase tortuosity.

The aqueous-phase tortuosity term for TETRAD was then calculated, as shown in Equation (5-3):

$$\tau_w = \frac{1}{\theta_w} \quad . \tag{5-3}$$

The end result of this application is to have greater tortuosity values assigned for drier conditions. Single tortuosity values were assigned for each sedimentary feature and for fractured basalt. Tortuosity values were determined using Equation (5-3) and are given in Table 5-21. Tortuosity values were based on the average simulated water content for each sedimentary feature from the base RI/FS model (shown in the second column of Table 5-21), and either the assigned porosity for surficial sediment and the A-B interbed or the average of the kriged values for the B-C and C-D interbeds (shown in the third column of Table 5-21). Fractured basalt has low-simulated moisture content, approximately the same as assigned residual water saturation; therefore, fractured basalt was arbitrarily assigned a high aqueous-phase tortuosity.

Table 5-21. Aqueous-phase tortuosity values for the remedial investigation and feasibility study model.

Material	Average Simulated Water Saturation (cm^3/cm^3)	Assigned or Average Porosity (cm^3/cm^3)	TETRAD Tortuosity (dimensionless)
Surficial sediment	0.59	0.50	3.4
A-B interbed	0.70	0.57	2.5
B-C interbed	0.68	0.354	4.2
C-D interbed	0.63	0.428	3.7
Fractured basalt	—	—	100

Longitudinal and transverse dispersivity values of 5.0 and 0.5 m (16.4 and 1.6 ft), respectively, were assigned in the vadose zone transport model. The longitudinal value is the same as was used in the IRA and ABRA models and was originally based on inverse modeling from the Large-Scale Infiltration Test (Magnuson 1995). The transverse dispersivity value of 0.5 m (1.6 ft) is the same as was used in the ABRA model and was assigned by using the modeling rule-of-thumb that the transverse dispersion is one-tenth the longitudinal dispersion (Freeze and Cherry 1979). The 5.0-m (16.4-ft) longitudinal value is smaller than would be assigned using the general rule-of-thumb that the dispersivity should be approximately one-tenth of the domain size (Gelhar 1986). In the absence of calibration data (e.g., the breakthrough of a nonsorbing contaminant), no basis is available to substantially adjust the dispersivity values from those used in the ABRA model. Ideally, higher concentrations would result for pulses of mobile contaminants because the lower dispersivity would produce a sharper simulated front. For a long slow release (e.g., a solubility-limited release of a lower mobility contaminant), the lower dispersivity ideally would result in a slightly later first arrival. Numerical dispersion was shown to not significantly impact the simulation results from the RI/FS model (see Appendix H of Magnuson and Sondrup 2006). No dispersivities were assigned for vapor-phase transport because diffusion would dominate the dispersive fluxes.

Half-lives for each radioactive contaminant of potential concern were assigned based on literature values (GE 1989) and were the same as those used in the ABRA model.

5.2.4.4.5 Interface from Vadose Zone Model into Aquifer Model—With separate vadose zone and aquifer domains, it was necessary to take the masses of water and contaminants emanating from the bottom of the vadose zone simulation domain and transfer them into the top of the aquifer simulation domain as a boundary condition. This was done on a gridblock-by-gridblock basis and, therefore, no spatial averaging was necessary. Gridblocks in the aquifer domain were refined to establish a one-to-one correspondence to vadose zone gridblocks. The complete time history of the flux of water and contaminants from the vadose zone model was transferred into the aquifer model.

5.2.4.5 Aquifer Flow Model. The objective in the aquifer simulation was to evaluate three-dimensional advective-dispersive transport in a predominantly horizontal flow regime. The aquifer flow model had been updated in the ABRA to take advantage of additional water level data (Whitmire 2001). For the RI/FS model, the aquifer domain was again revised to extend the domain farther to the south and west. This extension ensured that risk isopleths at the 1.E-05 level (see Section 6) were closed within the simulation domain. Permeability values were not adjusted to improve agreement between simulated and observed water levels for this extension to the ABRA domain. Appendix C of Magnuson and Sondrup (2006) contains the complete details of this aquifer domain extension. A summary of the domain extension is included here.

The domain was extended westward so that it was twice the width of the ABRA aquifer model domain (see Figure 5-26). The domain was extended southward so that it was three times the height (in a north-south sense) of the ABRA aquifer model domain. Hydrologic properties in the extended domain were taken from McCarthy et al. (1995) and are shown in Figure 5-27. These permeabilities were assigned isotropically in contrast to the vadose zone model, which had anisotropic permeabilities. The low-permeability region immediately south and southwest of the SDA was retained. Treatment of the low-permeability region as a continuous zone of similar properties is a key feature of the aquifer model because it influences water movement and, subsequently, contaminant movement and simulated concentrations.

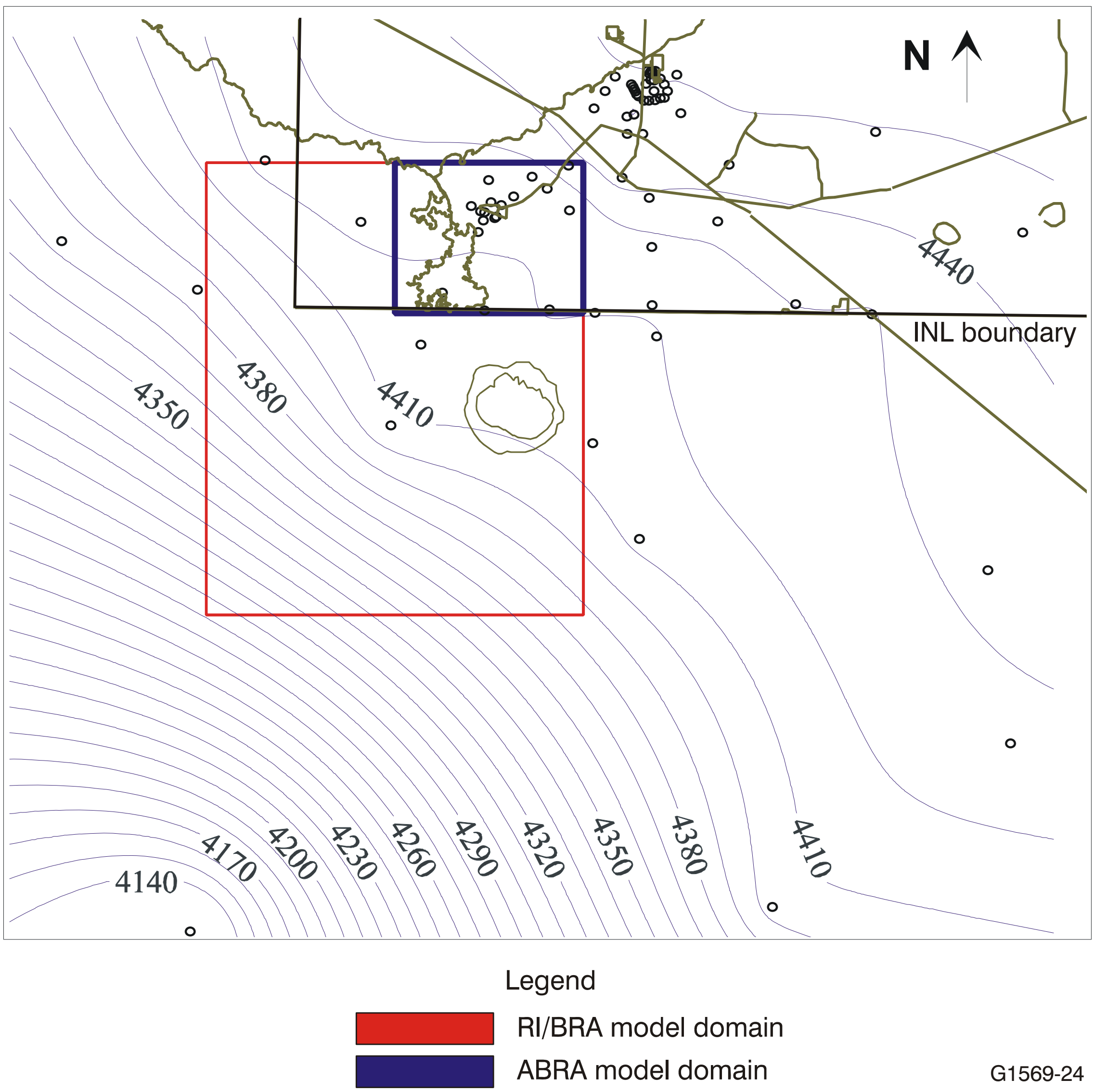

Figure 5-26. Remedial investigation and baseline risk assessment model domain with interpolated fall 2003 water table contours (feet). Symbols indicate locations used for interpolation.

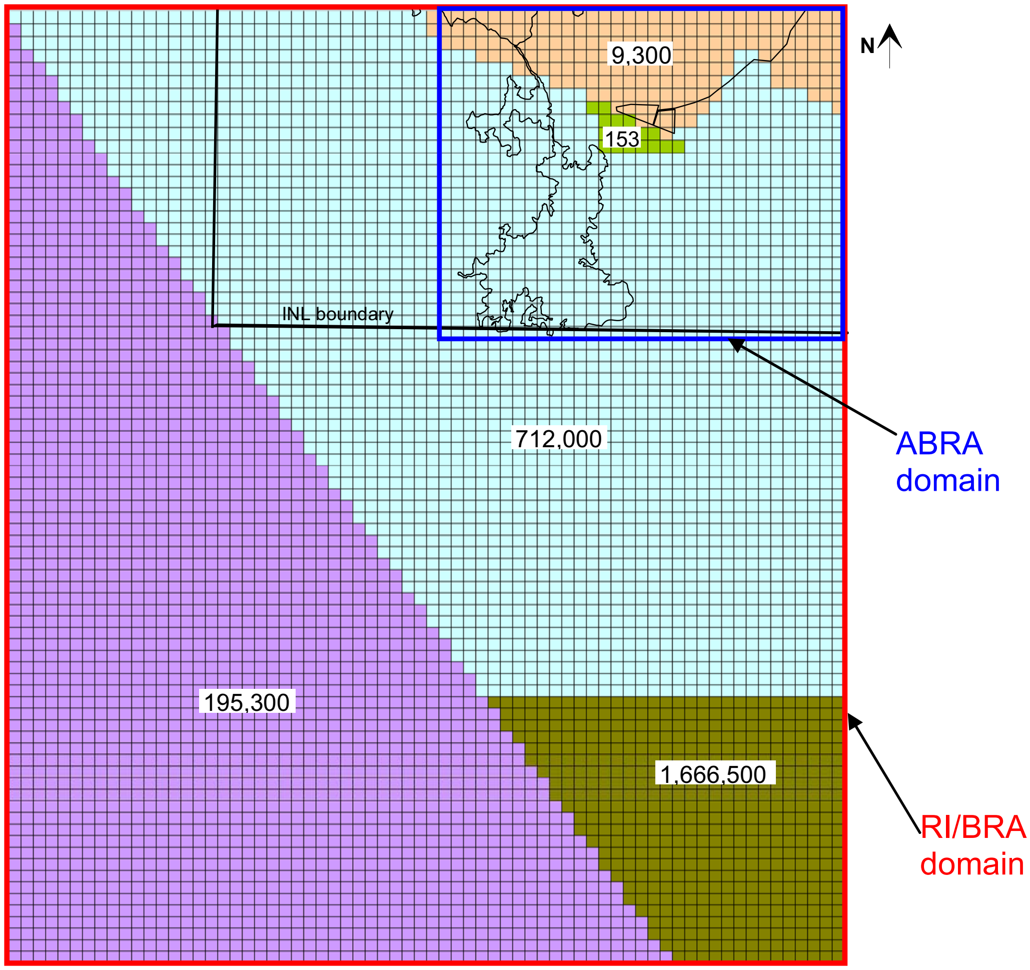

Figure 5-27. Permeability zones in the extended remedial investigation and baseline risk assessment aquifer model domain (values shown in millidarcy).

Prescribed head boundary conditions were based on interpolated water levels measured in 2003 and were applied with an assumption of hydrostatic conditions (see Figure 5-26). Porosity was assigned uniformly for the entire model domain and had the same value as in the ABRA model, 0.06. Simulated velocities in the new extended domain are compared to the old domain in Appendix C of the ABRA. With the larger domain, monitoring wells with considerably lower water levels got included in interpolating boundaries, and the head gradient imposed across the domain was greater, leading to increased velocities away from the SDA. However, with retention of the low-permeability region in the SDA vicinity, the velocities remain slow, keeping aquifer simulation results essentially consistent with the ABRA.

The thickness of the aquifer model was 76 m (250 ft). This thickness was discretized using seven vertical gridblocks varying in size from 8 m (26 ft) at the top to 18 m (59 ft) at the bottom. The 76-m (250-ft) thickness originated from generalizations of Robertson, Schoen, and Barraclough (1974) on the depth to which contaminants were detected in plumes in the southern part of the INL Site. This aquifer thickness was first implemented in simulations by Robertson (1974). Both the IRA and the ABRA aquifer models used this same 76-m (250-ft) thickness. Recent estimates of effective aquifer thickness show that it varies across the INL Site and is approximately 150 m (490 ft) in Well C1A, immediately northeast of the SDA (Arnett and Smith 2001). The effect of retaining the thinner aquifer in the ABRA simulations is conservative because less aquifer thickness is available for contaminant dispersion. Thus, resulting estimates of contaminant concentrations are higher than for a larger effective aquifer thickness. The resulting simulated hydraulic heads are shown in Figure 5-28 along with measured water levels from 2003.

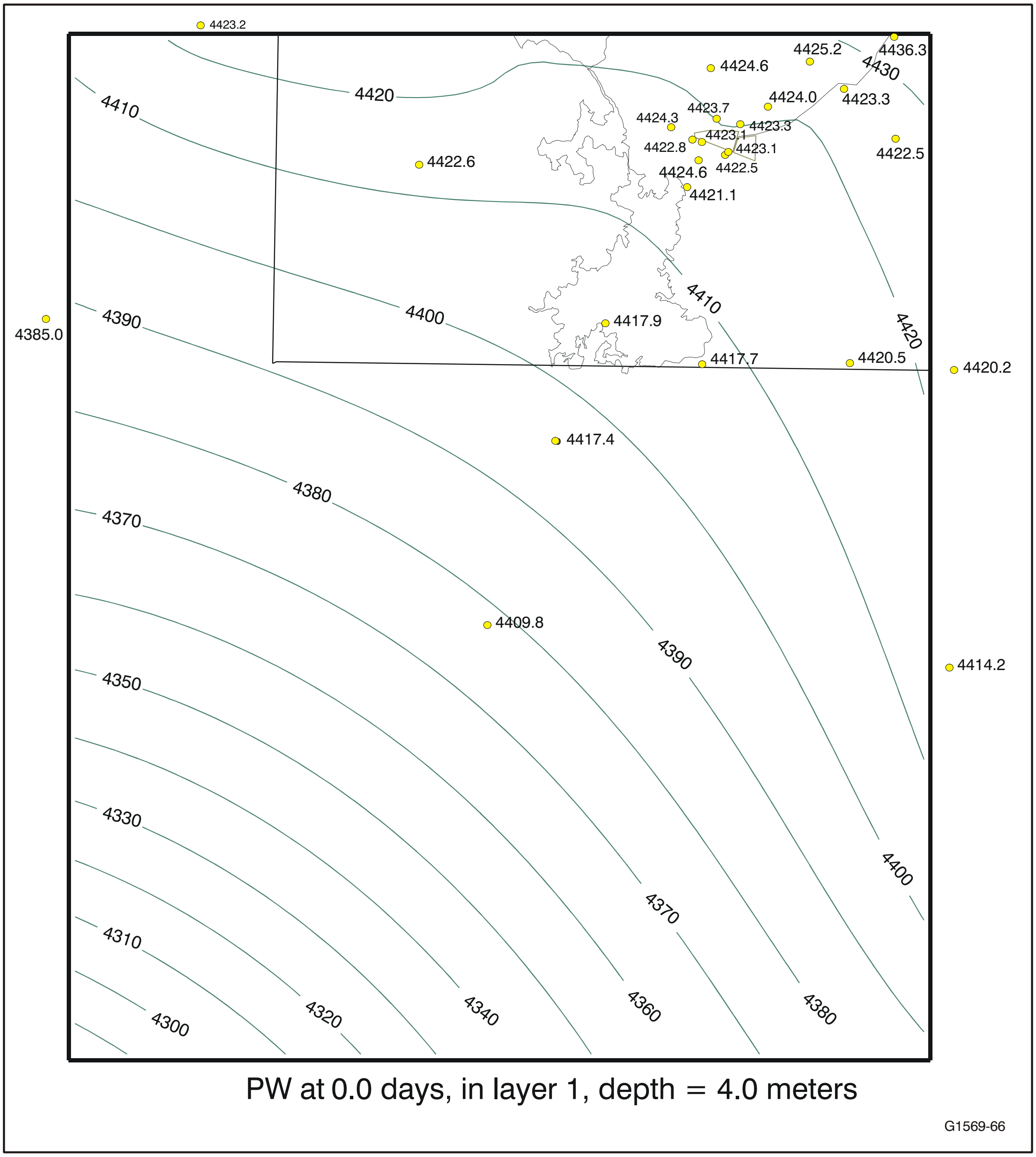

Figure 5-28. Contours of simulated water levels (feet) for the base aquifer model domain and water level measurements at indicated wells from 2003.

Simulated average linear groundwater velocities (also known as seepage or pore velocities) in the uppermost layer are shown in vector plots. Figure 5-29 shows the first-level refined grid, and Figure 5-30 shows the portion of the base aquifer domain that matches the ABRA domain. For readability, Figure 5-30 shows average linear velocity values in alternating gridblocks. Results for successively deeper model layers are essentially identical, given no vertical permeability contrasts in the model. The size of the vectors from each grid point is drawn on a scale relative to the maximum velocity in the model. The bottom plot in Figure 5-30 is for the refined grid and shows velocities, in meters per year, overlaid at each gridblock. The dominant influence of the low-permeability zone to the south and southwest of the SDA can be seen in the results, especially in the refined grid. Water movement is effectively blocked by the low-permeability region and has to diverge around the low-permeability zone. This divergence results in simulated westward velocities just northwest of the SDA and simulated southeastward velocities beneath the eastern half of the SDA. Simulated average linear velocities away from the low-permeability region agree favorably with estimates of flow velocity in the regional Snake River Plain Aquifer discussed in Section 2.2.9. Those estimates were 0.1 to 6.1 m/day (0.4 to 20 ft/day), which converts to 36 to 2,200 m/year (140 to 7,300 ft/year).

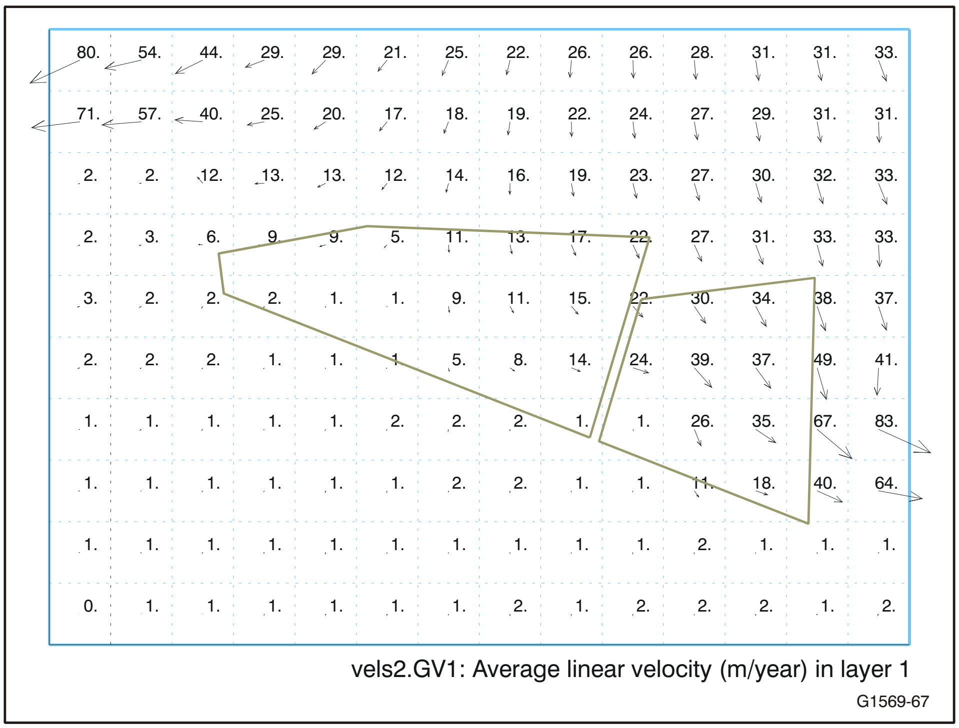

Figure 5-29. Simulated groundwater average linear velocities (meters/year) for the first-level refined grid in the aquifer domain that matches the vadose zone model domain.

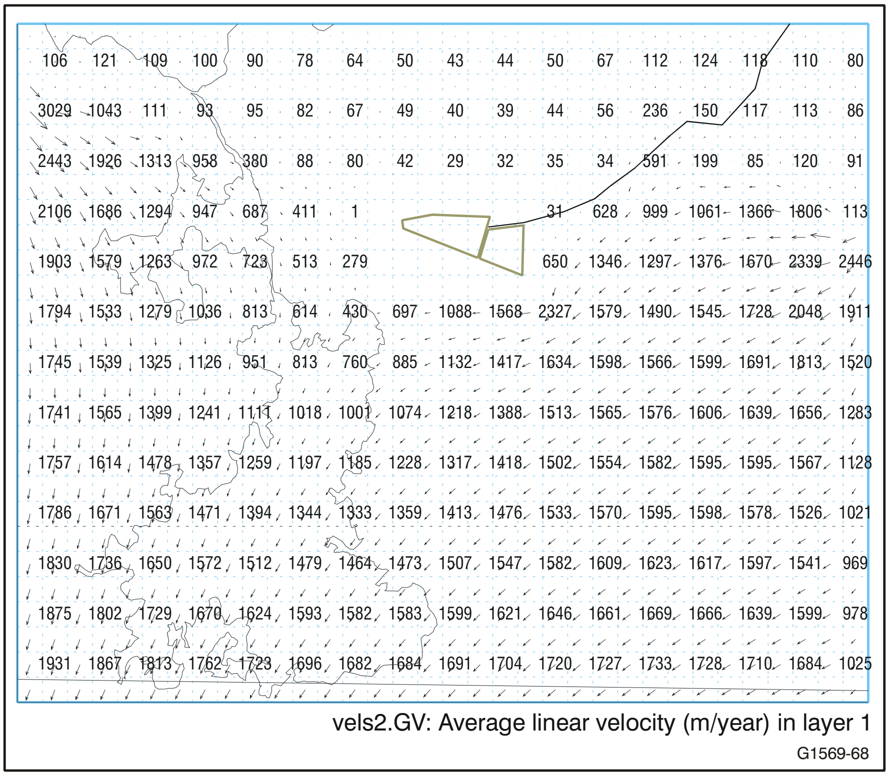

Figure 5-30. Simulated groundwater average linear velocities (meters/year) for the Ancillary Basis for Risk Analysis portion of the base aquifer model domain.

Velocities for the RI/BRA can be compared to those for the ABRA by referring to Figure 5-41 in the ABRA. The RI/BRA velocities in the immediate vicinity of the SDA are slightly higher, illustrating the effect of imposing much larger gradients across the extended aquifer domain compared to the smaller gradients across the ABRA aquifer domain.

An evaluation of flow directions in the aquifer near the SDA was conducted for the Operable Unit 7-13/14 Project (Appendix D of Magnuson and Sondrup 2006). In this evaluation, water levels were evaluated over time using three-point solutions with groupings of three wells to determine flow directions as a function of time. The flow directions are plotted using a rose diagram, similar to that normally used to plot wind velocities. Figure 5-31 shows the comparison of simulated and interpreted flow directions. Wells used for the comparison that are within the refined domain are labeled with blue text, and well triplets used to determine direction over time are labeled with purple text. The rose diagrams are plotted at the approximate centroid of each triplet. The larger the rose diagram in Figure 5-31, the larger the separation between wells and the less likelihood of errors due to very low gradients, which increase likelihood of measurement error influencing results. The interpreted flow directions often show a slight southeastward component beneath the eastern half of the SDA and beneath the Transuranic Storage Area, indicating some agreement with the flow directions from the RI/FS aquifer model.

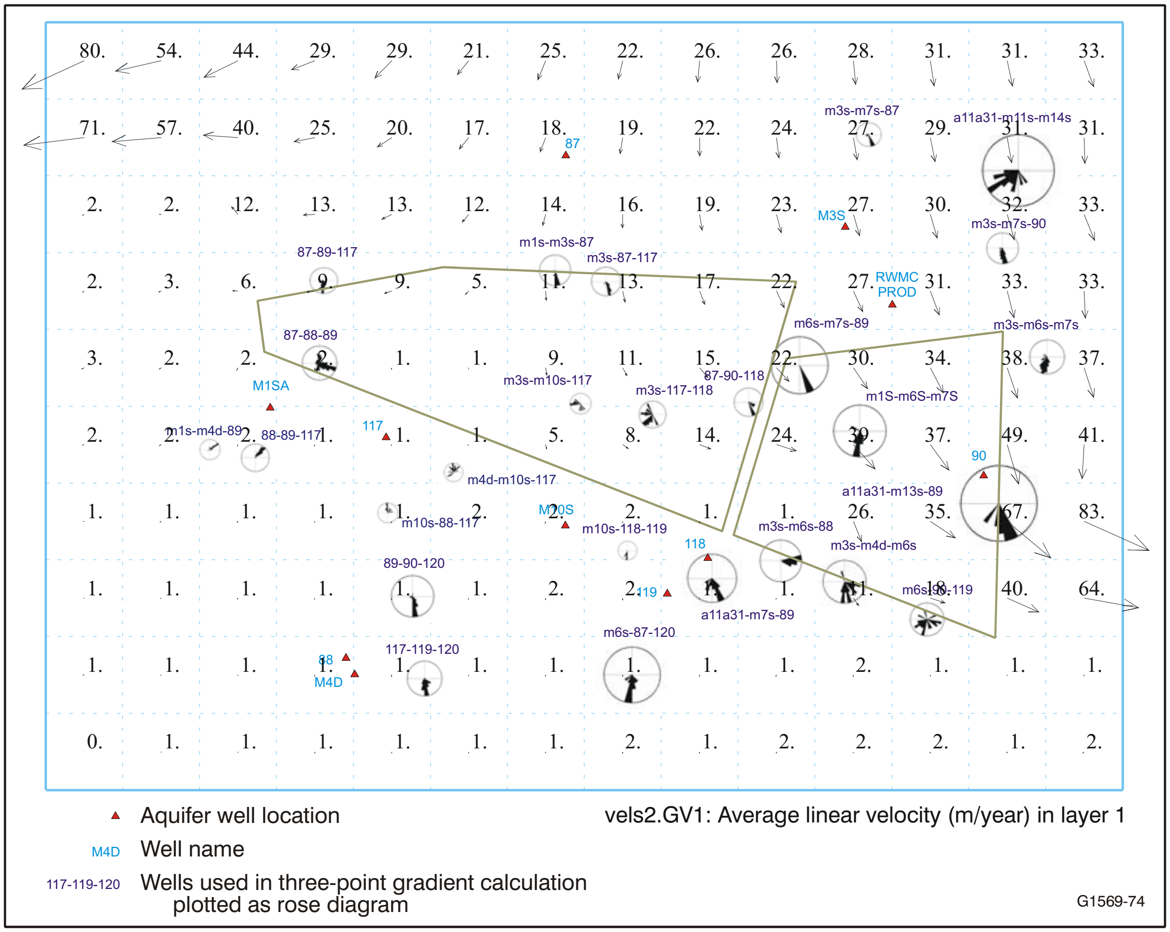

Figure 5-31. Simulated groundwater average linear velocities (meter/year) for the first-level refined grid in the aquifer domain, compared to interpreted aquifer flow directions, as a function of time.

Regarding the RI/FS aquifer flow model, general flatness of the water table in the immediate SDA vicinity, coupled with an apparent low-permeability region south-southwest of the SDA, precludes completely accurate determination of groundwater flow directions. The presence of a low-permeability region is hypothesized on an increasingly compelling body of supporting evidence and evaluations. This hypothesis also is consistent with the interpretation by Roback et al. (2001) that RWMC is in a low-permeability region extending southerly from the Lost River Range onto the INL Site. Furthermore, as discussed in Section 2, the low-permeability region immediately south of the SDA may be an extension of the Arco-Big Southern Butte volcanic rift zone.

The impact of increased velocities, from extending the aquifer simulation domain and reinterpolating head boundaries, demonstrates uncertainty in the aquifer simulation. Overall, treatment of water movement in the aquifer is simplistic with water movement being primarily two-dimensional with limited three-dimensional contaminant movement. Improving representation of the movement of water and contaminants within the aquifer is the scope of the Operable Unit 10-08 Groundwater Modeling Project (DOE-ID 2004b). The Operable Unit 10-08 groundwater model is currently under development to represent INL Site-scale transport, considering contaminant loading from all facilities concurrently. The potential effect of commingled plumes from INL Site facilities is one primary reason this model is being developed. This INL Site-wide model is being developed using information from the disciplines of geology, hydrology, contaminant chemistry, isotope chemistry, and thermal transport. This INL Site-wide model will use contaminant loading to the aquifer from individual waste area group facility models and has the stated goal of being consistent with the local velocities from waste area group models if they are based on local information (e.g., the Operable Unit 7-13/14 model's representation of the low-permeability zone).

5.2.4.6 Aquifer Transport Model. Simulating transport in the aquifer model was straightforward compared to the vadose zone. The flux of water and contaminants from the vadose zone model were applied as an upper-boundary condition in the refined portion of the model. The remainder of the upper surface of the model and the bottom surface of the model were assigned as no-flux boundaries. Contaminants could advect through external boundaries.

Because it was assumed that sorption did not occur within fractured basalt, and only fractured basalt was simulated in the aquifer portion of the model, no K_d values were necessary in the aquifer portion of the model. Diffusion was included and was parameterized the same as in the vadose zone model. Tortuosity was assigned using the same approach as in the vadose zone model (i.e., following the approach in Lerman [1988]), with a resulting value of 16.7 (dimensionless). Dispersion was parameterized differently in the aquifer model than in the vadose zone model. Longitudinal and transverse dispersivity values of 9 and 4 m (30 and 13 ft) were assigned, respectively. These values were the same as those used in the ABRA model. Similar to the vadose zone model, assigned longitudinal dispersivity values are small relative to the one-tenth domain size general rule of thumb. Dispersion is a fourth rank tensor and is assigned relative to principal flow direction, rather than by Cartesian coordinate direction. Through symmetry considerations, only two parameters are necessary: longitudinal and transverse dispersivity. Since the primary flow direction is horizontal to the south-southwest, transverse dispersion allows equal spreading of contaminants in directions orthogonal to this principal flow direction. The net effect of this implementation is to allow a contaminant plume to spread equally in the vertical and horizontal directions, transverse to the primary flow direction.

5.2.5 Base-Case Simulations for the Baseline Risk Assessment

The numerical model, implemented as discussed previously, was used to simulate each contaminant of potential concern for the RI/BRA base case. The source-release model (described in Section 5.1) provided contaminant inputs to the vadose zone model. This section presents comparisons of simulated results with observed concentrations for selected contaminants to illustrate model performance. These comparisons are presented in sequence for the vadose zone from 0 to 10.7 m (0 to 35 ft), the deeper vadose zone from 10.7 to 76.2 m (35 to 250 ft) that contains the B-C and C-D interbeds, and the aquifer. The comparisons are primarily time histories and aquifer concentration contours at points in time.
The contaminants, for which simulation results are presented in the vadose zone, are U-238, Tc-99, and nitrate. These contaminants were identified in Section 4 as showing either elevated concentrations relative to background or significant increasing trends. In the aquifer, the presentation focuses on simulation results for nitrate and chromium, because those contaminants can be discerned above background aquifer concentrations. Additionally, time histories are presented for all radionuclide contaminants with any detections.

Originally, scope for evaluating model performance included comparing simulated tritium concentrations in the vadose zone and aquifer to detected concentrations; hence, tritium is addressed in Section 4 and is identified as simulation Group 7 in Table 5-8. Unfortunately, despite numerous attempts, the vadose zone TETRAD simulations for tritium could not be made to preserve mass balance. Mass balance was successfully preserved for all other contaminants. The short half-life of tritium may be at the root of the problem. Because the discrepancy could not be resolved, tritium results are not presented in this section.